EFFECT OF MICHIGAN MULTI-AXLE TRUCKS ON PAVEMENT DISTRESS

Volume III – Rigid Pavements

Karim Chatti, Ph.D.
Anshu Manik, Ph.D.
Nicholas Brake, M.S.
Hassan Salama, Ph.D.
Syed W. Haider, Ph.D.

Michigan State University
Department of Civil and Environmental Engineering
Pavement Research Center of Excellence

Draft Final Report
Volume III
Project RC-1504

February 2009

Technical Report Documentation Page

1. Report No.	2. Government Accession No.	3. MDOT Project Manager
RC-1504		Mr. Mike Eacker

4. Title and Subtitle	5. Report Date
EFFECT OF MICHIGAN MULTI-AXLE TRUCKS ON PAVEMENT DISTRESS Volume III – Rigid Pavements	Februray 2009
	6. Performing Organization Code
7. Author(s) Karim Chatti, Anshu Manik, Hassan Salama, Nicholas Brake, Syed W. Haider, Chadi El Mohtar, Hyung Suk Lee	**8. Performing Org. Report No.**
9. Performing Organization Name and Address Department of Civil and Environmental Engineering Michigan State University East Lansing, MI 48823	**10. Work Unit No. (TRAIS)** **11. Contract No.** **11(a). Authorization No.**
12. Sponsoring Agency Name and Address Michigan Department of Transportation Construction & Technology Division 8885 Ricks Road Lansing, MI 48909	**13. Type of Report & Period Covered** Final Report **14. Sponsoring Agency Code**

15. Supplementary Notes
Volume III of III

16. Abstract
With the adoption of the new mechanistic-empirical pavement design method and the employment of axle load spectra, the question of evaluating the pavement damage resulting from different axle and truck configurations has become more relevant. In particular, the state of Michigan is unique in permitting several heavy truck axle configurations that are composed of up to 11 axles, sometimes with as many as 8 axles within one axle group. Thus, there is a need to identify the relative pavement damage resulting from these multiple axle trucks.
The study looked at both flexible and rigid pavement systems, and comprised of three main components: (1) in-service pavement performance data; (2) laboratory testing under multiple axles, and (3) mechanistic-empirical analyses. The results from in-service pavement performance data indicated that multiple axle groups appear to cause less damage in fatigue per load carried for both pavement types, whereas they cause more damage in rutting of flexible pavements and roughness for rigid pavements. Laboratory testing of asphalt concrete confirmed that multiple axles cause less fatigue damage per load carried, and that rutting is nearly proportional to the number of axles within an axle group. Results from flexural concrete beam fatigue testing showed significant variability; multiple linear regression analysis (independent variables: stress ratio, stress impulse and initial modulus of elasticity) indicated, on average, similar findings to asphalt concrete fatigue for a given stress ratio; however, mechanistic analysis showed that multiple axles cause considerable stress reduction leading to significantly lower fatigue damage. The mechanistic analysis also showed that multiple axles cause more faulting in rigid pavements. Mechanistic analyses of flexible pavements confirmed that multiple axles cause less fatigue damage per load carried, and rutting damage that is nearly proportional to the number of axles within an axle group. However, the mechanistic-empirical results suggest that the AASHTO Load Equivalency Factors (LEF) for large axle groups may be unconservative. Finally, Full scale slab testing to study joint/crack deterioration in plain concrete pavements was inconclusive.

17. Key Words	18. Distribution Statement
Multi-Axle Trucks, Michigan Trucks, Pavement Distress, Truck Factors	No restrictions. This document is available to the public through the Michigan Department of Transportation.

19. Security Classification - report	20. Security Classification - page	21. No. of Pages	22. Price
Unclassified	Unclassified	139	

TABLE OF CONTENTS

LIST OF FIGURES

LIST OF TABLES

CHAPTER 1
INTRODUCTION AND BACKGROUND

1.1 INTRODUCTION

The state of Michigan hosts several trucks that have unusual axle configurations, up to eleven axles and 164 kips in gross weight and 8 axles within an axle group. The relationship between these trucks and pavement distresses has not been determined, since earlier research studies have not addressed the damage caused by multiple axle/truck configurations. Therefore, there is a need to examine the relative effect of these heavy vehicles on pavement distresses using field data from in-service pavements, laboratory experimentation, and mechanistic analyses.

Analysis of in-service data, shown in Volume I of this report, indicated that multiple axles may be less damaging per load carried in cracking, while they may cause more roughness in rigid pavements. In this volume, the analyses are focused on concrete pavements by simulating the effect of these Michigan multiple axle trucks using laboratory testing in fatigue and mechanistic analysis (fatigue and faulting) to further explain their relative effect on concrete pavement damage. The conclusions and recommendations of this research can be accomplished by combining the findings using in-service data with those from mechanistic analysis and the laboratory experiments.

1.2 RESEARCH OBJECTIVES

The objective of the research conducted in this part of the study is to determine the effect of heavy multi-axle Michigan trucks on concrete pavement fatigue cracking and faulting. This was accomplished in the laboratory using cyclic beam fatigue testing under multiple load pulse configurations, and with mechanistic analysis. An attempt was made to test for crack deterioration in full-scale slabs; however, it was not possible to achieve the desired accelerated damage.

1.3 RESEARCH APPROACH

In addition to the investigation of in-service pavement traffic and distress data presented in volume I, the research problem was investigated using: 1) laboratory experimentation, and 2) mechanistic analysis. A brief description of each approach follows.

1.3.1 Laboratory Experiments

Four-point flexural fatigue tests were conducted on 4” X 4” X 24” beams to study the effect of fatigue cracking in PCC. Six different axle configurations were studied. A

55 kip MTS hydraulic actuator was used for the fatigue tests. Additionally, a 5' X 14' unreinforced concrete slab was used to study the performance of aggregate interlock under repetitive loading using two stationary 11 kip hydraulic actuators placed on either side of the joint. An out of phase loading sequence between each stationary actuator simulated the moving wheel load of a truck.

1.3.2 Mechanistic analysis

Two mechanistic based computer programs, DYNASLAB and KENSLAB, were used to analyze the effect of multiple axles on different pavement structures. For concrete fatigue and joint faulting, six different axle configurations were analyzed. The stress and displacement time history for each axle configuration was obtained and used in the flexural fatigue and full scale lab tests.

1.4 REPORT ORGANIZATION

This report consists of three volumes:

Volume I: Includes background information, literature review and statistical analyses using truck traffic and pavement performance data from in-service pavements.
Volume II: Contains the analyses pertaining to asphalt pavements, including laboratory fatigue and rut data, and mechanistic analysis.
Volume III: Contains the analyses pertaining to concrete pavements, including laboratory fatigue and joint deterioration data, and mechanistic analysis.

This volume is divided into six chapters:

Chapter 1 presents some background information, the research objective and approaches used.
Chapter 2 presents the laboratory fatigue investigation of concrete beams under multiple load pulses.
Chapter 3 contains the mechanistic analyses for concrete fatigue.
Chapter 4 presents the laboratory joint deterioration investigation of concrete slabs under multiple load pulses.
Chapter 5 contains the mechanistic analyses for faulting of concrete pavements.
Chapter 6 contains the conclusions from the study, implications for design and implementation recommendations.

CHAPTER 2
FATIGUE CRACKING – LABORATORY INVESTIGATION

2.1 INTRODUCTION

A detailed laboratory investigation was conducted to study the effect of multiple loading pulses on the fatigue performance of a standard PCC paving mix. The experimental testing matrix is similar to the one adopted for studying the fatigue response of asphalt mixture presented in Volume 2 of this report. The purpose of this experiment is to investigate the relative fatigue damage caused by different axle types (single, tandem, tridem, quad etc.) on PCC fatigue. The results from DYNASLAB computer runs were used to obtain the appropriate loading function and sequence to simulate a moving multi-axle group across the mid-point at the edge of the concrete slab. Because the focus of the research is on the relative effect of multiple axles on concrete fatigue and joint deterioration, the experiment was limited to one mix type (typical mix used by MDOT for PCC pavements-Grade P1). The same PCC mix was used for casting both beams and slabs. This enables a direct comparison of the effect of axle configuration on fatigue and joint/crack performance of concrete pavements.

2.2 FLEXURAL BEAM FATIGUE TEST

Concrete fatigue properties are an important design input. The general relationship between the flexural stress and the number of load repetitions is shown in figure 2.1, and it can be given by equation 2.1.

$$N_f = K_1 \left(\frac{\sigma}{M_r} \right)^4 \quad (2.1)$$

Where,

N_f = number of load repetitions to failure;
σ = applied flexural stress, psi;
M_r = modulus of rupture, psi; and
K_l = material constant.

The test uses a third point repeated flexural loading on beam specimens as shown in figure 2.2. Loading is generally applied at the rate of 1 to 2 pulses per second, with load duration of 0.1 second. This third point-loading configuration applies a constant bending moment over the middle third of the beam specimen.

The extreme fiber stress in the beam is calculated and plotted against the number of loads at that stress, which produces failure as shown in figure 2.2. In these tests, it is generally recognized that concrete will not fail in fatigue when the ratio of applied stress to modulus of rupture is below approximately 0.5, although no real limit has been shown up to 10-20 million load applications.

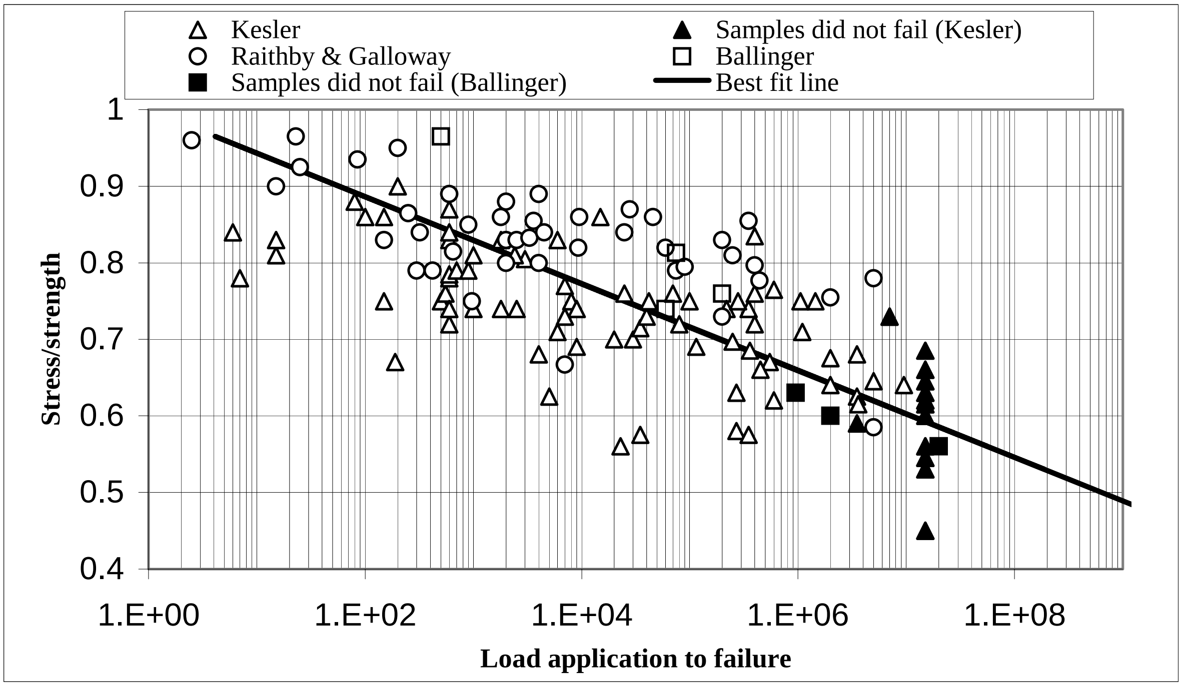

Figure 2.1. Typical failure curve for Portland Cement Concrete (from PCA)

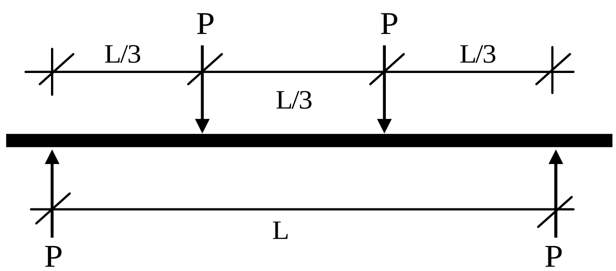

Figure 2.2. Schematic representation of flexural beam with third point loading

2.2.1 Beam Dimensions for Fatigue Testing

Review of previous research shows that a variety of beam sizes have been used for the beam fatigue testing. However, the rationale behind the selection of beam sizes was not apparent mainly because of lack of standard testing procedure for this type of test. Therefore, to select an appropriate beam dimension for fatigue testing an investigation of size effects was required. The key element in the beam fatigue testing is the fatigue of the beam in “flexure” only (i.e., no shear). This means that the beam size should be selected based on flexural stresses at the center bottom of the beam. Figure 2.2 shows the schematic of beam loading for fatigue testing.

The flexural response in the beam can be ensured if the following conditions are fulfilled:

(a) Flexural capacity should be less than the shear capacity, i.e., the beam should not fail in shear.

(b) The beam should be slender, i.e., shear span slenderness should be at least three.
(c) Flexural deformations should be more than shear deformations, i.e., this ratio should be at least two to three.

The first objective can be accomplished if the next two conditions are met in deciding the beam dimensions. Equation 2.2 is used to calculate the bending (flexural) stress at the bottom of a beam under a third point loading as shown in figure 2.1.

$$\sigma_c = \frac{2PL}{bh^2} \tag{2.2}$$

Where,

σ_c = flexural stress at the center of the beam, psi
P = load, lbs
b = width of beam, inches
h = depth of beam, inches

The flexural strength, or Modulus of Rupture (MOR), will be equal to the flexural stress, σ_c, at failure; i.e. corresponding to the load, P in equation 2.2 equal to the peak load at failure.

The allowable shear capacity of the beam can be determined by using equation 2.3. Therefore, to meet the first assumption, the shear force should always be less than allowable shear capacity of the beam.

$$V_{allowable} = 2\sqrt{f_c^{'}} \times bh \tag{2.3}$$

Where,

f_c' = compressive strength of concrete, psi
b = width of beam, inches
h = depth of beam, inches

The deflection at the bottom of the beam due to bending can be calculated using equation 2.4. This equation can be derived using the unit response method. The negative sign in the equation shows a downward deflection.

$$\delta_{c,\,flexure} = \frac{-23}{648} \times \frac{PL^3}{EI} \tag{2.4}$$

Where;

$\delta_{c,\ flexure}$ = deflection at the center of the beam due to flexural, inches
E = modulus of elasticity for concrete, psi

Once the deflection at the bottom center is known, the tensile strain at the same location can be calculated using the Hook's law. Equation 2.5 can be used to calculate the elastic strain at the bottom of the beam under third point loading.

$$\varepsilon_c = \frac{108}{23} \times \frac{\delta_{c,\ flexure} h}{L^2} \tag{2.5}$$

Similarly, the bending stress can be calculated by using equation 2.6.

$$\sigma_c = \frac{108}{23} \times \frac{\delta_{c,\ flexure} Eh}{L^2} \tag{2.6}$$

The vertical deformation in the same beam due to shear only can be calculated using equation 2.7.

$$\delta_{c,shear} = \frac{-1.5\ Pa}{Gbh} = \frac{PL}{2Gbh} \tag{2.7}$$

Where,

$\delta_{c,\ shear}$ = deflection at the center of the beam due to shear, inches

G = shear modulus of concrete, psi, $G = \frac{E}{2(1+\mu)}$

μ = Poisson's ratio of concrete

From equations 2.6 and 2.7, the ratio of the flexure to shear deformation can be calculated. Equation 2.8 shows this ratio for the beam shown in Figure 2.3. This equation shows that the ratio of the bending to shear deformation varies as the square of the length/depth ratio.

$$\frac{\delta_{flexure}}{\delta_{Shear}} = \frac{46}{15}\left(\frac{a}{h}\right)^2 = \frac{46}{135}\left(\frac{L}{h}\right)^2 \tag{2.8}$$

This function was plotted in figure 2.3 and reveals that large depth/span ratio ($L/h > 10$), the shear deformation is less than 3 percent of the bending deflection. At an L/h ratio of unity, the shear deformation is approximately three times the bending deflection. Although this curve is for a particular beam and loading, it is generally true that for the large span/depth ratio, i.e., $L/h > 10$, the shear deflections are practically negligible compared to the bending deflection. Conversely, shear deflections should be investigated for beams with relatively small length/depth ratios. For a 4 × 4 inch beam, assuming a span of 24 inches will translate into an $L/h = 6$, which will give a ratio slightly greater than 10. Also, the share of shear in the total deformation at the center of the beam will be less than 10% (see Figure 2.3).

Table 2.1 shows the detailed calculations of deflections by failure mode (flexure and shear) for a 4 × 4 inch beam along with the slenderness ratio. The rule of thumb for slenderness is given in equation 2.9.

$$slenderness = \frac{L}{2h} \geq 3 \tag{2.9}$$

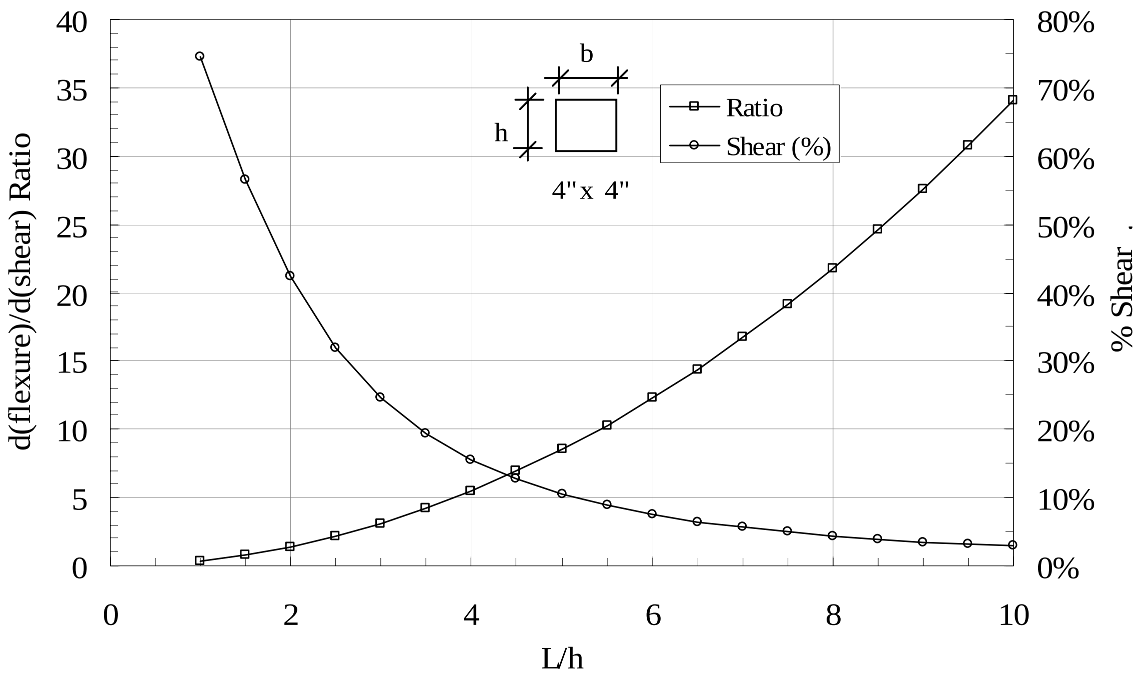

Figure 2.3 Flexure to shear deformations for beam third point loading

Table 2.1. Effect of beam span on the shear and flexural deformations

Span	P	I	Deflection (inches)		Ratio	L/h	Total Deflection	Shear (%)	Total Load	Slenderness
inches	lbs	in^4	Shear	Flexure			inches		lbs	L/(2h)
4	4400	21.33	0.00041	0.00014	0.34	1.0	0.000547	75%	8,800	0.50
6	2933	21.33	0.00041	0.00031	0.77	1.5	0.000720	57%	5,867	0.75
8	2200	21.33	0.00041	0.00056	1.36	2.0	0.000963	42%	4,400	1.00
10	1760	21.33	0.00041	0.00087	2.13	2.5	0.001276	32%	3,520	1.25
12	1467	21.33	0.00041	0.00125	3.07	3.0	0.001658	25%	2,933	1.50
14	1257	21.33	0.00041	0.00170	4.17	3.5	0.002110	19%	2,514	1.75
16	1100	21.33	0.00041	0.00222	5.45	4.0	0.002631	15%	2,200	2.00
18	978	21.33	0.00041	0.00281	6.90	4.5	0.003221	13%	1,956	2.25
20	880	21.33	0.00041	0.00347	8.52	5.0	0.003881	11%	1,760	2.50
22	800	21.33	0.00041	0.00420	10.31	5.5	0.004611	9%	1,600	2.75
24	733	21.33	0.00041	0.00500	12.27	6.0	0.005409	8%	1,467	3.00
26	677	21.33	0.00041	0.00587	14.40	6.5	0.006278	6%	1,354	3.25
28	629	21.33	0.00041	0.00681	16.70	7.0	0.007216	6%	1,257	3.50
30	587	21.33	0.00041	0.00782	19.17	7.5	0.008223	5%	1,173	3.75
32	550	21.33	0.00041	0.00889	21.81	8.0	0.009300	4%	1,100	4.00
34	518	21.33	0.00041	0.01004	24.62	8.5	0.010446	4%	1,035	4.25
36	489	21.33	0.00041	0.01125	27.60	9.0	0.011662	3%	978	4.50
38	463	21.33	0.00041	0.01254	30.75	9.5	0.012947	3%	926	4.75
40	440	21.33	0.00041	0.01389	34.07	10.0	0.014301	3%	880	5.00

The results in table 2.1 show that in order to achieve a slenderness ratio of at least 3, a span of 24 inches will be required. Therefore, based on the above analysis a beam size ($b \times h \times L$) of 4 × 4× 24 inches was selected for this research.

2.2.2 Beam Test Set-up

For the beam test, there are two possible scenarios that can be simulated in the laboratory: 1) longitudinal stress 2) transverse stress. As an example, Figures 2.4 (a) and (b) show the longitudinal and transverse stresses at the bottom of the slab shown in Figure 2.5 at node 302 (2 ft from the edge at the middle of the slab). As Figures 2.4 (a) and (b) show, unlike the transverse direction, the longitudinal stress has a significant compressive component. It should be noted that fatigue cracking in concrete pavement slabs is most likely due to longitudinal stress along the edge of the slabs.

An attempt was made to simulate the longitudinal force using the beam test. The beam fixture to simulate stress-reversal (tension-compression) at the center of the beam was designed and fabricated to enhance the capabilities of the MTS machine in the civil infrastructure research laboratory. Figures 2.6 and 2.7 show different views of this beam fixture. Unfortunately, this setup was unsuccessful due to problems with grabbing the beam sample (several samples were broken prior to testing during set-up). The research team decided to eliminate the compression part from the longitudinal pulse and run the test in tension only using a simple third point loading test fixture (Figure 2.8). Figure 2.4 (c) shows the truncated longitudinal pulse that was used to simulate the tridem axles. Figure 2.4 (d) shows the output pulses from the MTS machine for the tridem axles.

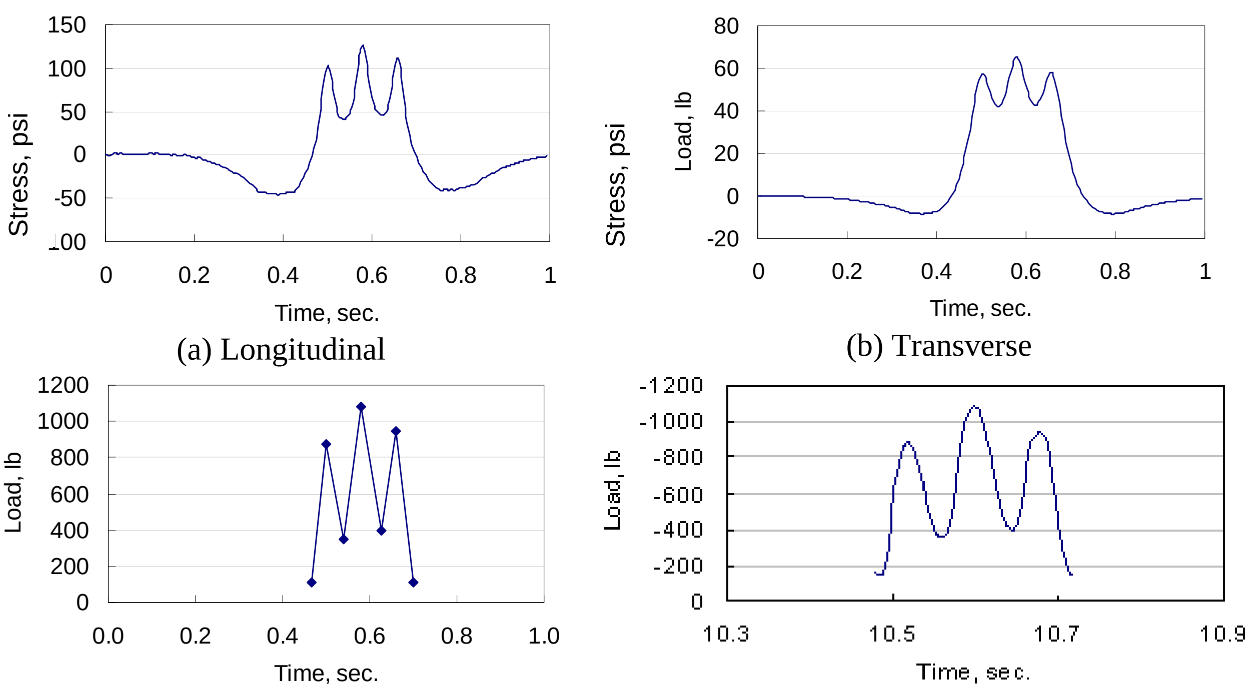

(a) Longitudinal

(b) Transverse

(c) Longitudinal – tension only (SR=0.6)

(d) Longitudinal – tension only from MTS (SR=0.6)

Figure 2.4 Load pulses for tridem axles

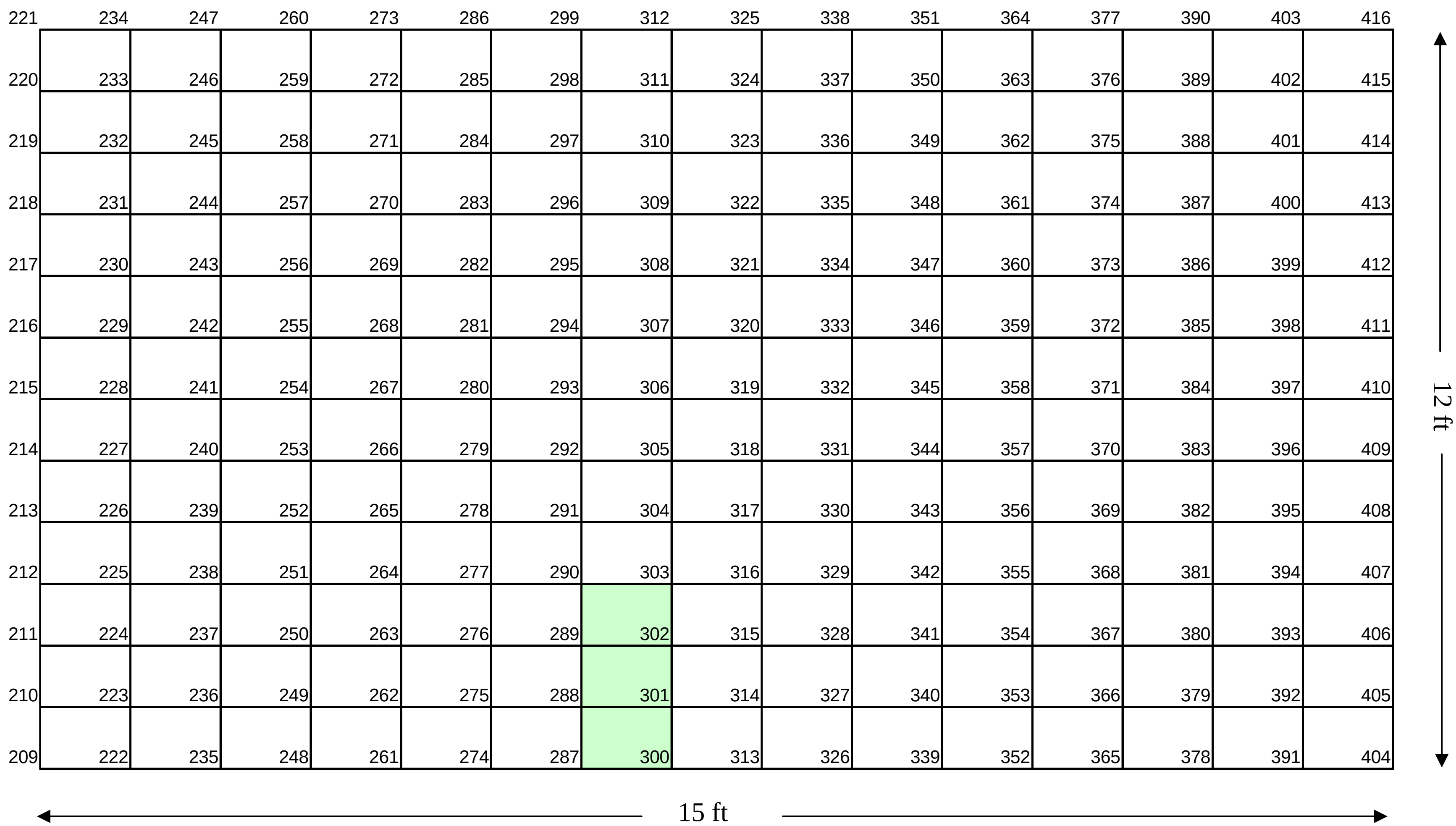

Figure 2.5 Middle slab nodes and elements used for finite element analysis

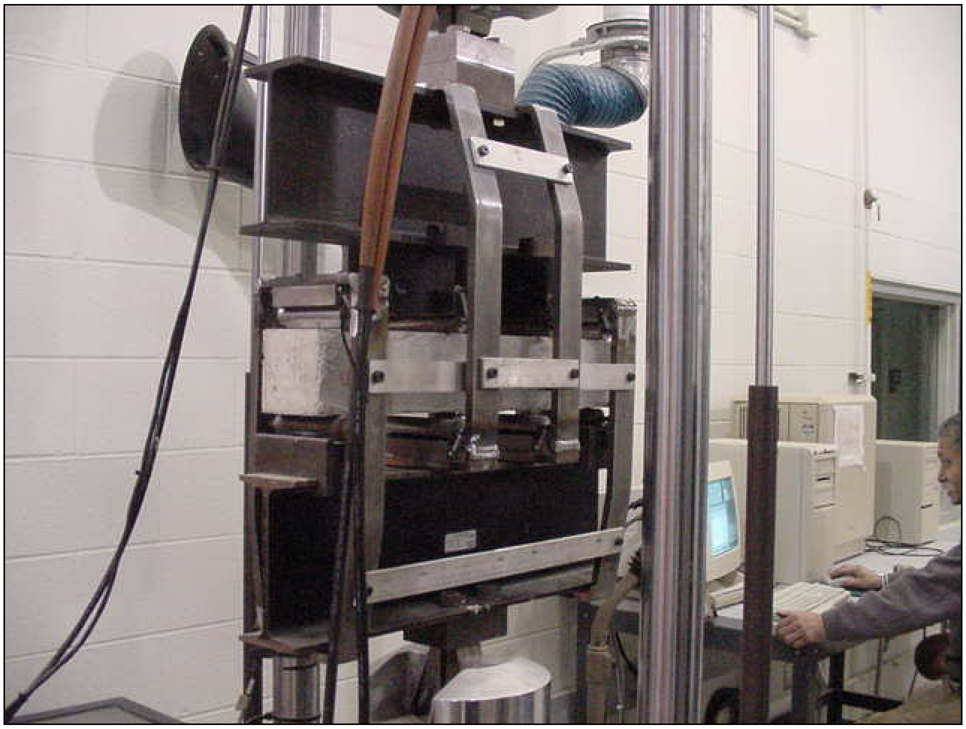

Figure 2.6 Beam Fatigue Fixture with Data Acquisition System

Figure 2.7 Side View of the Beam Fatigue Fixture

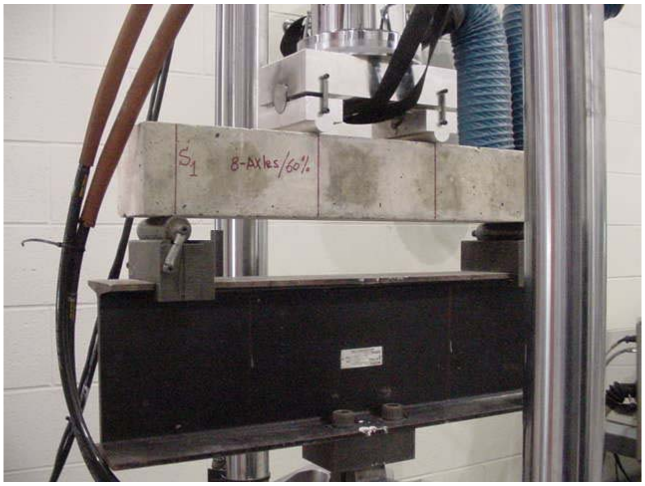

Figure 2.8 Beam Fatigue Fixture with Simple Third-Point Loading

To calculate the response (deflection, transverse stress, and longitudinal stress) of different axle configurations, the axle spacing was calculated from MDOT traffic data (WIM) for axle groups and trucks. Traffic data (65535 records) from station no. 26545309 was analyzed to calculate the axle spacing as well as the spacing between the axle groups for different trucks considered in this study. These distances between the axles were used for calculating the longitudinal and transverse stresses in the DYNASLAB computer program.

2.3 EXPERIMENT DESIGN

The main objective of this research is to investigate the effects of multi-axle trucks on the fatigue performance of concrete pavements. Traditionally, due to economic and efficiency reasons, PCC beams have been used to study the flexural fatigue of concrete slabs. The experiment design adopted for this research is shown in Table 2.2. The stress ratio and axle type are considered to be the main factors affecting the fatigue life of the concrete.

Table 2.2 Beam Test Matrix

	Axle Type						
Stress Ratio	**Single**	**Tandem**	**Tridem**	**Quad**	**Six**	**Eight**	**Total**
0.9	5	X	X	X	X	X	5
0.85	X	5	5	5	6	6	27
0.8	5	7	X	X	X	X	12
0.75	X	X	6	4	6	5	21
0.67	4	4	4	4	4	4	24
0.59	X	5	5	X	X	X	10
0.52	4	X	5	6	4	4	23
0.46	X	X	X	X	X	4	4
Sum	18	21	25	19	20	23	126

The replication of the experimental units was decided based on the variability of the results encountered in the laboratory. As shown in Table 2.2, several stress levels were chosen for the six axle configurations. The beams were tested at specific stress ratios that directly correspond to the amount of stress reduction from the multiple axle configurations. Additionally, it should be noted that the stress ratios used in this study were modified for strength gains after the completion of the fatigue testing (see section 2.5.3). Four different batches were cast to complete the beam test matrix. The first batch was a trial batch and was not used in the actual experiments.

2.3.1 Load Input for Testing

The concrete specimens in batch 2 were used to test the single, tandem, tridem, quad, six and eight axles at stress ratios of 67% and 52%. Figure 2.9 shows the load pulses that were input in the MTS test machine for batch 2. The concrete specimens in batch 3 were used to test the single, tandem, tridem, quad, six and eight axle at specific stress ratios in an attempt to complete the test matrix. Figure 2.10 shows the load pulses for batch 3. Because of the large variability in test results, the number of samples required was more than initially planned. Therefore, a fourth batch of specimen was prepared. The concrete specimens in batch 4 were used to test the tridem, quad, six and eight axles at specific stress ratios in an attempt to complete the test matrix. Figure 2.11 shows the load pulses for batch 4.

2.4 LABORATORY TESTING

Before pursuing the fatigue testing, typical concrete tests were performed to determine important concrete properties. The tests normally conducted on cured concrete can be grouped (according to the use of the test results) into two general categories:

1. Mix design tests including:
    a) Compressive strength
    b) Diametral tensile strength
    c) Slump
    d) Consistency
    e) Air content

2. General design tests including:
    a) Unconfined compressive strength tests
    b) Modulus of elasticity and Poisson's ratio tests
    c) Coefficient of thermal expansion tests
    d) Fatigue characteristic tests
    e) Flexural tests

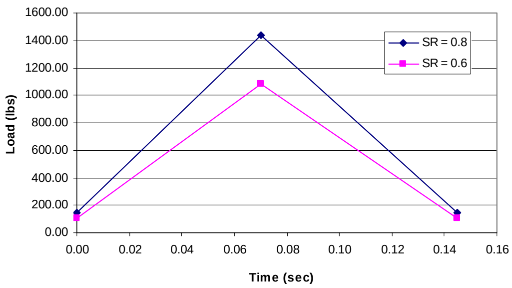

Single Axle

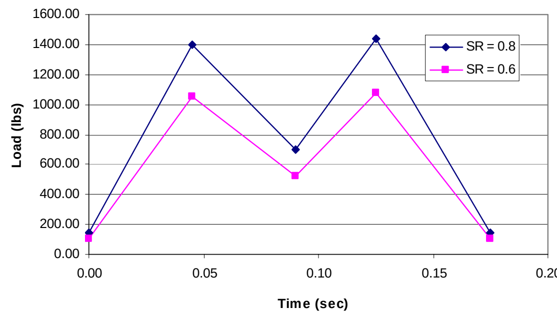

Tandem Axle

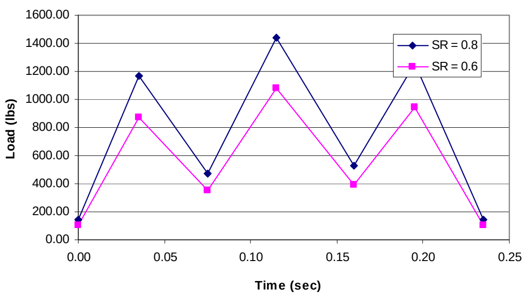

Tridem Axle

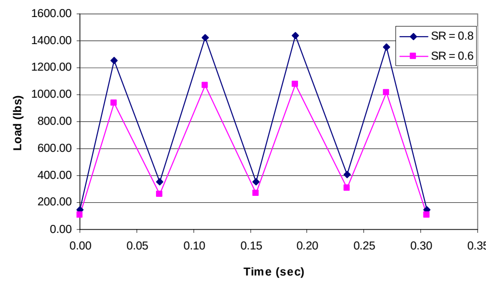

Quad Axle `

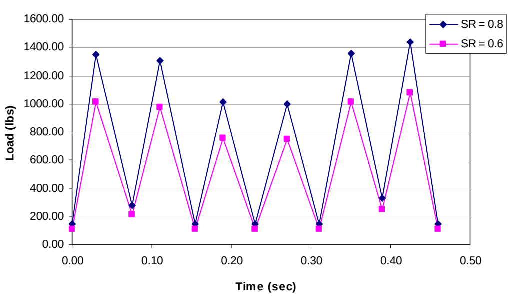

Six Axle

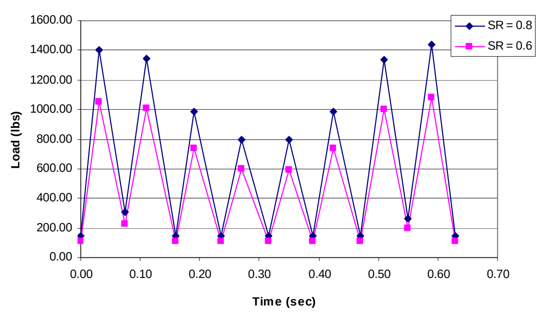

Eight Axle

Figure 2.9 Load input into MTS testing machine for Batch 2

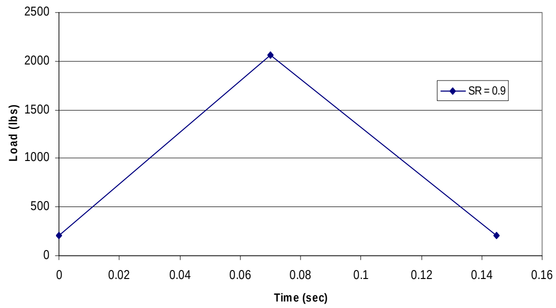

Single Axle

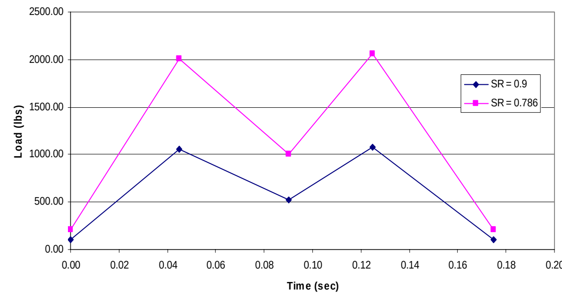

Tandem Axle

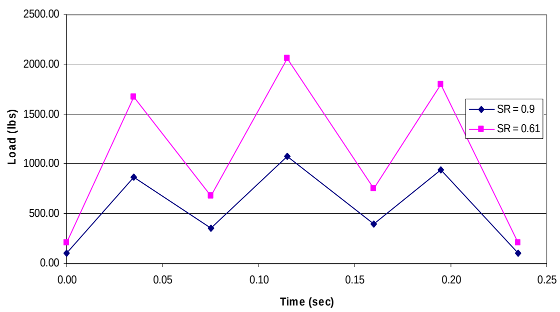

Tridem Axle

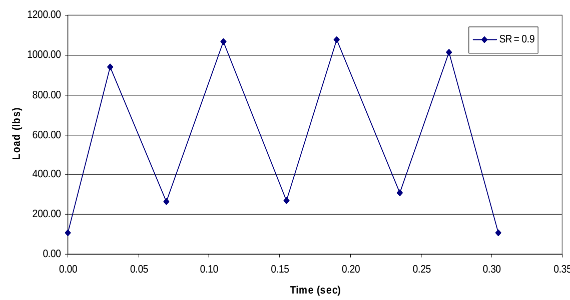

Quad Axle

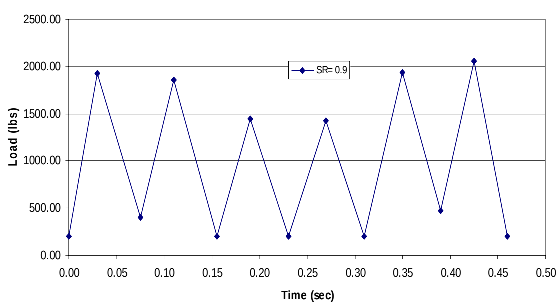

Six Axle

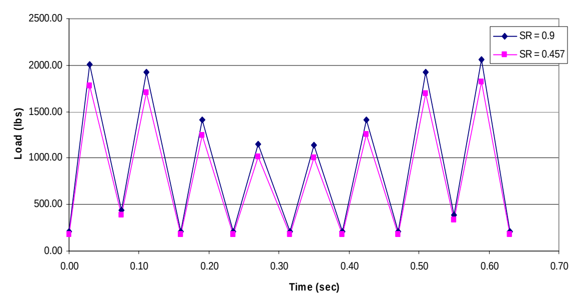

Eight Axle

Figure 2.10 Load input into MTS testing machine for Batch 3

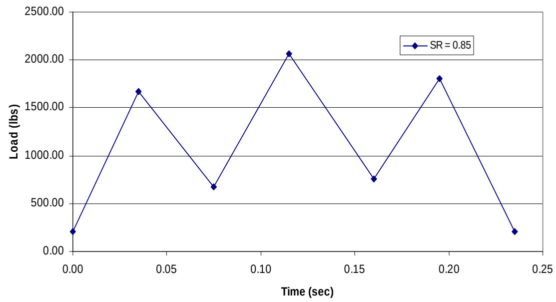

Tridem Axle

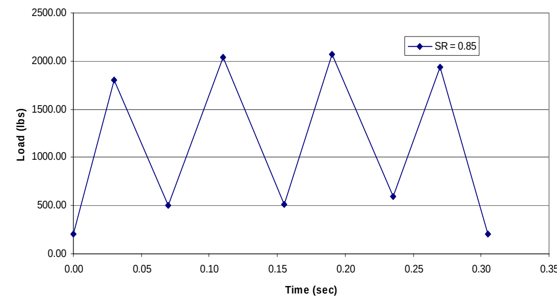

Quad Axle

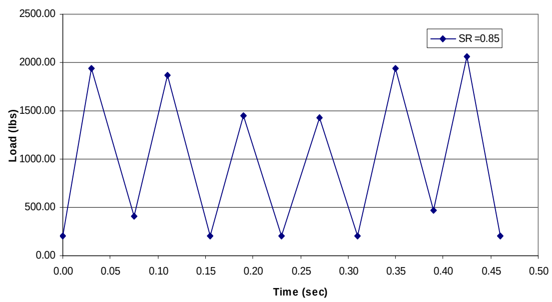

Six Axle

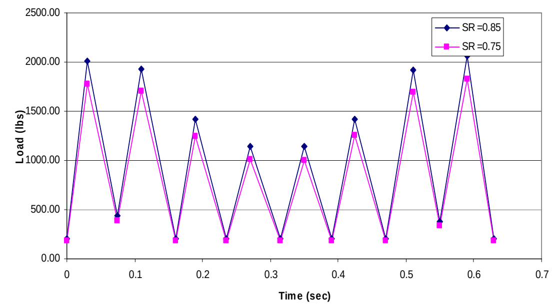

Eight Axle

Figure 2.11 Load input into MTS testing machine for Batch 4

These test values are interrelated and statistical correlations between the various tests have been developed, allowing different test values to be estimated. The laboratory tests other than fatigue testing comprise of the following tests.

(a) Compressive Strength: The compressive strength (f'_c) of concrete is considered a universal measure of concrete quality and durability. A high compressive strength is an indicator of high quality concrete. The concrete compressive strength is a function of aggregate size, aggregate type, coarse aggregate shape, cement composition and additives incorporated in the concrete as well as the compositional factors mentioned above (Neville 1996).

The modulus of rupture (f_r), tensile strength (f_t) and the modulus of elasticity (E_c) can be related to compressive strength by the following empirical equations:

$$f_r = 0.6\sqrt{w \times f_c'} \tag{2.10}$$

$$f_t = \tfrac{1}{3}\sqrt{w \times f_c'} \tag{2.11}$$

$$E_c = 33 \times w^{3/2}\sqrt{f_c'} \tag{2.12}$$

Where,

w = unit weight of concrete, pcf; and

f_c' = compressive strength, psi.

The compressive strength of concrete is related to a combined effect of time and temperature, which can be defined as maturity. Concrete maturity is a summation of the integrals of time-temperature of the concrete above a selected datum temperature. The datum temperature for maturity may be defined as the curing temperature at which the strength of the concrete remains constant regardless of age. Therefore, the maturity is calculated as the time of curing, in hours, multiplied by the temperature, in degrees, above the datum temperature. Experimental data indicates that the datum temperature equals to 11°F (-11°C). Figure 2.12 shows a typical age, curing temperature and strength relationship. It should be noted that the 28-days strength, which is normally used in concrete pavement design, may be slightly lower than the strength at later age. Keeping in consideration the testing time for fatigue testing, for this research all the beams were cured in the curing room for at least 90-days. It is assumed that at this age the strength gain is negligible during the fatigue testing of these beams, which took a few more months. Nonetheless, strength gain was monitored during the entire testing program. Figures 2.13 through 2.16 show the compressive strength gain for all the four batches of concrete beams.

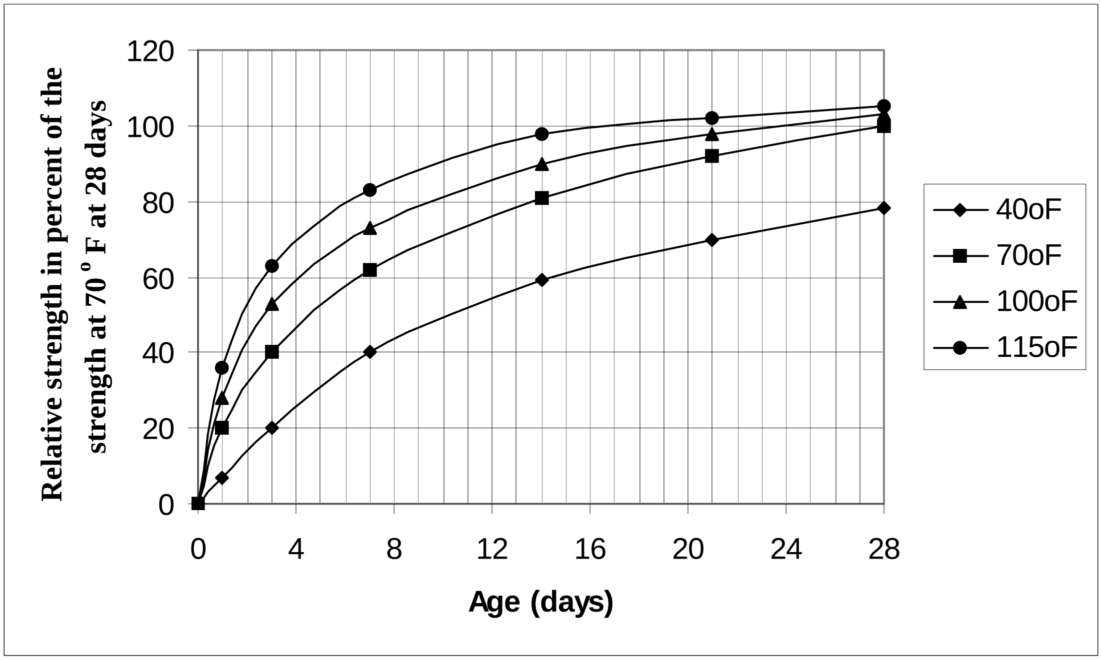

Figure 2.12 Effect of casting and curing temperature on the strength of concrete (Neville 1996)

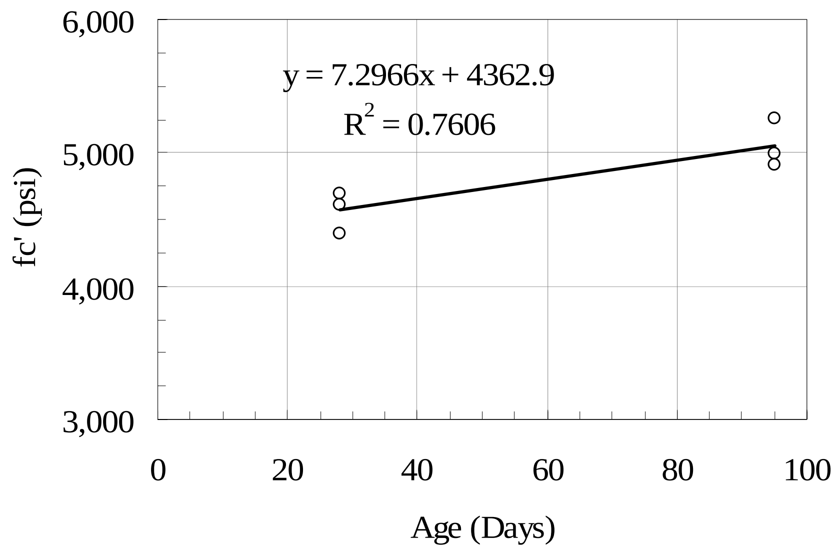

Figure 2.13 Compressive Strength Gain (28 to 95 Day) derived from flexural testing— Batch 1

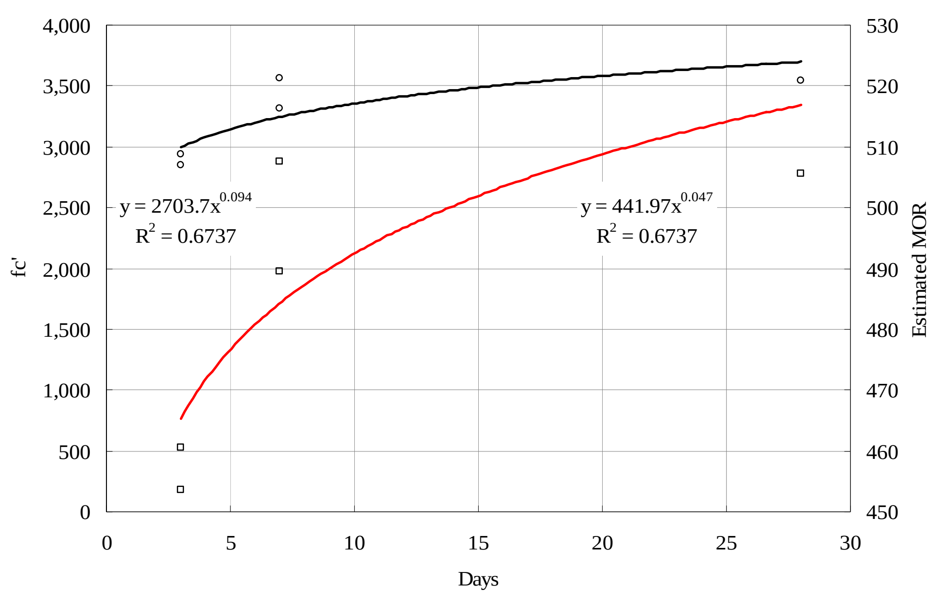

Figure 2.14 Compressive Strength Gain (3 to 28 Day) — Batch 2

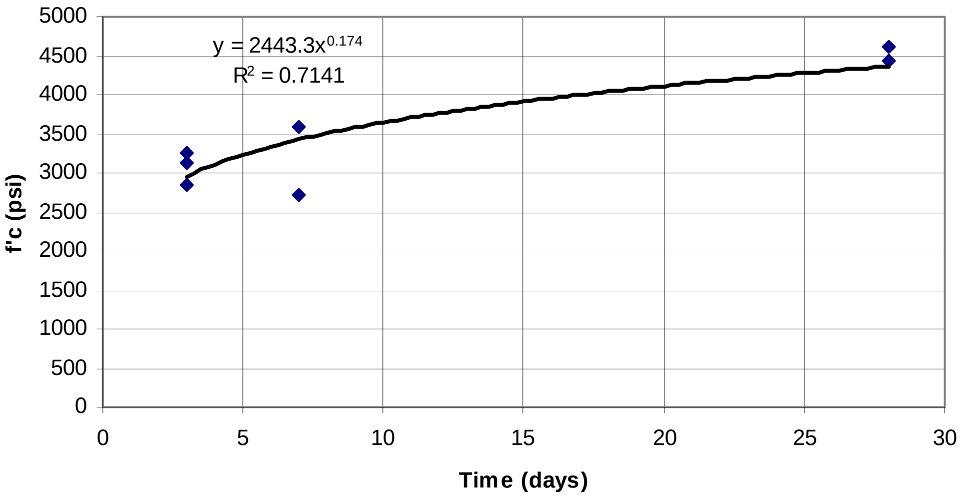

Figure 2.15 Compressive Strength Gain (3 to 28 Day) — Batch 3

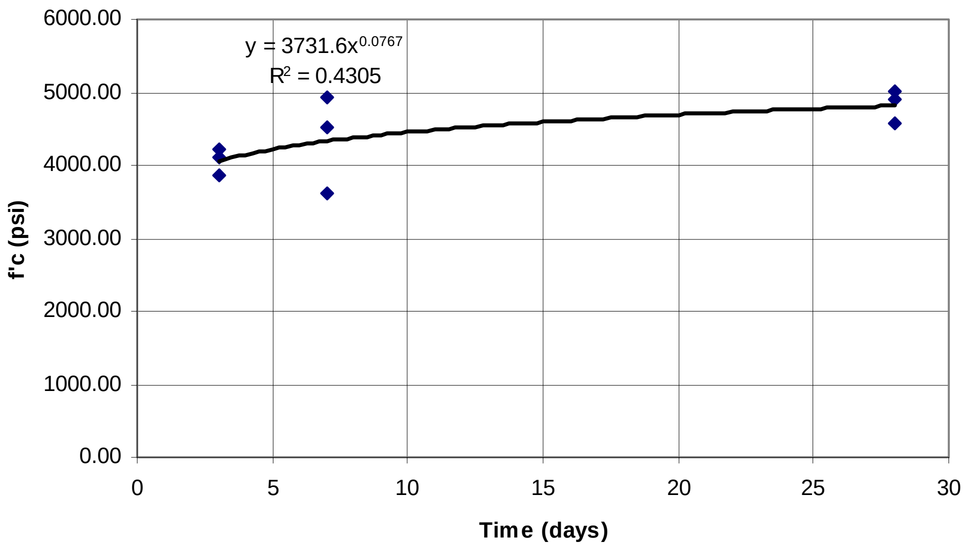

Figure 2.16 Compressive Strength Gain (3 to 28 Day) — Batch 4

(b) Tensile Strength: Tensile strength is not normally measured directly. A flexure or indirect tension test is normally conducted. The indirect (splitting) tensile test is most often used to determine tensile strength of concrete. The modulus of elasticity can be determined from these tensile tests. The indirect tensile strength is given by equation 2.13.

$$f_t' = \frac{2P}{\pi D t} \tag{2.13}$$

Where,

f_t' = indirect tensile strength, psi;
P = applied load, pounds;
D = diameter, inches; and
t = thickness, inches.

The indirect tensile strength and the unconfined compressive strength of concrete have been correlated. It has been shown that for concrete pavement design purposes, the tensile strength can be taken as 0.40 to 0.50 f_r, where f_r is the modulus of rupture; or

$$f_t' = 0.24 \times 0.3\sqrt{w \times f_c'} \tag{2.14}$$

where all variables are as defined before.

(c) Modulus of Rupture (Flexural Strength): For pavement design purposes, the allowable stress in a rigid pavement is calculated by using the modulus of rupture, which is the extreme fiber stress under the breaking load (maximum load). The modulus of rupture is given by the following equation.

$$f_r = \frac{M \times c}{I} \tag{2.15}$$

Where,

f_r = modulus of rupture, psi;
M = bending moment at breaking load, lb-in;
c = one half the beam depth, inches; and
I = moment of inertia, $inches^4$.

The flexural test is conducted on a beam using a third point loading. The modulus of rupture determined by any other configuration will not be the same as that from the third point loading, and suitable correlations must be developed if another test is to be used. Such a correlation would be the relationship between modulus of rupture and indirect tensile strength. The 1986 AASHTO Design Guide requires that the average modulus of rupture be used rather than the commonly used working stress.

(d) Modulus of Elasticity: The rigidity of the pavement slab and its ability to distribute loads is represented by its modulus of elasticity (E_c). The rigid pavement deflections, curvature, stresses and strains are directly influenced by the modulus of elasticity of the concrete layers.

The tensile stresses and strains developed in the concrete slab are also functions of the modulus of elasticity. The modulus of elasticity will become more important as the mechanistic empirical design procedures gain more popularity. The elastic modulus of the concrete is a major input into the newer finite element programs for accurate stress and strain calculations. The modulus of elasticity can be approximated from the modulus of rupture data as:

$$f_r = 43.5\frac{E_c}{10^6} + 488.5 \tag{2.16}$$

Where,

f_r = modulus of rupture, psi; and
E_c = modulus of elasticity of PCC, psi.

2.4.1 Casting of Beams

After deciding the beam dimensions, four separate batches were cast (Table 2.3). Each batch consisted of 72 beams and 20 cylinders. Figures 17 through 19 show the preparation of beam formwork, and casting and finishing of the beams. Figure 20 shows the concrete cylinders for compressive strength testing. For each batch, several beams were used for the Modulus of Rupture (MOR) and the rest were used for fatigue testing.

Table 2.3 Concrete casting dates

	Cast Dates
Batch 1	7/1/2005
Batch 2	10/17/2005
Batch 3	5/19/2006
Batch 4	11/13/2006

2.4.2 Modulus of Rupture (Flexural Strength)

The flexural test was conducted on a beam using a third point loading for a conventional 12-inch long beam; also a similar test using the MTS machine was done for the larger (4x4x24 in) ‘fatigue’ beam using a ramp load. Figures 2.21 through 2.25 present the summary of flexural strength (modulus of rupture) for four PCC concrete batches. Figures 2.26 through 2.30 show the load-deformation curves for PCC fatigue beams used to determine the failure loads.

(a) The wooden formwork for casting 72 beams simultaneously

(b) Oiling of the formwork one day before pouring concrete

Figure 2.17 Preparation of beam formwork for casting (July 21, 2005)

(a) Casting of beams

(b) Finished beams

Figure 2.18 Casting and finishing of beams (July 22, 2005)

(a) De-molded beams

(a) De-molded beams with numbering

Figure 2.19 De-molding and numbering of beams before transfer to curing room (July 26, 2005)

(a) De-molded 4 x 8 inch cylinders with numbering

(b) De-molded 4 x 8 inch 15 cylinders

Figure 2.20 De-molded cylinder for compressive strength (July 27, 2005)

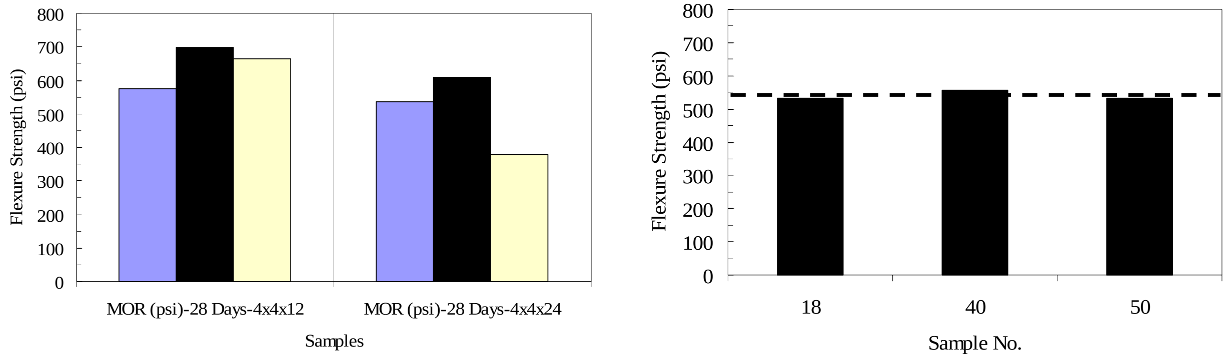

(a) Flexural Strength at 28 Days

(b) Flexural Strength at 95 Days

Figure 2.21 Effect of Beam Size on Flexural Strength (28 to 95 Day) — Batch 1

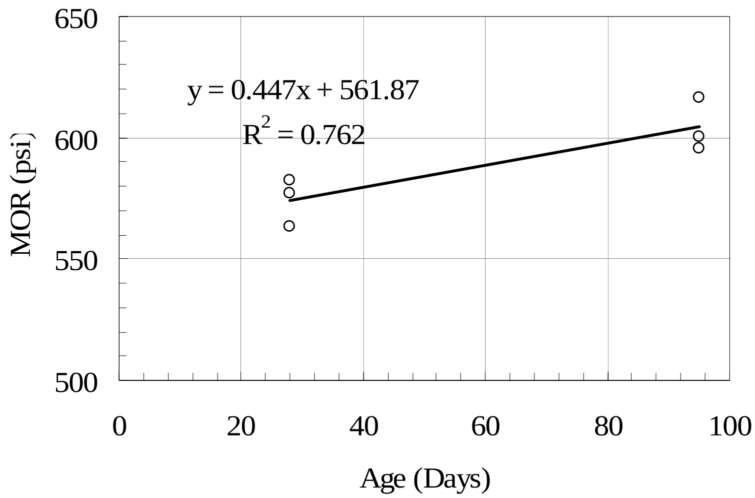

Figure 2.22 Flexure Strength Gain (28 to 95 Day) — Batch 1

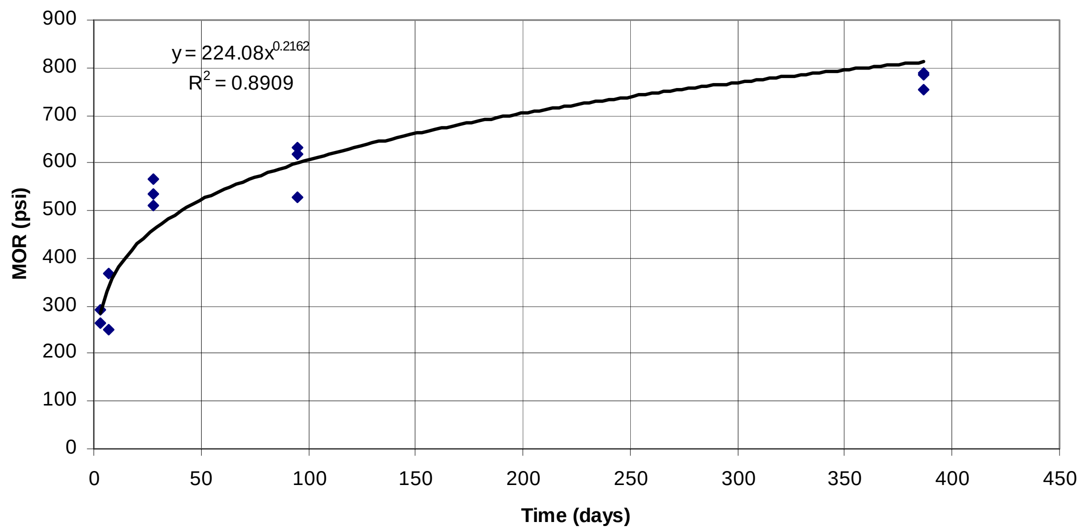

Figure 2.23 Flexure Strength Gain (3 to 387 Day) — Batch 2

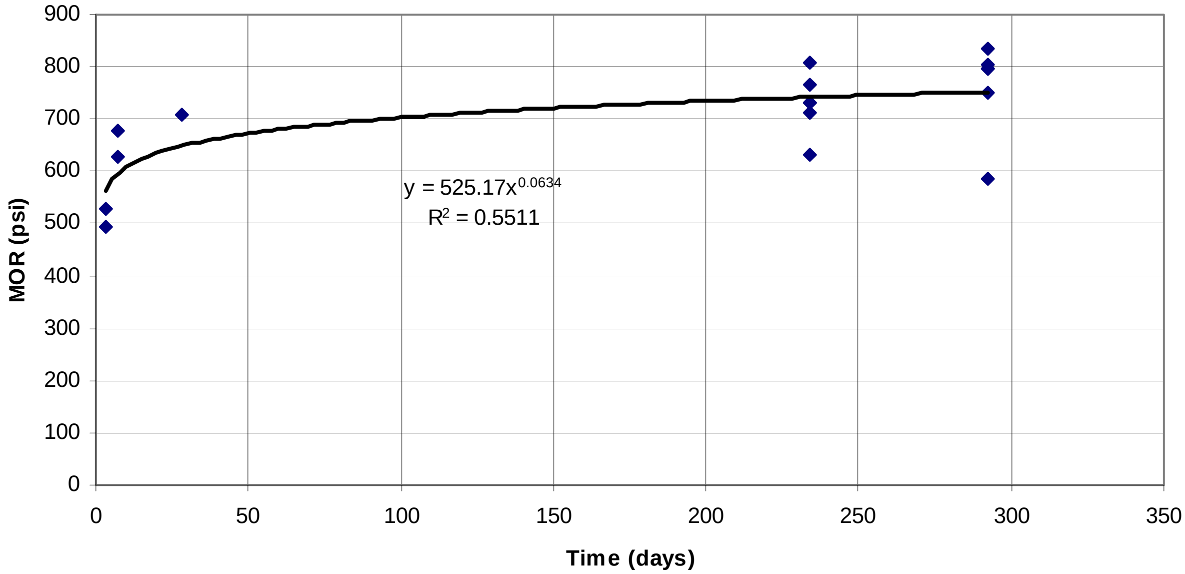

Figure 2.24 Flexure Strength Gain (3 to 292 Day) — Batch 3

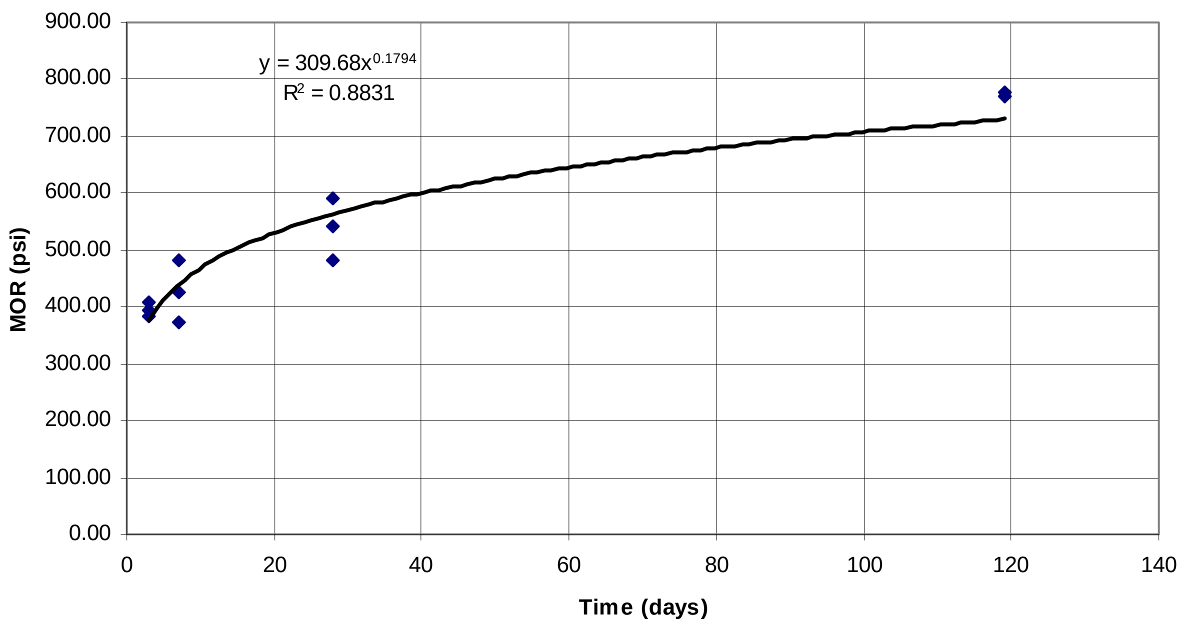

Figure 2.25 Flexure Strength Gain (3 to 292 Day) — Batch 4

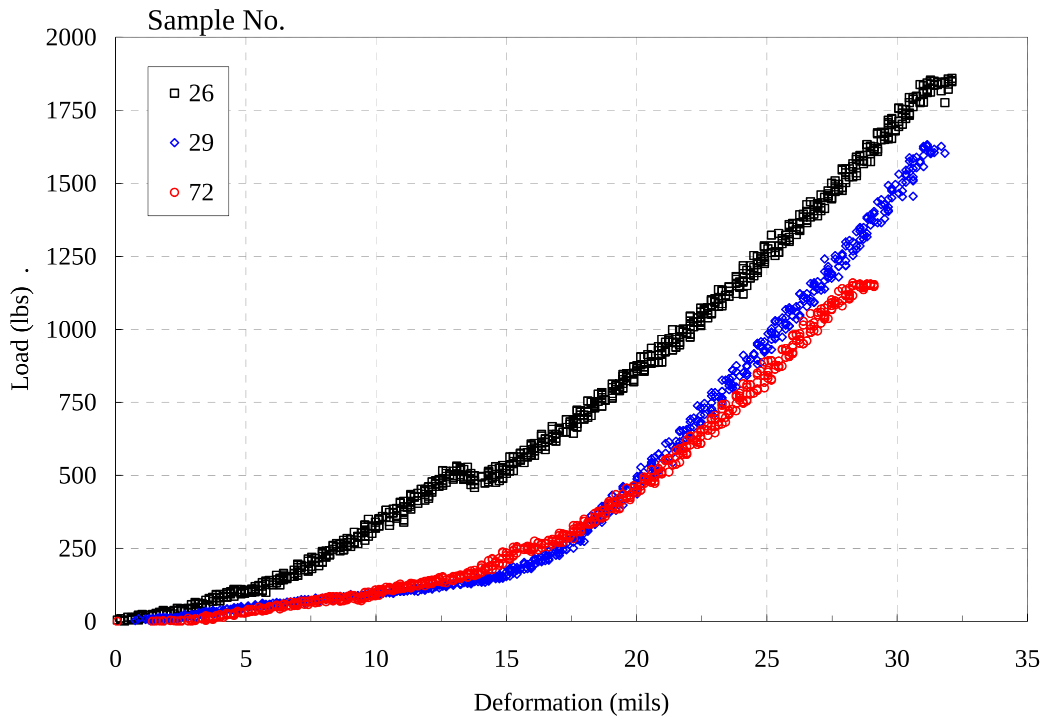

Figure 2.26 Load-Deformation Curves for Three Beam Samples (28 Day) — Batch 1

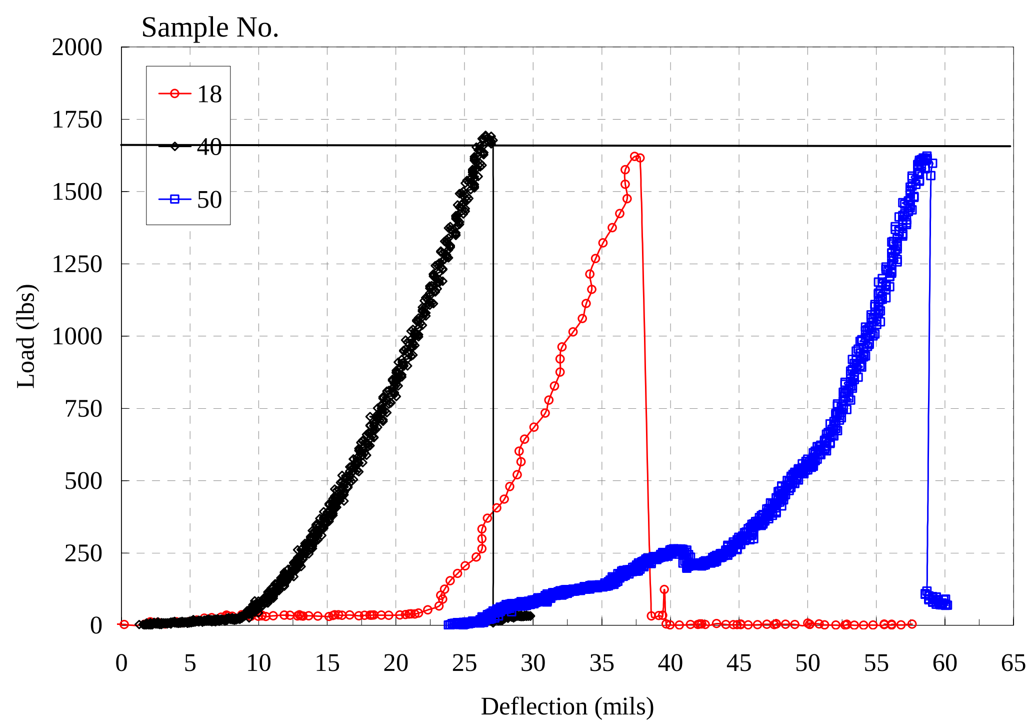

Figure 2.27 Load-Deformation Curves for Three Beam Samples (95 Day) — Batch 1

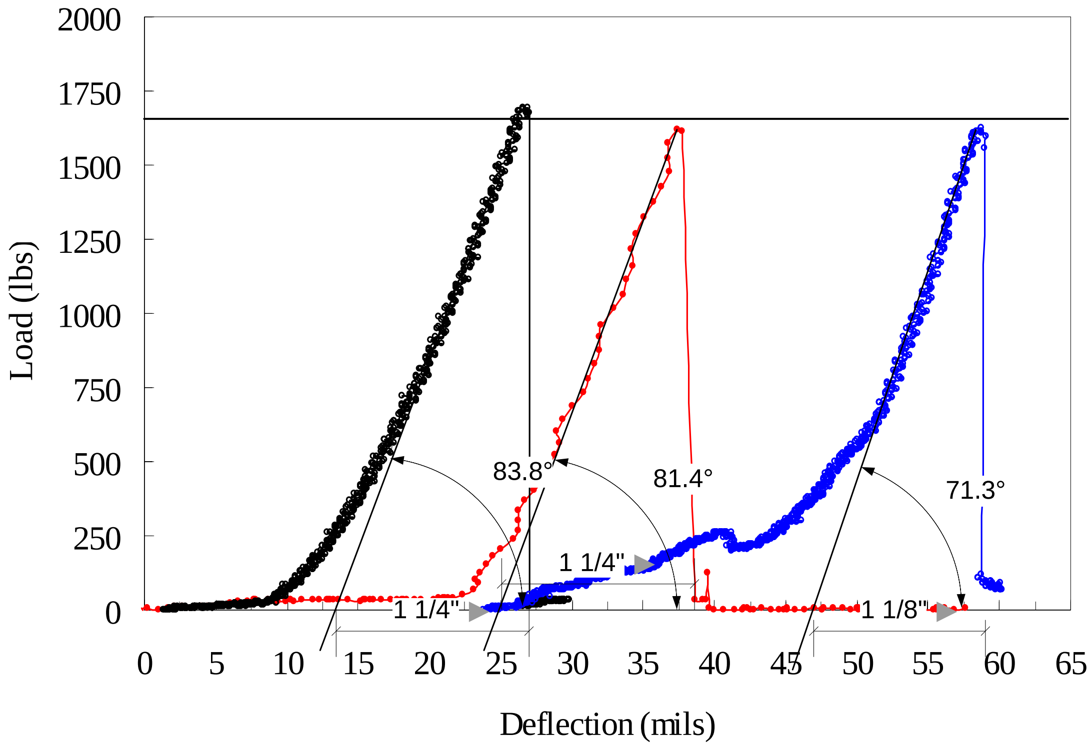

Figure 2.28 Load-Deformation Curves Analysis (95 Day) — Batch 1

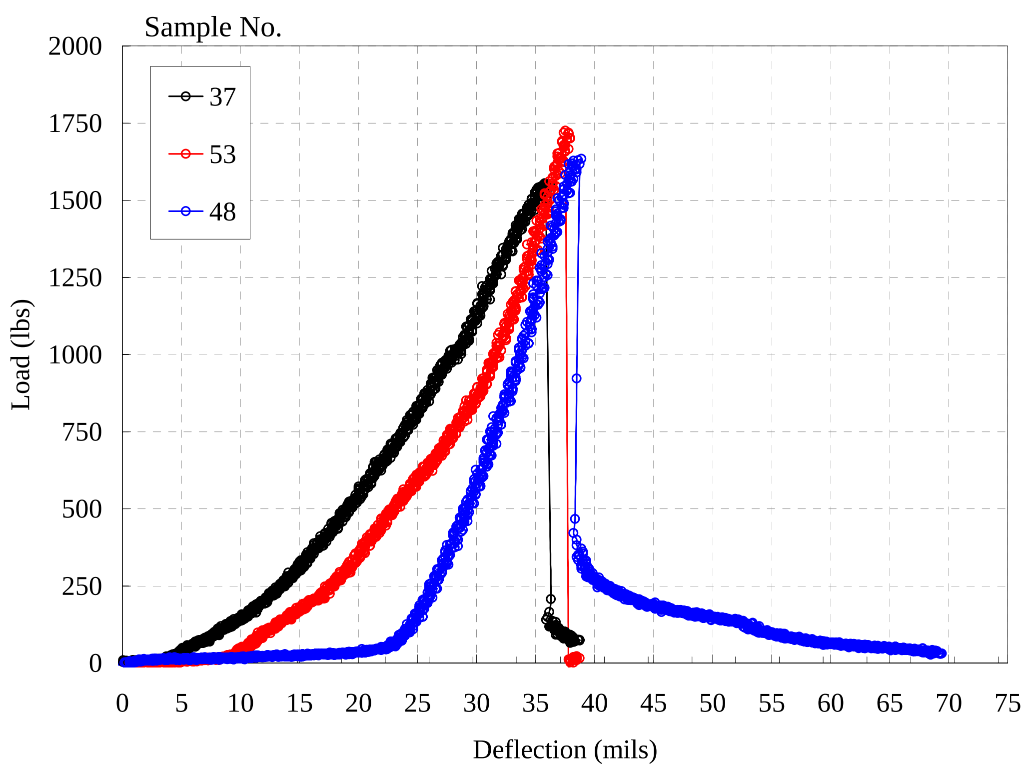

Figure 2.29 Load-Deformation Curves for Three Beam Samples (28 Day) — Batch 2

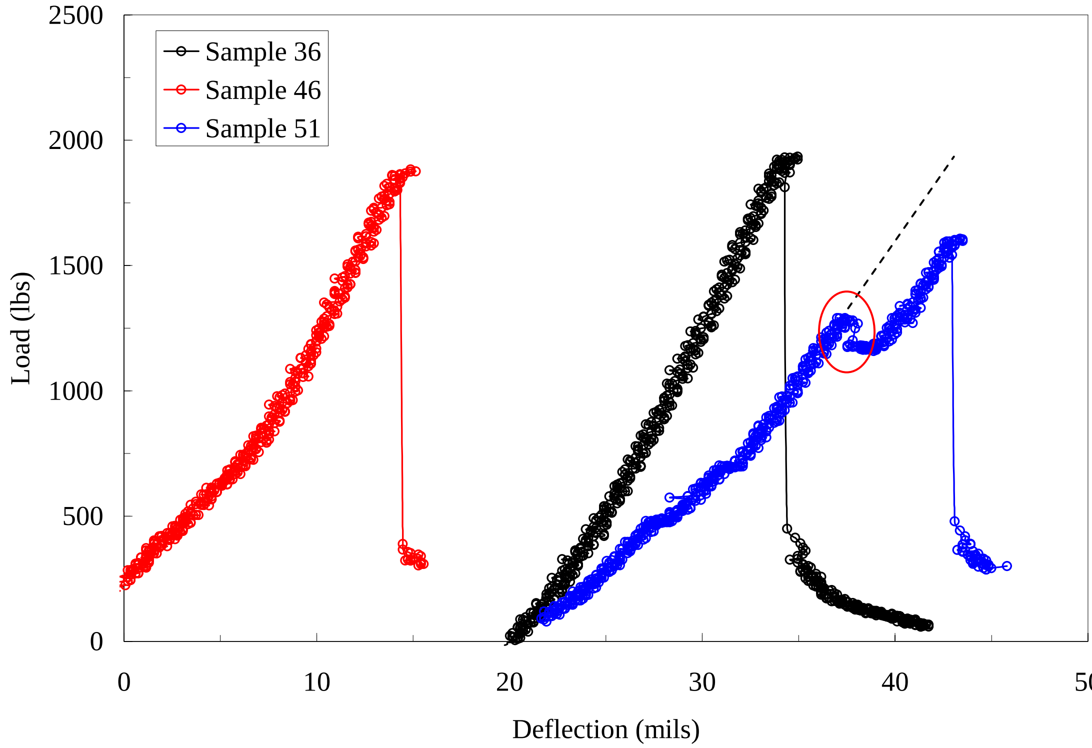

Figure 2.30 Load-Deformation Curves for Three Beam Samples (95 Day) — Batch 2

2.4.3 Strength Adjustment due to Age

Concrete strength increases with time at a decreasing rate, with the highest strength gain occurring in its early life up 28 days. Figure 2.31 shows typical strength gain of concrete for different curing conditions. The figure shows that if the concrete is stored in air after the initial curing period, the strength will increase over a period of about 14 days, then stabilizes and remains fairly constant over its life. However, if the concrete is continuously moist cured, the strength gain continues even beyond 90 days, with strength linearly increasing with time. In our case, the beams were kept in the curing room throughout the experiment. Fatigue testing was done after 90 days, extending into about a year or so. Therefore there was a need to estimate the strength of each beam at the time of fatigue testing. Because strength gain is linear after 90 days, strength tests were done just before fatigue testing started and just after it ended, and strength was estimated by linearly interpolating the strength value, knowing the age at which each specimen was tested for fatigue. Tables 2.4 and 2.5 show a summary of the strength gain (per day) for batches 2 and 3. The beams in batch 4 were tested very quickly (high stress ratio) so the strength gain observed before and after fatigue testing was insignificant. The stress ratios were modified according to the amount of strength gain observed in the concrete. Batch 2 showed a greater strength gain than batch 3.

Table 2.4 Summary of strength gain for batch 2

Day	Load @ Failure (lbs)	Strength per day (lbs)	Stress (psi)	Strength per day (psi)
90	1800	1.88	590.6	0.62
387	2360		774.4	

Table 2.5 Summary of strength gain for batch 3

Day	Load @ Failure (lbs)	Strength per day (lbs)	Stress (psi)	Strength per day (psi)
234	2284.4	2.46	749.6	0.81
292	2427.2		796.4	

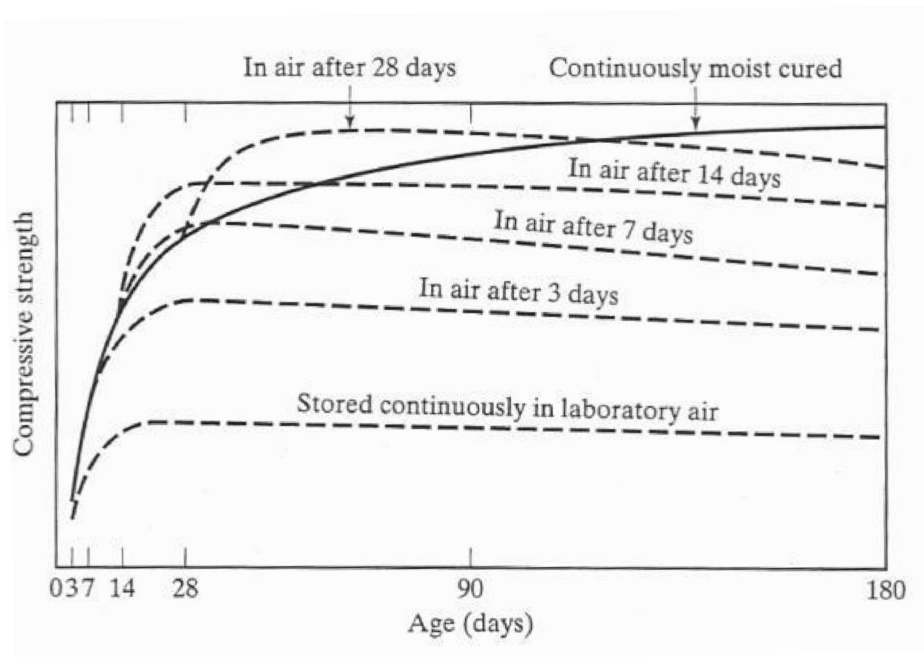

Figure 2.31 Typical gain in compressive strength with time

2.5 RESULTS AND DISCUSSION

All 126 beams were tested and their corresponding test results analyzed. The fatigue test for each axle configuration ran until the complete failure of the beam; i.e., until the middle portion of the beam is completely fractured.

2.5.1 Univariate Regression

The S-N curves for single, tandem, tridem, quad, six and eight axles are shown in Figure 2.32. At first glance, the slopes of the S-N curves for each axle type appear to be different from one another, with six and eight axles having the steepest slopes. However, after a statistical analysis of the regression models was completed, it was determined that the slopes for the given axles are not significantly different from each other. This is caused by the large error within each of the models. Table 2.6 shows the detailed regression analysis for each of the axle types. The last two columns of Table 2.6 show the upper and lower 95 percent confidence limits of the slope. For each axle type, the upper and lower confidence limits intersect one another, thus making the difference in the slope values statistically insignificant. This means that the slopes for each axle type are essentially the same. Thus, the data from different axle types can be combined and interpreted using a multiple linear regression.

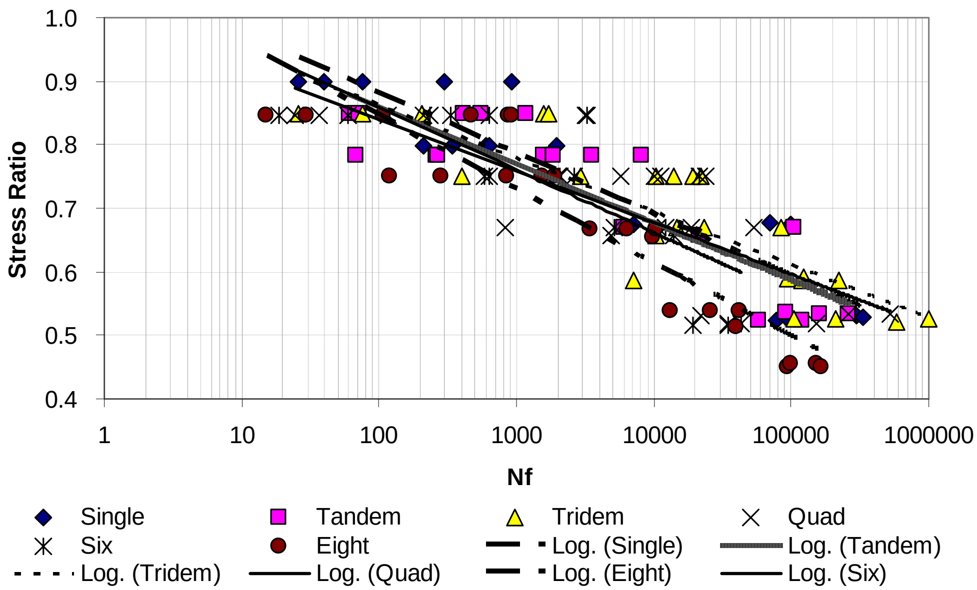

Figure 2.32 Fatigue curves for various axle configurations

Table 2.6 Results from regression analysis

Axle Type		Regression Equation	DF	R^2	Type	SE	95 % Slope Lower Confidence Limit	95 % Slope Upper Confidence Limit
Single Axle		SR = -0.0416LogNf + 1.0733	16	0.86	Intercept	0.0370	0.9949	1.1518
					Slope	0.0043	-0.0324	-0.0508
Tandem Axle		SR = -0.0396LogNf + 1.0432	19	0.79	Intercept	0.04222	0.9548	1.1315
					Slope	0.004882	-0.0293	-0.0498
Tridem Axle		SR = -0.0363LogNf + 1.0290	23	0.76	Intercept	0.04343	0.9391	1.1188
					Slope	0.004404	-0.0271	-0.0454
Quad Axle		SR = -0.0353LogNf + 1.0028	17	0.67	Intercept	0.05719	0.8821	1.1234
					Slope	0.006264	-0.0221	-0.0485
Six Axle		SR = -0.0427LogNf + 1.0554	18	0.66	Intercept	0.06002	0.9293	1.1815
					Slope	0.00751	-0.0270	-0.0585
Eight Axle		SR = -0.0500LogNf + 1.0745	22	0.85	Intercept	0.03929	0.9930	1.1560
					Slope	0.004619	-0.0404	-0.0596

2.5.1.1 Comparison to previous research

The single axle regression line was compared to the regression lines from previous fatigue experiments to see if similar results were produced. The regression line produced from the current research shows a reasonably similar trend to those from other experiments, as shown in Figure 2.33.

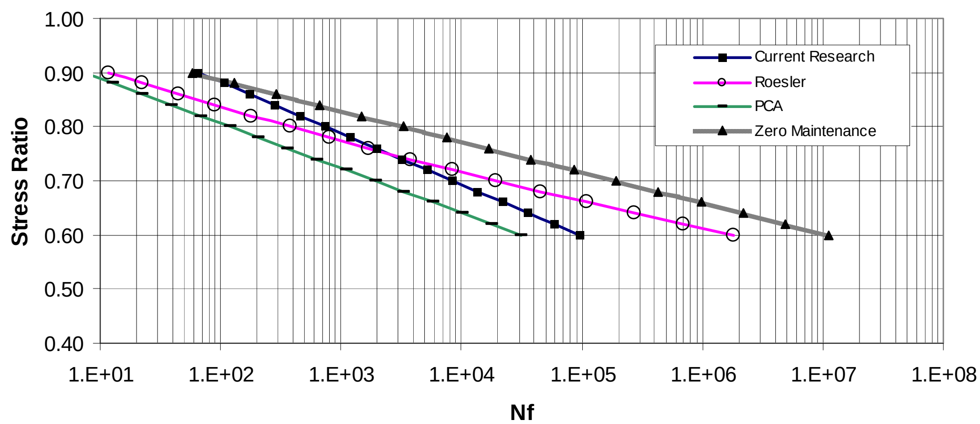

Figure 2.33 Comparison of S-N curve for single axles to previously published curves

2.5.1.2 Axle factors from univariate analysis

The number of cycles to failure (N_f) was calculated using the individual regression equation corresponding to each axle configuration. Axle factors (*AF*) were then calculated for each axle configuration using equation 2.17 in order to quantify the relative damage from the different configurations. For example, the tandem axle factors were calculated by dividing the number of cycles to failure for each single axle over the number of cycles to failure for a tandem axle.

$$AF = \frac{\text{Damage of the axle group}}{\text{Damage of the single axle}} = \frac{\dfrac{1}{N_{f \text{ axle group}}}}{\dfrac{1}{N_{f \text{ single axle}}}} = \frac{N_{f \text{ single axle}}}{N_{f \text{ axle group}}} \tag{2.17}$$

Figure 2.34 shows the variation of the AF with respect to stress ratio and axle configuration. The figure shows that the six- and eight- axle groups are behaving differently from the rest of the axle configurations (The AF's are greater). The results also show that as the stress ratio increases, the axle factors tend to decrease for the larger axle groups. The effect of time (longevity of the pulse) might have a greater effect on the fatigue life at lower stress levels, thus increasing the axle factors. However, the trend is much weaker for the smaller axle groups, making the observation tentative.

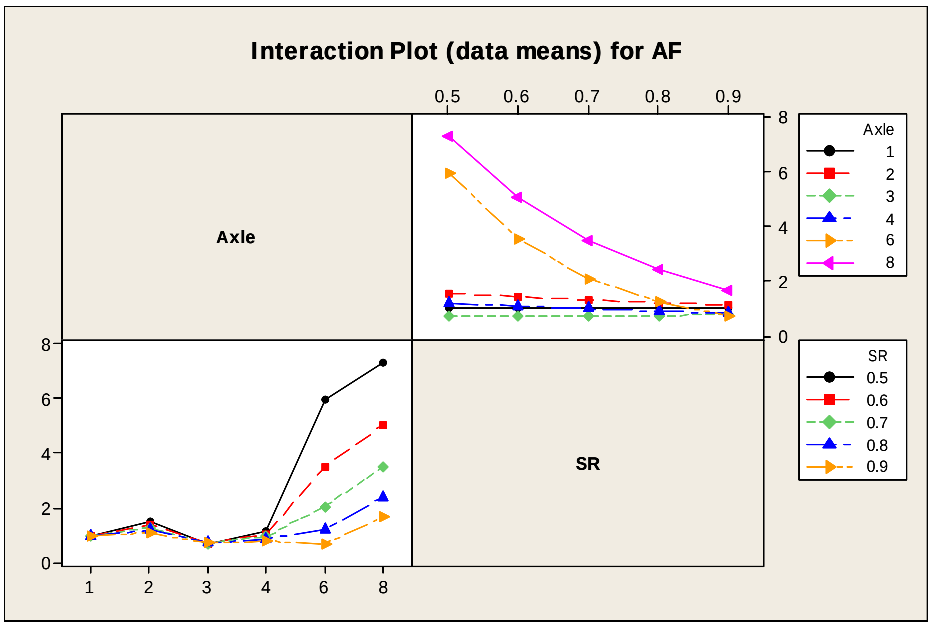

Figure 2.34 Interaction plot for axle factors in terms of axle configuration and stress ratio

2.5.2 Multiple Linear Regression

A multiple linear regression analysis was also conducted to further investigate the behavior between stress ratio and axle types in the hope that the model can provide a more conclusive answer than the individual S-N curves. One of the advantages of using a multiple linear regression equation is that all of the data from the experiments can be used at once, which subsequently increases the degrees of freedom in the model, and ultimately decreases the margin of error.

Since axle type is not a continuous variable, a new variable needed to be created for the regression analysis. A normalized stress impulse, SI, was used for this purpose. SI is a continuous quantity that represents a specific axle type. The equation for SI is as follows:

$$SI = \frac{IMPULSE}{PEAKSTRESS} \quad \text{(sec)} \tag{2.18}$$

The impulse is the area under the stress pulse and the peak stress corresponds to the largest stress within a given pulse. The SI quantity is constant for a given axle type, regardless of the applied stress. Thus, it is a good indicator of axle type. Figure 2.35 shows the relationship between stress impulse and the number of axles.

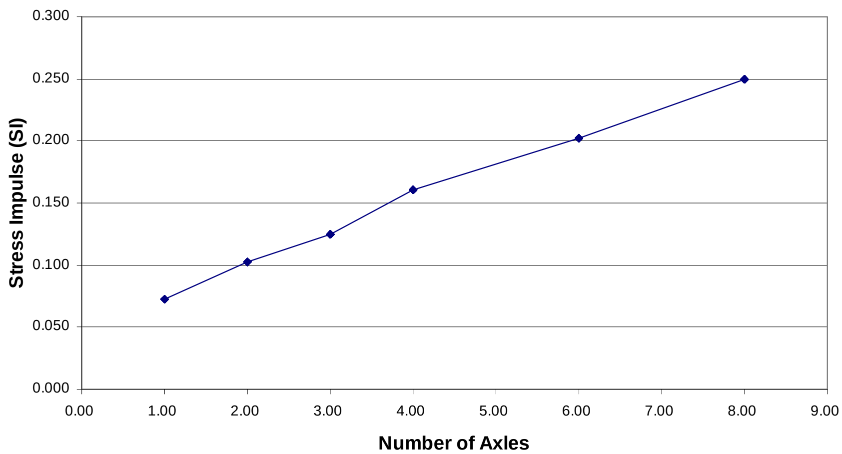

Figure 2.35 Stress Impulse vs. Number of Axles

Also, the initial elastic modulus, E_o, for each beam was added as a variable to account for specimen-to-specimen material variability. The initial elastic modulus was calculated through beam theory using the initial measured displacement over the first cycles of the fatigue test. Table 2.7 shows the results from the multiple linear regression analysis. The analysis shows that SR, SI and E_o are all statistically significant variables ($p < 0.05$), with fatigue life increasing with decreasing stress ratio, increasing modulus and decreasing stress impulse (i.e., decreasing axle number).

Table 2.7 Multiple Linear Regression Analysis*

Predictor	Coefficient	SE	t	p
Constant	21.222	1.112	19.08	0.000
SR	-20.838	1.355	-15.38	0.000
SI	-6.970	1.722	-4.05	0.000
Initial Elastic Modulus	1.84E-06	9.20E-07	2.01	0.047

* $R^2 = 0.772$ Adjusted $R^2 = 0.766$

2.5.2.1 Axle factors from multiple linear regression

Axle factors (AF) were defined as the ratio of damage ($1/N_f$) due to the axle group to that due to a single axle, with N_f being the fatigue life obtained from the results of the multiple regression analysis for a constant SR and E_o (Table 2.7). This was done first by using the same peak stress value for all axle groups (laboratory condition). Then, recognizing that the peak longitudinal stress decreases with increasing number of axles because of the interaction between individual axles within an axle group (Figure 2.36) the AFs were recalculated after accounting for this stress reduction. Figure 2.37 shows the AFs for the various axle configurations for the same peak stress value and accounting for the stress reduction.

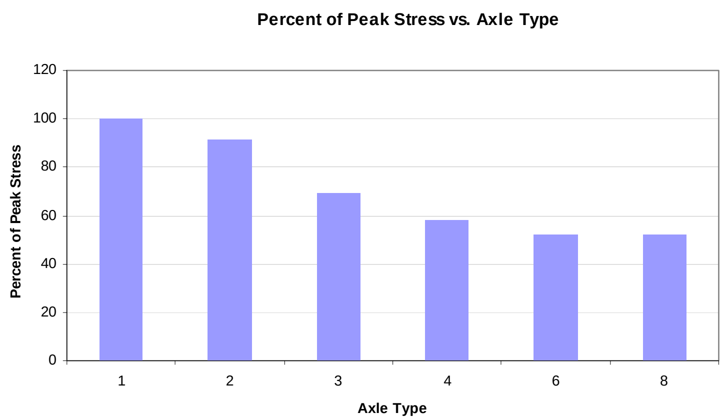

Figure 2.36 Peak stress under multiple axles expressed as a percentage of stress caused by a single axle

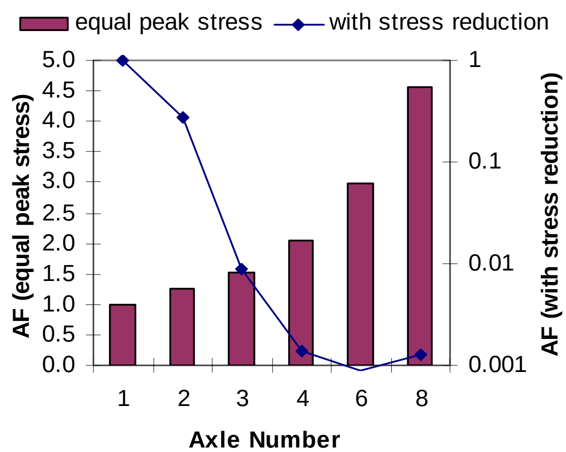

Figure 2.37 Axle factors versus axle configuration with and without stress reduction

When the peak stress is the same for all axle groups, the axle factors increase as the number of axles increases. The results are similar to those from the individual regression equations. The axle factor for the eight-axle group is approximately 4.5, which suggests that it is 4.5 times as damaging as the single axle. However, the effect of stress reduction is not present within this relationship. If one takes into account the reduction in longitudinal stress caused by stress interaction under multiple axles, as shown in Figure 2.36, the damage from multiple axles and the corresponding axle factors become much smaller. Next we compare the AF value for tandem and tridem axles with stress reduction from Figure 2.37 to those obtained from the PCA design manual. From the design example provided in the manual for a 9.5 inch slab on an untreated base, the allowable number of repetitions for a 26 kip tandem axle is 1.1×10^6, while that for a 13 kip single axle is 230,000. This leads to an axle factor for the tandem axle of 0.21 compared to 0.28 from Figure 2.37, suggesting that they are reasonably close. For the tridem axle, the example in Appendix C of the PCA manual shows an unlimited number of allowable repetitions of a 36 kip tridem for the same design. This agrees fairly well with the AF value of about 0.01 from Figure 2.37, which is close to zero.

2.5.2.2 Truck factors from laboratory AF and AASHTO LEF

This study was charged with determining the relative damage caused by multiple axles within an axle group; i.e., how much damage is caused by grouping multiple axles into one axle group. The scope of the study did not include verifying the AASHTO's "Fourth Power" damage law; i.e., we were not charged with determining how much damage is caused by increasing the load of a given axle relative to the standard 18-kip single axle. To do so would require extensive full-scale testing similar to what had been done in the original AASHO road test. Therefore, the TF's were obtained by converting multiple axle groups within each truck configuration into an equivalent number of single axles using the AF's obtained in this study, calculating the LEF of each axle group by multiplying the AF values obtained from the laboratory (Figure 2.37) with the Load Equivalency Factor (LEF) from AASHTO corresponding to the single axle at the legal load limit, and then summing the LEF of the different axle groups within a truck. This was done for different slab thicknesses. Table 2.8 summarizes the results.

Table 2.8 Truck Factors from Laboratory AF (fatigue) and AASHTO LEF

Truck	Truck No.	Total Wt. (kips)	Truck Factors - Fatigue (AASHTO Framework) Slab thickness, D (in): 8	9	10	11	12	13
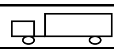	1	33.4	1.519	1.512	1.509	1.508	1.507	1.507
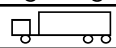	2	47.4	1.288	1.273	1.266	1.263	1.262	1.261
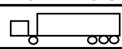	3	54.4	0.902	0.887	0.881	0.878	0.876	0.876
	4	67.4	1.046	1.028	1.021	1.017	1.016	1.015
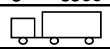	5	51.4	2.519	2.512	2.509	2.508	2.507	2.507
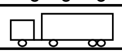	6	65.4	2.288	2.273	2.266	2.263	2.262	2.261
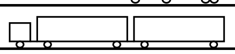	7	87.4	4.519	4.512	4.509	4.508	4.507	4.507
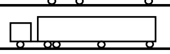	8	83.4	3.288	3.273	3.266	3.263	3.262	3.261
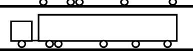	9	101.4	4.288	4.273	4.266	4.263	4.262	4.261
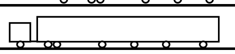	10	119.4	5.288	5.273	5.266	5.263	5.262	5.261
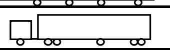	11	91.4	2.607	2.586	2.576	2.572	2.570	2.569
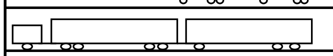	12	117.4	2.927	2.898	2.886	2.880	2.878	2.877
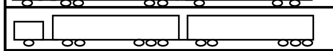	13	151.4	2.372	2.335	2.319	2.311	2.308	2.306
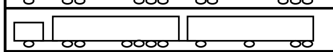	14	161.4	4.134	4.102	4.087	4.081	4.078	4.077
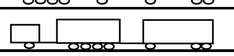	15	117.4	2.815	2.789	2.778	2.773	2.770	2.769
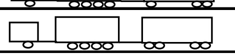	16	125.4	2.134	2.102	2.087	2.081	2.078	2.077
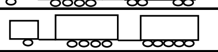	17	132.4	1.685	1.654	1.640	1.634	1.632	1.630
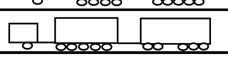	18	143.4	2.121	2.089	2.074	2.068	2.065	2.064
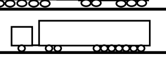	19	138.4	2.180	2.146	2.132	2.125	2.122	2.121
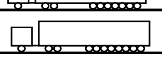	20	151.4	2.443	2.404	2.387	2.380	2.376	2.375
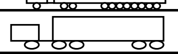	21	79.4	2.057	2.034	2.023	2.019	2.016	2.015

2.5.3 Strength Adjustment by Cube Compression Tests

Due to the large scatter in the flexural fatigue test, which may be caused by the variation between the flexural strength of the beam samples, each tested (failed) beam was sawed into four separate 4” x 4” x 4” cubes, as shown in Figure 2.38. These cubes were tested in compression to determine the compressive strength of each individual beam. Also, the distance between the crack and the cubes was recorded to study the effect of the hairline cracks developed during the cyclic test on the compressive strength of the cubes. The flexural strength was calculated through a series of regression equations that relate the concrete strength for nonstandard specimens to that of standard ones. Figures 2.39 (a) and (b) compare the flexural strength of the interior cubes (the ones close to the cracks) and exterior cubes (the ones far from the cracks). The results show that the flexural strength of interior cubes is always slightly less than the exterior cubes. This result is expected since the interior cubes are affected by the cyclic loading which generates more hairline cracks in the interior cubes than in the exterior ones. These results can be confirmed through the relation between the flexural strength versus the distance from the crack as shown in Figure 2.39(c).

Figure 2.38 Cubes sawed out of failed beams in fatigue test

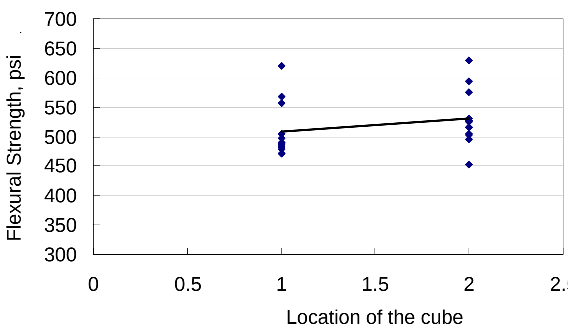

(a) Interior vs. exterior flexural strength

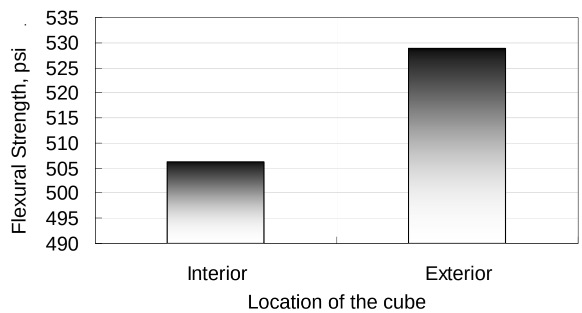

(b) Average flexural strength

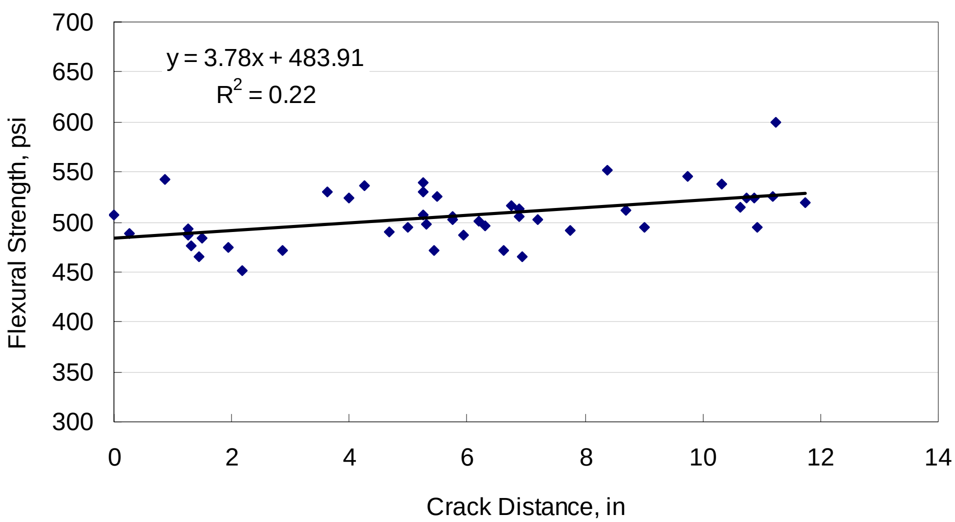

(c) Flexural strength vs. crack distance

Figure 2.39 Flexural strength of the sawed cubes

The cubes compressive strength was used to normalize the stress ratio for each individual beam instead of assuming a constant flexural strength for all beams, which is not a valid assumption. It should be noted that the compressive strength was used to avoid the errors from regression analyses that correlate the flexural strength to the compressive strength. Figures 2.40 and 2.41 show uncorrected and corrected (for strength) stress ratio versus N_f for the different axle configurations for 52% and 67% nominal stress levels. Table 2.9 shows the R^2 values for both cases. Comparing the two cases, it can be concluded that accounting for strength does not improve the relationships.

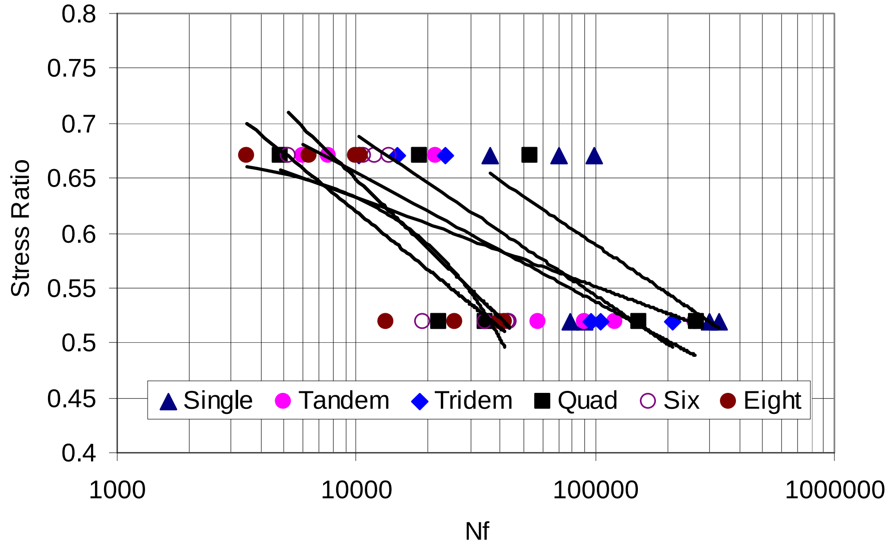

Figure 2.40 Stress ratio vs. N_f for different axle configurations

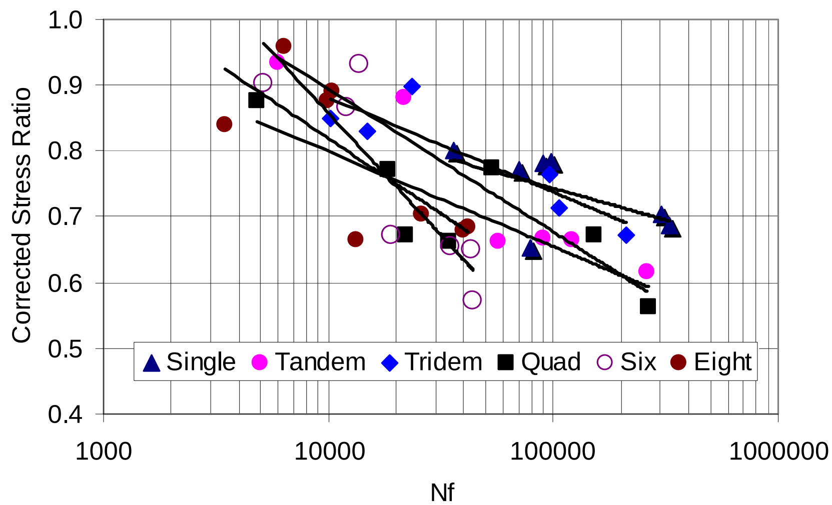

Figure 2.41 Stress ratio corrected for strength vs. N_f for different axle configurations

Table 2.9 Comparison of R^2 values with and without correction for strength

Axle Type	R^2 Original Strength	R^2 Corrected Strength
Single	0.41	0.33
Tandem	0.83	0.85
Tridem	0.90	0.79
Quad	0.35	0.68
Six	0.75	0.71
Eight	0.70	0.56
Average	0.66	0.65

2.6 DISSIPATED ENERGY CURVES

In an attempt to further understand the fatigue behavior caused by different axle types, the Dissipated Energy per cycle was calculated at specified intervals within each individual beam test. The Dissipated Energy was calculated by summing the area under the stress-strain curve under a given cycle. Figure 2.42 illustrates the behavior between the dissipated energy per cycle and log N_f.

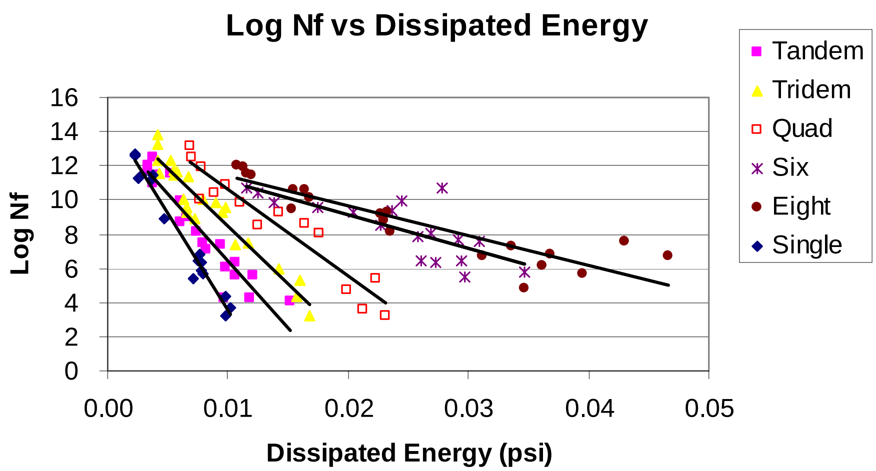

Figure 2.42 Log N_f vs. Dissipated Energy

Figure 2.42 shows that the behavior between dissipated energy and axle type is not unique. As the number of axles increases, the dissipated energy also increases. However, log N_f is not affected by this extra dissipated energy and thus there is a visible shift in the graph between axle types. The dissipated energy increases but log N_f remains relatively unaffected. In order for the behavior to be unique, the curves between axle types should collapse over one another and no visible shift should be present. Although the behavior between the dissipated energy and log N_f is not unique, the trends are much more discernable than for the individual S-N curves.

If dissipated energy is to be used, however, there must be a unique curve. Thus, several methods were used in an attempt to normalize the dissipated energies in such a way that would cause the data points to collapse over one another. The research team was not able to come up with a truly viable method to normalize the data. However, several methods have been attempted and have yielded reasonably adequate results.

2.6.1 Normalizing by SI

Figure 2.43 illustrates the behavior between dissipated energy and SI. As SI increases, the dissipated energy increases by a power of 1.3364. Given this relationship, the dissipated energy can be normalized to the SI corresponding to single axle through the following relationship:

$$CF = \frac{DE_M}{DE_1} = \left(\frac{SI_M}{SI_1}\right)^{1.3364} \qquad (2.19)$$

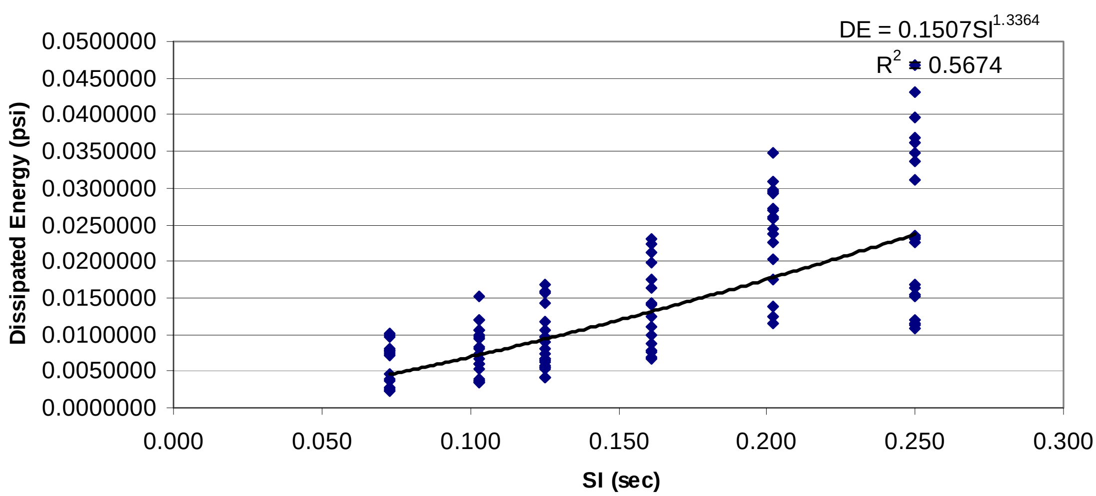

Figure 2.43 Dissipated Energy vs. SI

Figure 2.44 shows the relationship between normalized dissipated energy and log N_f. The data from the multiple axles has collapsed substantially due to the normalization of the dissipated energy. However, if the data points for different axle types are observed individually, as shown in Figure 2.45, not all curves are parallel. This contradicts the notion that the behavior, although it has collapsed, is unique. Thus, further investigation of dissipated energy must be conducted.

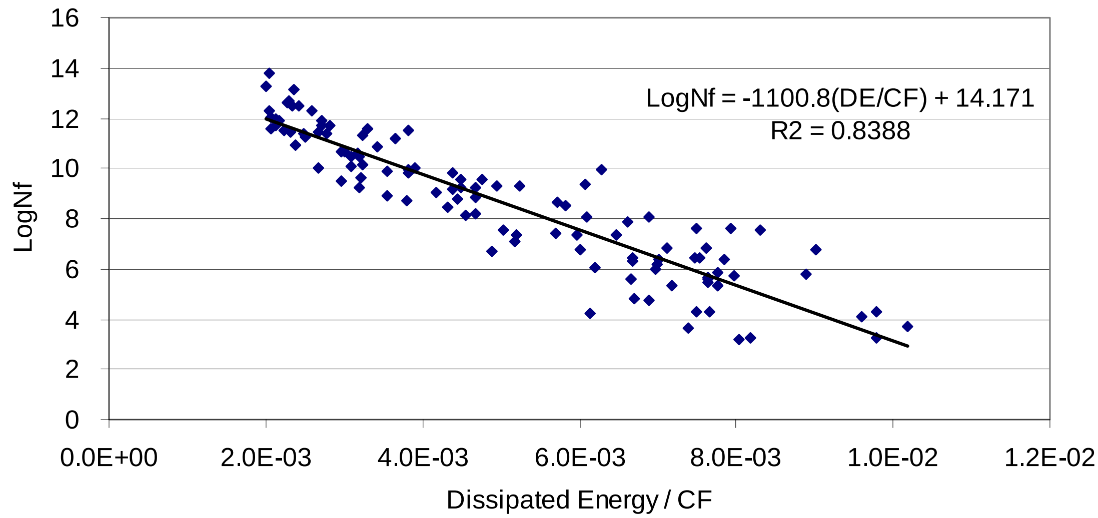

Figure 2.44 Log N_f vs. Dissipated Energy/Correction Factor

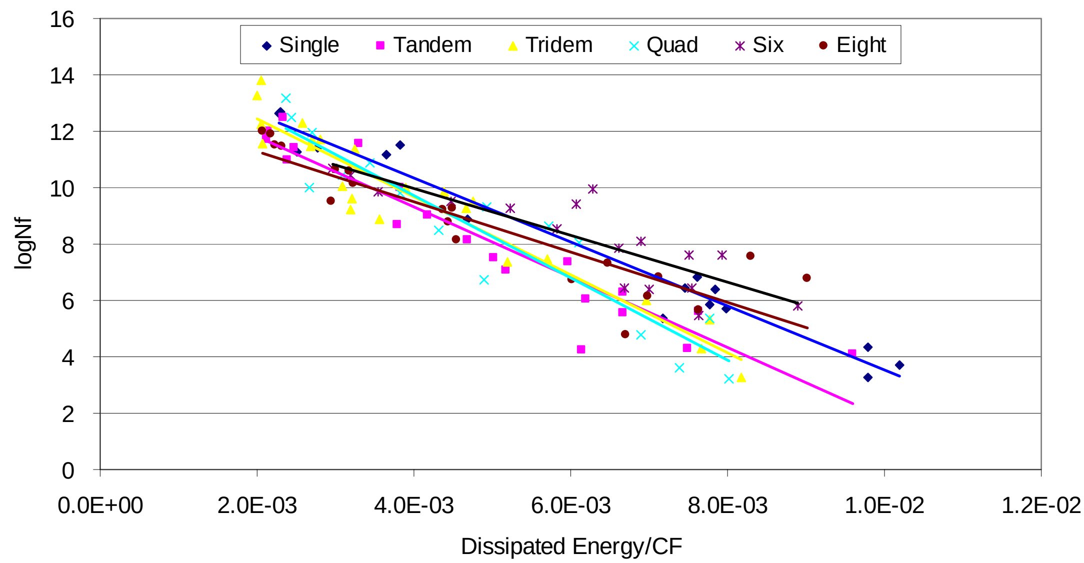

Figure 2.45 Log N_f vs. Dissipated Energy/Correction Factor for different axle types

2.7 MORTAR BEAMS

It was observed that the fatigue data was quite variable. Therefore, it was decided to try a limited fatigue experiment using mortar beams. It was our hope that because of the smaller aggregates the mix in mortar beams would be much more uniform and it might lead to more consistent results.

Two different beam dimensions were tested: 2 in x 2in x 11in and 3 in x 3 in x 11 in (Figure 2.46). Four 2 in. beams and three 3 in. beams were tested, for a total of seven beams. Each beam was tested under 85% stress ratio.

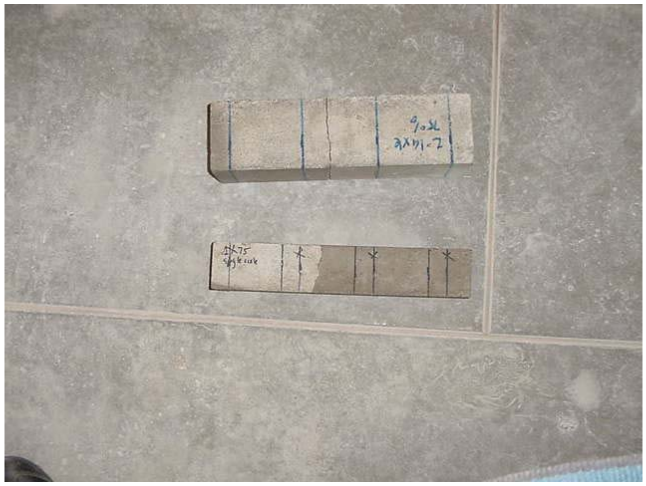

Figure 2.46 Photo of 3x3x11 and 2x2x11 Mortar Beams

2.7.1 Results

Table 2.10 shows the results for the seven tests. As shown below, there is still some variability within the test specimens. The smaller beam specimens show slightly higher variability when compared to the larger beams. However, the desired result of minimum variability was not attained. Therefore, it was decided to no longer pursue mortar beam testing.

Table 2.10. Mortar fatigue results

Specimen	Dimension	Nf	lnNf	Average	St Dev
1.00	2X2X11	707	6.56	7.14	1.83
2.00	2X2X11	4599	8.43		
3.00	2X2X11	6303	8.75		
4.00	2X2X11	122	4.80		
1.00	3X3X11	560.00	6.33	5.60	1.35
2.00	3X3X11	613.00	6.42		
3.00	3X3X11	57.00	4.04		

2.8 SUMMARY

The laboratory fatigue testing was conducted on concrete beams using the four-point bending test and cyclic loading corresponding to various axle configurations. These tests were done at various stress ratios and for a minimum of four replicates. The axle factors for the various axle groups were obtained using a multi-variate linear regression analysis taking into account the beam-to-beam variability using the elastic modulus of the individual beams, and accounting for the different axles through a continuous variable in the form of the stress impulse (SI). The results are shown in Figure 2.37.The reduction in longitudinal stresses due to the interaction between multiple axles within an axle group was obtained using the DYNASLAB computer program. The axle factors modified to account for this stress reduction are also shown in the figure.

An attempt was made to account for the variability in beam strength by normalizing the stress ratio using the compressive strength values obtained by testing individual cubes that were cut out from each beam after fatigue testing. However, this did not improve the fatigue relationships.

Also, an effort was made to come up with a unique relationship between dissipated energy and fatigue failure similar to the one obtained for the asphalt concrete mixture. While there was some convergence in the fatigue curves for different axle configurations, no unique relationship could be established.

Finally, the possibility of reducing test variability by using mortar beams in lieu of concrete mix beams was explored through additional testing. Interestingly, this did not reduce the variability in fatigue test results.

CHAPTER 3
FATIGUE OF RIGID PAVEMENTS: MECHANISTIC ANALYSIS

3.1 INTRODUCTION

In parallel with the lab experiments an analysis was performed using the computer program DYNASLAB to determine the relative damage to jointed plain concrete (JPCP) pavements caused by trucks with different axle configurations. This chapter presents the analyses relating to fatigue near the edge and at mid-slab. Chapter 5 gives details of similar work done for faulting at the joint.

3.2 FATIGUE ANALYSIS UNDER MULTIPLE AXLES

3.2.1 Detailed Sample Analysis for Calculating Axle and Truck Factors

Four different types of trucks, as shown in figure 3.1, were considered in the analysis. The slab chosen in the analysis was 16 feet long and 12 feet wide with a thickness of 10 inches.

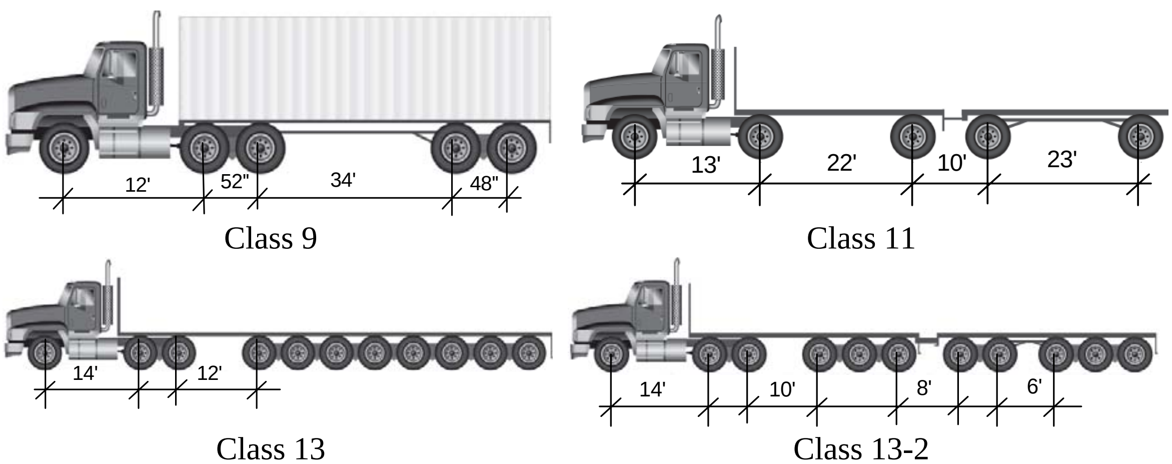

Figure 3.1 Types of trucks used in faulting and fatigue analyses

Loading per axle as applied in this analysis was as follows:

- Steering axle: 15,400 lbs
- Single axle: 18,000 lbs
- Tandem axle: 16,000 lbs
- Tridem and higher axles: 13,000 lbs

Figure 3.2 shows the longitudinal stress response for the four trucks. The results indicate: (1) significant interaction between the axles, which leads to reduction in longitudinal stress, and (2) relatively large compressive stresses (tensile stresses at the top of the slab). Figure 3.3 shows the longitudinal stresses under different axle configurations. The plots show a significant reduction in stress as the number of axles within an axle group increases.

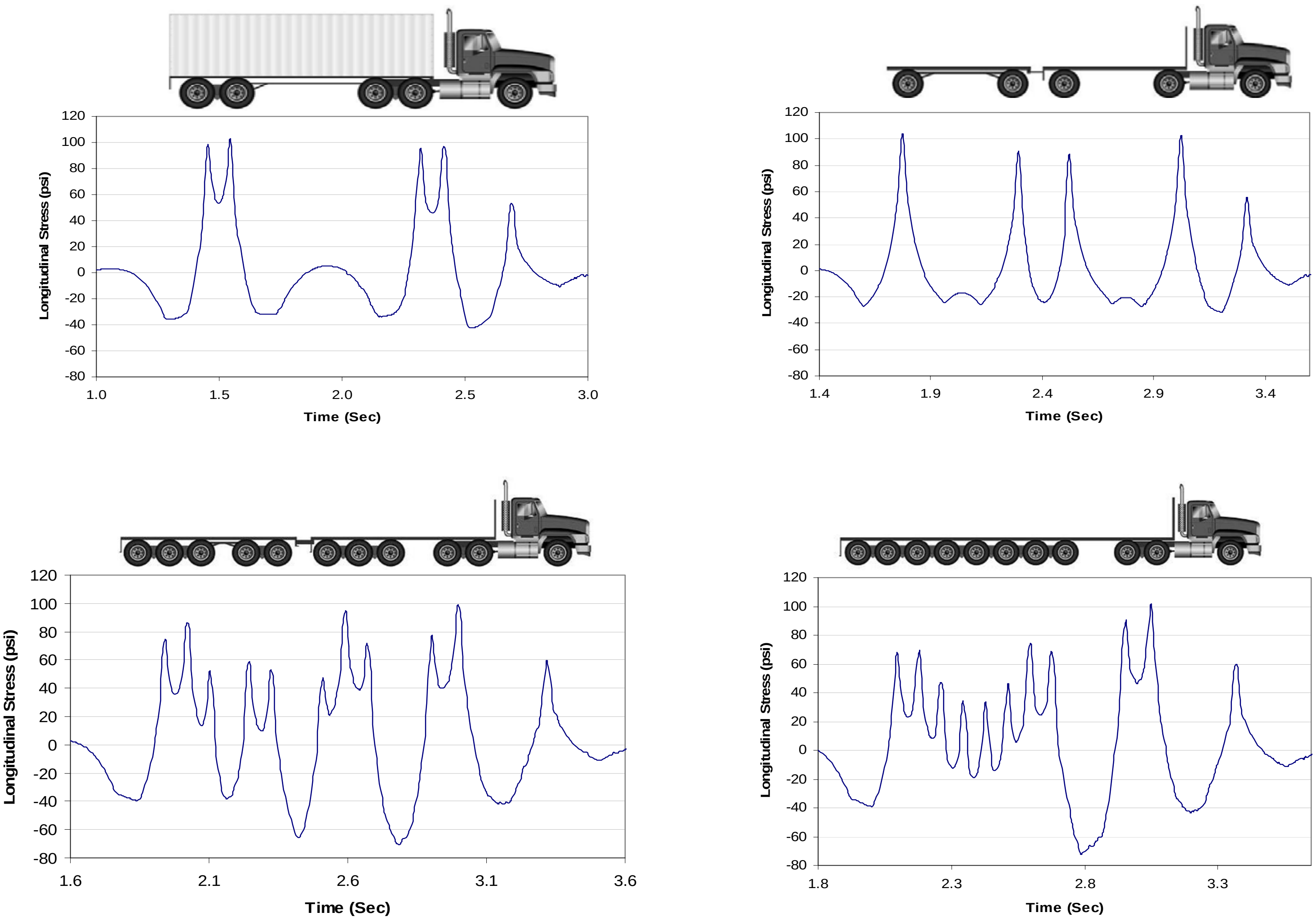

Figure 3.2 Longitudinal stress responses under various Michigan truck axle configurations

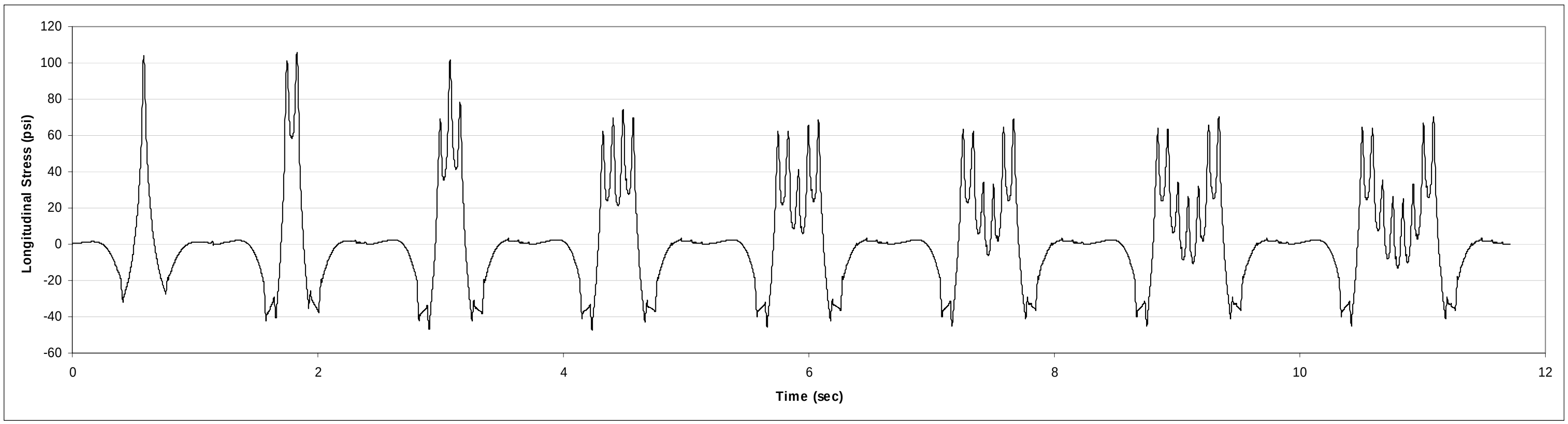

Figure 3.3 Longitudinal stresses under different axle groups (13 kips per axle)

Fatigue life is generally related to the longitudinal stress at the mid slab in the wheel path under the moving load. However, because of environmental effects the slab may also be undergoing curling. Curling stress at the mid-slab would superimpose itself onto the stress caused by the moving load. Curling stress would vary with gradual changes in the environment throughout the day. However, for the sake of simplicity in the preliminary analysis, a constant curling stress of 179 psi was assumed. This corresponds to the maximum daytime thermal stress for such a slab with a temperature difference of 31 ^{o}F between the top and bottom surfaces. Table 3.1 presents the resulting longitudinal stress at the bottom of the slab.

The M-E PDG uses the following model for estimating fatigue life in concrete pavements.

$$\log\left(N_{i,j,k,l,m,n}\right) = C_1 \cdot \left(\frac{MR_i}{\sigma_{i,j,k,l,m,n}}\right)^{C_2} + 0.4371 \qquad (3.1)$$

Using this model, the number of load repetitions to fatigue failure was calculated, as presented in table 3.2. Fatigue life was then used to determine the damage to the pavement by taking its inverse (one over the number of repetitions to fatigue failure). The damage values were then normalized using a standard 18 kip single axle as the reference. Table 3.3 presents the axle factors thus calculated along with the resulting truck factors, assuming 100% LTE.

Since different classes of trucks have varying axle and gross vehicle loads, each truck factor was divided by its gross vehicle weight (GVW). Also, to be able to compare the trucks relative to each other, the truck factor per unit GVW was normalized using the class 9 truck as the reference truck, since it accounts for the majority of trucks in the U.S. (see table 3.4). The results show that class 13 trucks (with multiple axles) are less damaging than class 9 trucks. Within class 13, the truck with the 8-axle group is the least damaging in fatigue. On the other hand, the most damaging truck is that of class 11, which is comprised of single axles.

3.2.2 Axle Factors for Different Configurations

The trucks analyzed so far had single, tandem, tridem and 8-axle groups. To be able to compare various axle groups to each other with respect to fatigue damage, the same analysis was repeated with 1, 2, 3, 4, 5, 6, 7 and 8 axles. All the axles in this case had a load of 13 kips individually. Tables 3.5 through 3.8 present the calculated stresses and the resulting axle factors. A tandem axle group with a total load of 26 kips is found to be 1.88 times more damaging than a 13 kip single axle. However, adding more axles to the same axle group leads to reduced fatigue damage although the total load being carried increases with each additional axle. This is due to the stress reduction in the slab caused by the interaction among axles.

Table 3.1 Longitudinal stress at the bottom of the slab for different trucks

Truck Type	Gross Vehicle	Longitudinal Stresses (psi)										
		Axle 1	Axle 2	Axle 3	Axle 4	Axle 5	Axle 6	Axle 7	Axle 8	Axle 9	Axle 10	Axle 11
Class 9	**79400**	281	293	294	303	297						
Class 11	**87400**	284	321	306	308	321						
Class 13	**151400**	288	301	292	245	247	212	203	204	214	243	242
Class 13-2	**151400**	288	299	282	246	275	223	245	241	224	270	246

Table 3.2 Number of load repetitions to fatigue failure for different trucks

Axle Group	Gross Axle Wt.	No. of Repititions to Failure (in 1000s)										
		Axle 1	Axle 2	Axle 3	Axle 4	Axle 5	Axle 6	Axle 7	Axle 8	Axle 9	Axle 10	Axle 11
Class 9	**79400**	3300	1639	1574	993	1320						
Class 11	**87400**	2845	407	840	757	408						
Class 13	**151400**	2281	1111	1778	43684	36370	1071767	3011941	2847631	875729	51960	55927
Class 13-2	**151400**	2279	1207	3186	41067	4854	335580	41851	60489	297721	6978	40333

Table 3.3 Axle factors and truck factors relative to 18 kip single axle with dual wheels

Axle Group	Gross Axle	Axle Factors											Truck factors
		Axle 1	Axle 2	Axle 3	Axle 4	Axle 5	Axle 6	Axle 7	Axle 8	Axle 9	Axle 10	Axle 11	
Class 9	**79400**	0.124	0.249	0.259	0.411	0.309							1.352
Class 11	**87400**	0.143	1.004	0.486	0.539	1.000							3.172
Class 13	**151400**	0.179	0.367	0.230	0.009	0.011	0.000	0.000	0.000	0.000	0.008	0.007	0.813
Class 13-2	**151400**	0.179	0.338	0.128	0.010	0.084	0.001	0.010	0.007	0.001	0.058	0.010	0.827

Table 3.4 Truck factors normalized to gross vehicle weight

Axle Group	Gross Axle	Truck factors	TF/GVW	Normalized AF/GAW
Class 9	**79400**	1.352	1.7E-05	1
Class 11	**87400**	3.172	3.6E-05	2.131
Class 13	**151400**	0.813	5.4E-06	0.315
Class 13-2	**151400**	0.827	5.5E-06	0.321

Figure 3.4 shows the axle factors for each axle group normalized for the total load carried by the axle group. The results show that every additional axle makes the axle group less damaging. This gain becomes even greater when the axle group has 4 or more axles. For an 8-axle group normalized axle factor is 0.037 only relative to a single axle. This observation can be explained by the fact that additional axles actually spread the load to a greater area of the slabs, leading to much lower bending stresses.

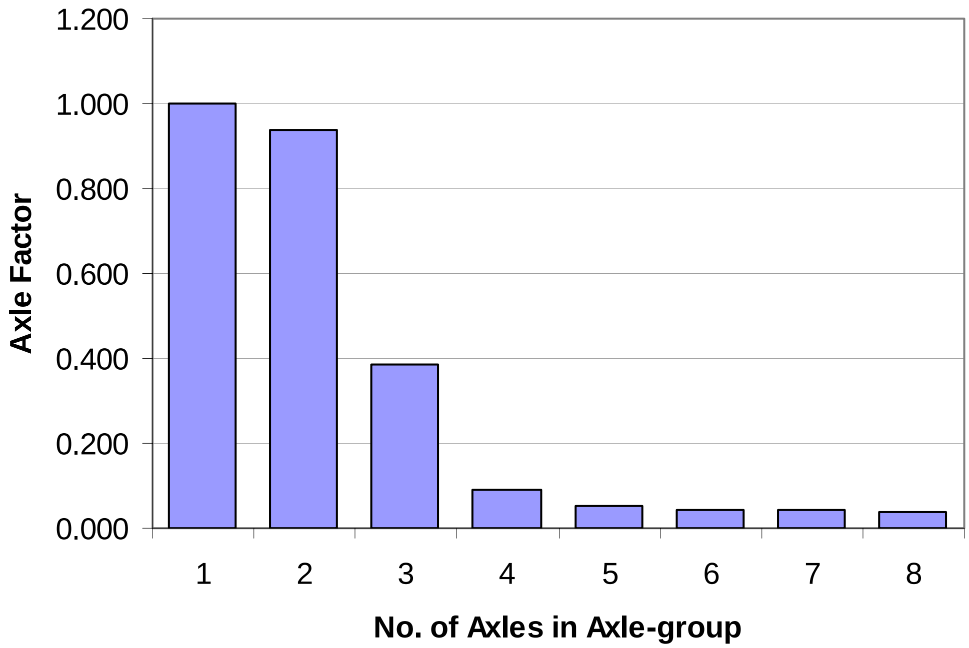

Figure 3.4 Axle factors normalized by total weight for different axle groups

3.2.3 Truck Factors for Legal Load Limits

This analysis was extended to include the different axle load configurations at their legal load limits. Table 3.9 lists the corresponding axle factors for each axle group. Table 3.10 shows the final truck factors relative to a standard 18 kip single axle with dual wheels. As expected, the results show trucks with multi-axle groups to be less damaging in fatigue as compared to those with single or tandem axles.

Table 3.5 Longitudinal stress at the bottom of the slab for different axle groups

Axle Group	Gross Axle Wt. (lb)	Longitudinal Stress At the Bottom of the Slab (psi)							
		Axle 1	Axle 2	Axle 3	Axle 4	Axle 5	Axle 6	Axle 7	Axle 8
1 Axle	13000	283							
2 Axles	26000	285	279						
3 Axles	39000	257	281	248					
4 Axles	52000	248	253	248	241				
5 Axles	65000	247	245	220	241	241			
6 Axles	78000	248	244	212	213	241	242		
7 Axles	91000	249	245	211	205	213	242	243	
8 Axles	104000	249	246	212	204	204	214	243	243

Table 3.6 Number of load repetitions (thousands) to fatigue failure for different trucks

Axle Group	Gross Axle Wt. (lb)	No. of Repititions to Failure							
		Axle 1	Axle 2	Axle 3	Axle 4	Axle 5	Axle 6	Axle 7	Axle 8
1 Axle	13000	3014							
2 Axles	26000	2727	3890						
3 Axles	39000	16869	3386	32782					
4 Axles	52000	32677	22608	32599	60179				
5 Axles	65000	35873	44302	427286	58407	59718			
6 Axles	78000	33205	48344	1047651	896556	59260	53971		
7 Axles	91000	30878	44192	1171781	2381155	896556	53653	51917	
8 Axles	104000	31224	41236	1044085	2689692	2598239	820903	50116	49366

Table 3.7 Axle group factors relative to 13 kip single axle with dual wheels

Axle Group	Gross Axle Wt. (lb)	Axle Factor								AF (Axle Gr.)
		Axle 1	Axle 2	Axle 3	Axle 4	Axle 5	Axle 6	Axle 7	Axle 8	
1 Axle	13000	1.000								1.000
2 Axles	26000	1.105	0.775							1.880
3 Axles	39000	0.179	0.890	0.092						1.161
4 Axles	52000	0.092	0.133	0.092	0.050					0.368
5 Axles	65000	0.084	0.068	0.007	0.052	0.050				0.261
6 Axles	78000	0.091	0.062	0.003	0.003	0.051	0.056			0.266
7 Axles	91000	0.098	0.068	0.003	0.001	0.003	0.056	0.058		0.287
8 Axles	104000	0.097	0.073	0.003	0.001	0.001	0.004	0.060	0.061	0.300

Table 3.8 Axle group factors normalized to gross vehicle weight

Axle Group	Gross Axle Wt. (lb)	AF (Axle Gr.)	AF/GAW	Normalized AF/GAW
1 Axle	13000	1.000	7.692E-05	1.000
2 Axles	26000	1.880	7.232E-05	0.940
3 Axles	39000	1.161	2.977E-05	0.387
4 Axles	52000	0.368	7.080E-06	0.092
5 Axles	65000	0.261	4.019E-06	0.052
6 Axles	78000	0.266	3.412E-06	0.044
7 Axles	91000	0.287	3.157E-06	0.041
8 Axles	104000	0.300	2.882E-06	0.037

Table 3.9 Axle group factors (fatigue) for legal load limits

Axle Group	Gross Axle Wt. (lb)	Axle Factors								Axle Factor (Group)
		Axle 1	Axle 2	Axle 3	Axle 4	Axle 5	Axle 6	Axle 7	Axle 8	
Front Axle	15400	0.1435								0.143
Single Axle	18000	1.0000								1.000
2 Axles-16k	32000	0.411	0.309							0.720
2 Axles-13k	26000	0.150	0.105							0.255
2 Axles-9k	18000	0.0166	0.0131							0.030
3 Axles	39000	0.0242	0.1205	0.0124						0.157
4 Axles	52000	0.0125	0.0181	0.0125	0.0068					0.050
5 Axles	65000	0.0114	0.0092	0.0010	0.0070	0.0068				0.035
6 Axles	78000	0.0123	0.0084	0.0004	0.0005	0.0069	0.0076			0.036
7 Axles	91000	0.0132	0.0092	0.0003	0.0002	0.0005	0.0076	0.0079		0.039
8 Axles	104000	0.0131	0.0099	0.0004	0.0002	0.0002	0.0005	0.0081	0.0083	0.041

Table 3.10 Truck factors (fatigue)

Truck	Truck No.	Total Wt. (kips)	TF
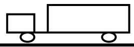	1	*33.4*	1.143
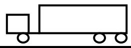	2	*47.4*	0.864
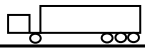	3	*54.4*	0.301
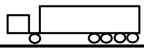	4	*67.4*	0.193
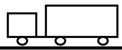	5	*51.4*	2.143
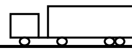	6	*65.4*	1.864
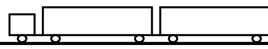	7	*87.4*	4.143
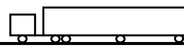	8	*83.4*	2.864
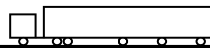	9	*101.4*	3.864
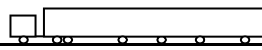	10	*119.4*	4.864
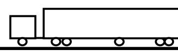	11	*91.4*	2.118
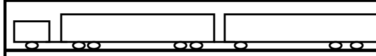	12	*117.4*	2.373
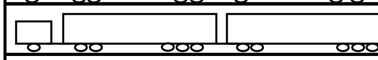	13	*151.4*	1.433
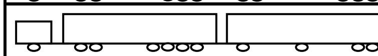	14	*161.4*	3.168
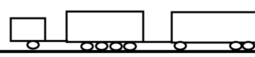	15	*117.4*	1.914
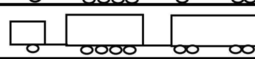	16	*125.4*	1.168
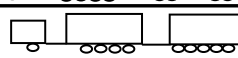	17	*132.4*	0.229
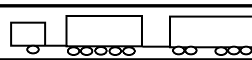	18	*143.4*	1.208
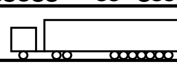	19	*138.4*	0.903
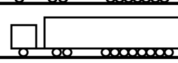	20	*151.4*	0.904
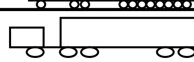	21	*79.4*	1.584

3.3 PAVEMENT PERFORMANCE WITH DIFFERENT AXLE GROUPS USING MEPDG

Similar to the analyses conducted for flexible pavements, the objective behind this analysis was to compare relative damage to rigid pavements caused by the passage of different axle groups. To this end, four types of axle groups were separately simulated using MEPDG. The simulation was done using a 9 inch JPCP pavement with 8 inch thick granular base of A-1-b material as shown in figure 3.5. The traffic loading applied was equivalent to 4000 axle groups per day. Each run has only one type of axle group traffic. The axle groups simulated in this analysis were (a) Single, (b) Tandem, (c) Tridem, and (d) Quad axles.

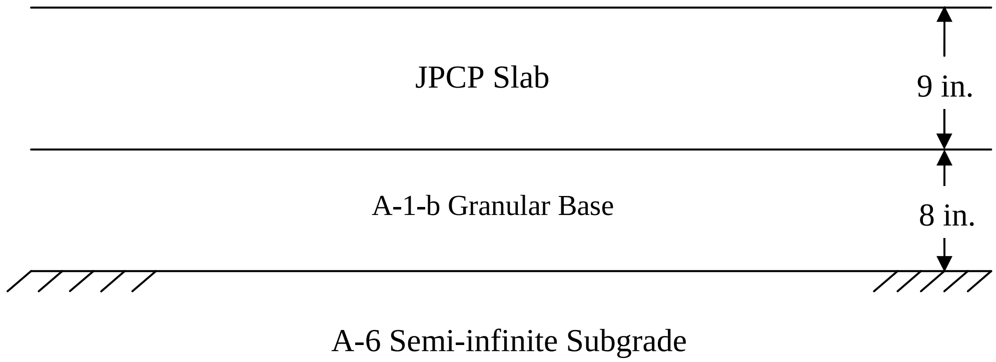

Figure 3.5 Pavement structure used in the MEPDG simulation

Figures 3.6 and 3.7 show the performance curves output by M-E PDG for cracking and roughness. A severe discrepancy is noted for tandem axles in the case of cracking. The percent of slabs cracked reaches one hundred percent right at the beginning of the pavement life. This seems to be an anomaly resulting from the deficiency of the cracking model used in the MEPDG software. These runs were performed using MEPDG version 1.003. When version 0.91 was run for the same cases, the percent slabs cracked reached the one hundred percent level only after 70 months. Percent slabs cracked in the other three cases were also significantly lower in version 0.91 than those obtained from version 1.003 as shown here. The IRI plot also shows the apparent anomaly in the case of tandem axles. This is because the percent of slabs cracked is a direct input in the IRI model.

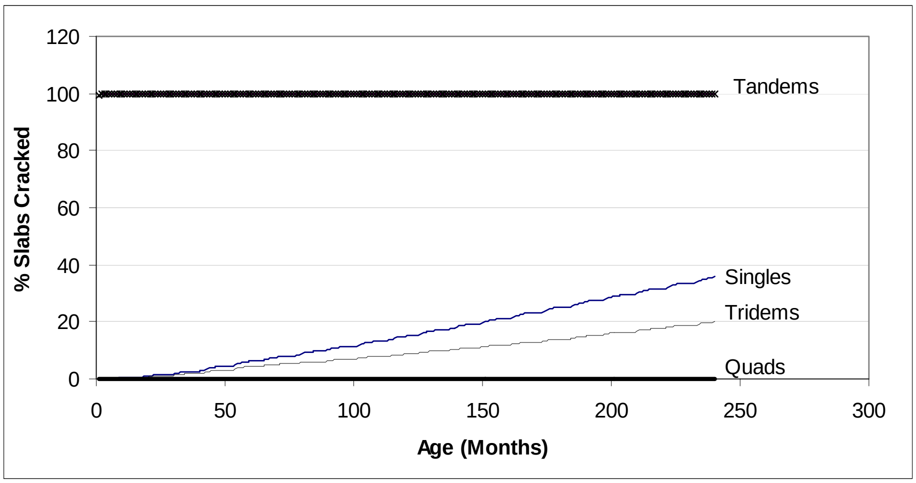

Figure 3.6 Percent slabs cracked under different axle group loadings

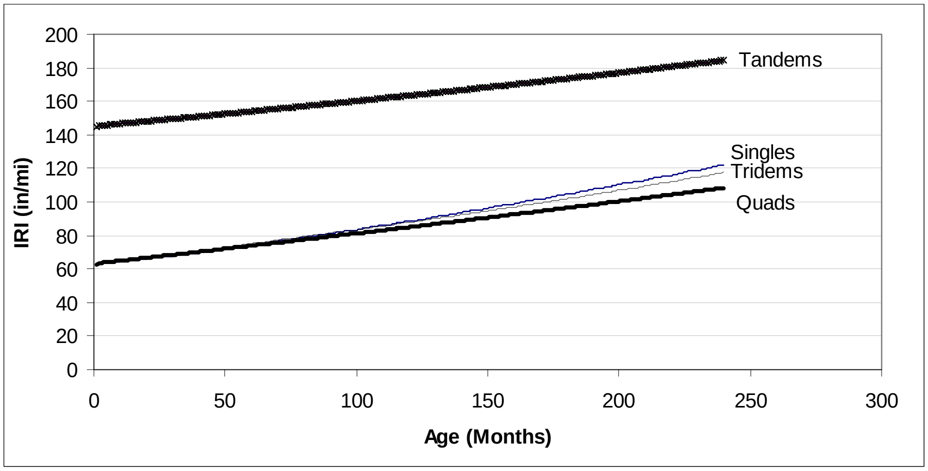

Figure 3.7 IRI as a result of different axle group loadings

3.4 POTENTIAL FOR TOP-DOWN CRACKING IN JPCP PAVEMENTS

There have been speculation that positioning of different axles or axle groups relative to joint spacing may lead to top-down cracking in jointed plain concrete pavements. This analysis was aimed at exploring a few case scenarios. To this end, a JPCP slab was loaded with three axle groups. The slab chosen in the analysis was 16 feet long and 12 feet wide with a thickness of 10 inches. The three axle groups analyzed were: (a) a single steering axle with single wheels and a single drive axle with dual wheels, (b) a single axle with single wheels with a tandem axle simulating the front tandem axle, and (c) two tandem axles simulating the drive and rear axles. The spacing between the axle groups were adjusted so that the two groups would exactly fit on one slab of 16 feet length. This is shown pictorially in figure 3.8 (not-to-scale). Note that we did not include tridem and quad axles because the 16 foot slab could not accommodate these larger axles; hence they are not critical for the end-loading condition. It is expected that when the two axles groups are at the two ends of the slab it would lead to maximum compressive stresses in the bottom of the mid-slab which; i.e., maximum tensile stresses at the top, which may lead to top-down cracking. Therefore, the main focus in this analysis is on the magnitude of compressive stresses at the critical point in the slab.

Figure 3.9 shows the critical stresses in the same slab caused by the passage of one standard 18 kip single axle (base case). This would help in ascertaining the relative magnitudes of compressive and tensile stresses in the other three cases described above. Figures 3.10 to 3.12 show the critical stresses in the slab as the three axle groups pass over it with a speed of 30 mi/hr (528 in/sec).

In figure 3.9, the magnitude of maximum compressive stress experienced by a JPCP slab because of the passage of a standard 18 kip single axle is 80 psi. The maximum tensile stress in the same situation, however, is around 144 psi. Since the maximum compressive stress is much smaller than maximum tensile stress, top-down cracking under these conditions would not be a concern.

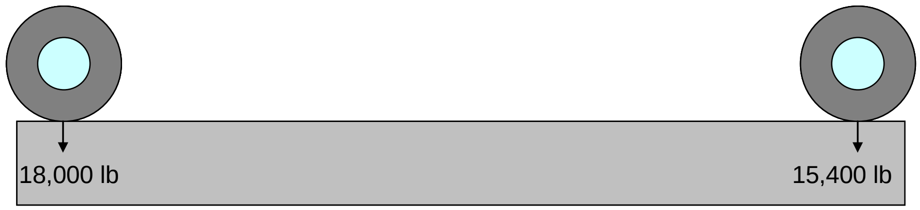

(a) A single steering axle with single wheels and a single drive axle with dual wheels

(b) A single axle with single wheels with a tandem axle simulating the front tandem axle

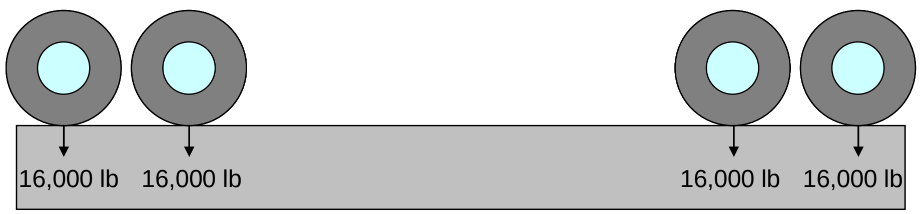

(c) Two tandem axles simulating the drive and rear axles

Figure 3.8 Relative locations of axles and axle loads used in the analysis (not-to-scale)

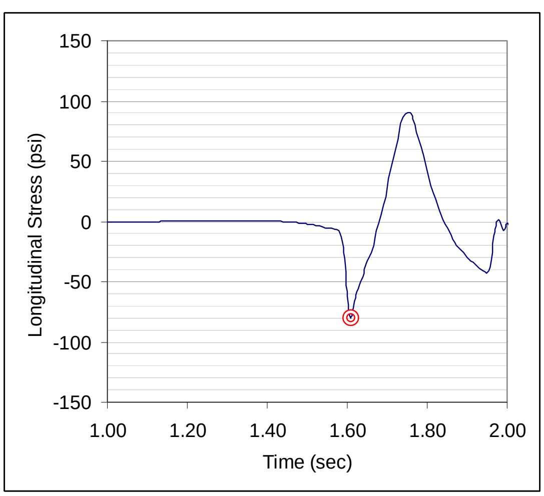

(a) Critical compressive stress

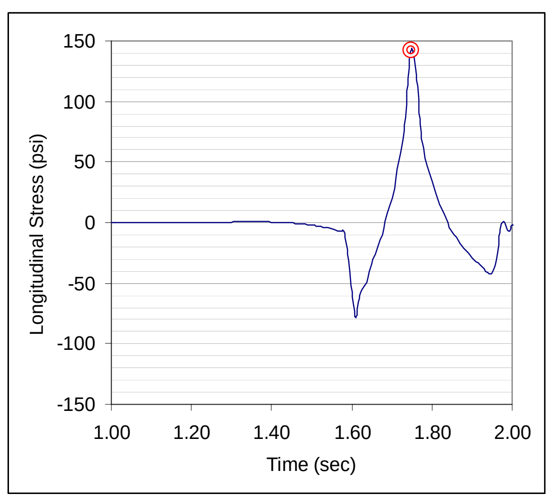

(b) Critical tensile stress

Figure 3.9 Critical stresses under passage of one standard 18 kip single axle

Figure 3.10 shows that the maximum tensile stress caused by two single axles (case "a") is very similar to that caused by the standard 18 kip single axle. However, because of the presence of the second single axle the maximum compressive stress at the bottom of the slab is as high as 108 psi. This is 28 psi higher than that caused by one standard single axle. In the case of a single axle and a tandem axle combination (case "b") the bottom compressive stress is even higher (118 psi) as shown in figure 3.11. In the case of two tandem axles (case "c"), it is lower (108 psi), as shown in figure 3.12. Therefore case "b" is the most critical of the cases studied here. However, even in this case the maximum compressive stress, being 118 psi, is 20 percent lower than the maximum tensile stress experienced by the slab. Therefore, it seems that under the given conditions top-down cracking, because of certain critical axle placements, should not be of concern. However, once negative curling is introduced in the pavement maximum compressive stresses may be much higher.

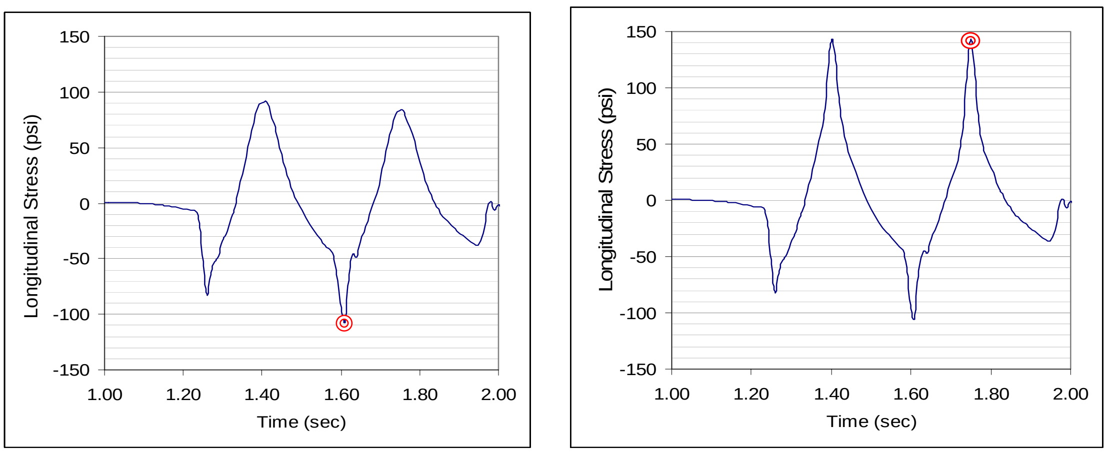

(a) Critical compressive stress (b) Critical Tensile stress

Figure 3.10 Critical stresses with one single wheel single axle and one dual wheel single axle

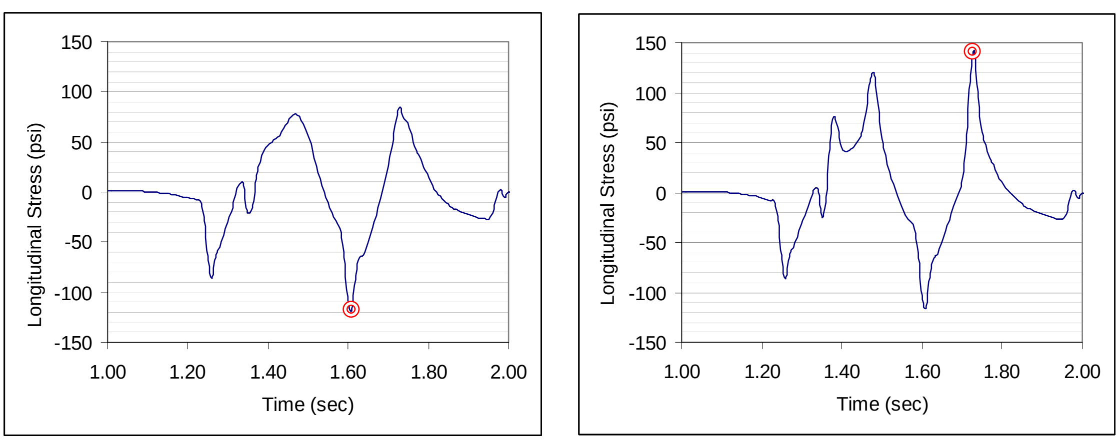

(a) Critical compressive stress (b) Critical Tensile stress

Figure 3.11 Critical stresses with one single-wheel single axle and one dual-wheel tandem axle

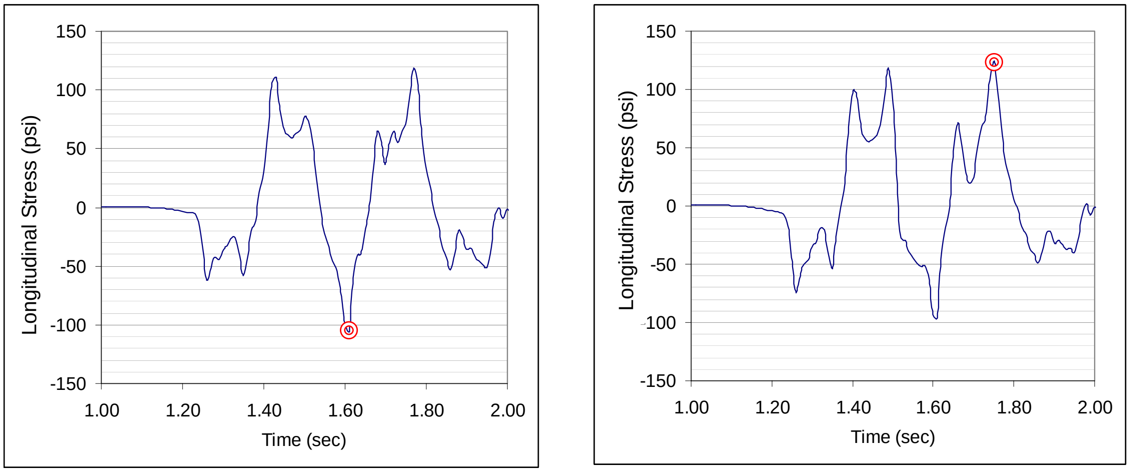

(a) Critical compressive stress (b) Critical Tensile stress

Figure 3.12 Critical stresses with two dual wheel tandem axles

3.5 POTENTIAL FOR CRACKING IN CURLED JPCP SLABS

The analysis presented in the preceding section looked at positioning of different axles or axle groups relative to joint spacing that may lead to top-down cracking in jointed plain concrete pavements. The next step in the analysis was to include the effect of temperature curling on slab stresses. In the analysis presented so far either a constant curling stress was assumed or no curling stresses were considered. The following analysis was preformed using the computer program KENSLABS because it allows for curled slabs and gaps underneath the slab system. The analysis focused on the potential for top down cracking in the middle of the slab because of different relative positioning of axle groups

The same pavement conditions, as in the preceding section, were used: 16 ft long, 12 ft wide and 10 inch thick slabs. The axles (single and tandem axle combinations) were placed at both ends of the slab. The results in terms of longitudinal and transverse stresses and deflections were compared to those when there is no curling/gaps, and to the case when a single axle is at mid-point.

The axle groups analyzed were: (a) a single steering axle with single wheels and a single drive axle with dual wheels, (b) a single axle with single wheels with a tandem axle simulating the front tandem axle, and (c) two tandem axles simulating the drive and rear axles. The spacing between the axle groups were adjusted so that the two groups would exactly fit on one slab of 16 feet length. Recall that we did not include tridem and quad axles because the 16 foot slab could not accommodate these larger axles; hence they are not critical for the end-loading condition. This is shown pictorially in figure 3.8 (not-to-scale). It is expected that when the two axles groups are at the two ends of the slab it would lead to maximum compressive stresses in the bottom of the mid-slab which; i.e., maximum tensile stresses at the top, which may lead to top-down cracking. Therefore, the main focus in this analysis is on the magnitude of compressive stresses at the critical point in the slab.

Figure 3.13 shows the critical stresses in the same slab caused by the different axle combinations on curled slabs with gap. Figure 3.14 shows the longitudinal and transverse stresses under single axle at mid-slab and at slab ends without curling. Figure 3.15 shows longitudinal and transverse curling stresses with no loading.

It is clear that negative (upward) curling with inclusion of gaps causes the stresses to increase significantly, with the tensile stress at the top of slab caused by the axles at the slab ends can be as much as 2.4 times as high as the tensile at the bottom of the slab caused by the axle at mid-point of the slab. In this case a temperature difference of 12.2 ^{o}C (22 ^{o}F) was assumed with the top surface being colder than the bottom. When there is no curling, the effect of placing axles at the slab ends is not significant. It is clear from the results presented in table 3.11 that curling with inclusion of gaps causes the stresses to increase significantly.

Table 3.11 Maximum longitudinal stresses for top-down cracking

Loading	Longitudinal Stress					
	Max Long. Stress (psi)	Location (in)		Min Long. Stress (psi)	Location (in)	
		X	Y		X	Y
Curling Only	132.1	96	72	0	0	Joint
Single + Single Load Only	125.4	48	36	0	0	Joint
Single + Single & Curling	287.2	96	72	0	0, 192	Joint
Single + Tandem & Curling	284.8	108	72	0	0, 192	Joint
Tandem + Tandem & Curling	281.6	96	48	0	0, 192	Joint

In the case of positive (downward) curling the load was placed at mid-slab. Such load position would cause maximum tensile stresses at the bottom of the mid-slab leading to the possibility of bottom-up cracking. Table 3.12 shows the longitudinal stresses due to different axle groups with and without curling. When the slab is flat, i.e. without curling, the stresses decrease as the number of axles within a group increases from one to four. This decrease is because of the bridging effect from additional axles leading to less flexure in the longitudinal direction. When the slab is curled downward (positive curling), longitudinal stresses increase by two to almost five folds. A component of this stress is the positive curling stress. In this case a temperature difference of 17.2 ^{o}C (31 ^{o}F) was assumed with the top surface being warmer than the bottom. In addition, the upward curvature of the slab produces higher bending moment leading to higher load-related stresses as well. Interestingly the percent increase in longitudinal stress increases significantly as the number of axles increases from one to four. However the absolute maximum value of longitudinal stress at the bottom of mid-slab goes down with increasing number of axles. This means that the bridging effect in multiple axles is smaller when the slab is curled (downward) than when it is flat.

Table 3.12 Stresses due to different axle groups for bottom-up cracking

Loading Axle	Maximum Longitudinal Stress (psi)		% Increase in Max Stress
	No Curling	With Curling	
Single	132.8	393.8	197
Tandem	114.0	347.4	205
Tridem	73.3	334.3	356
Quad	48.4	279.8	478

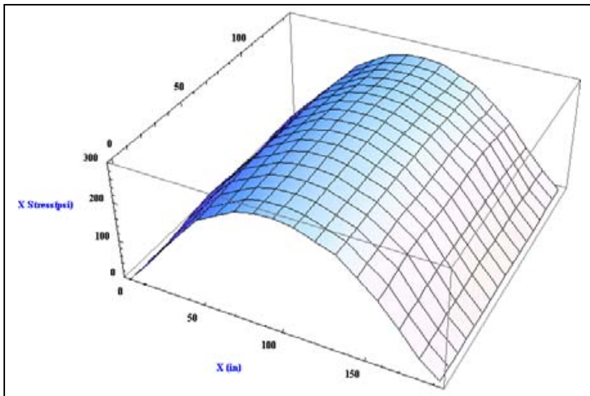

Single + Single axles longitudinal stress

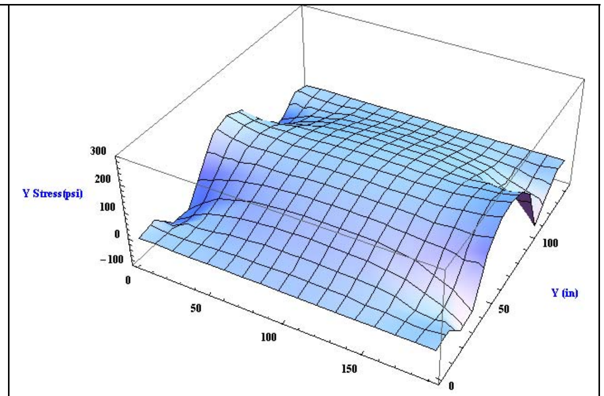

Single + Single axles transverse stress

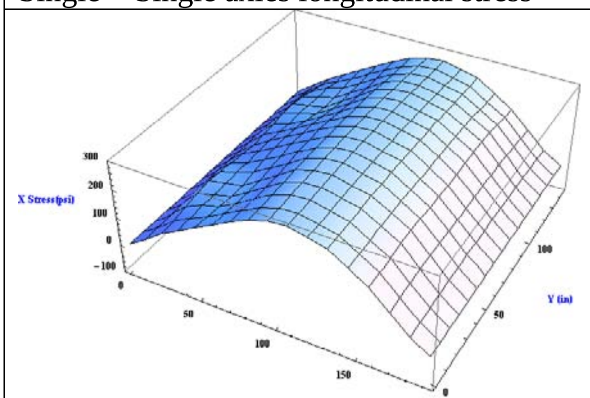

Single + Tandem axles longitudinal stress

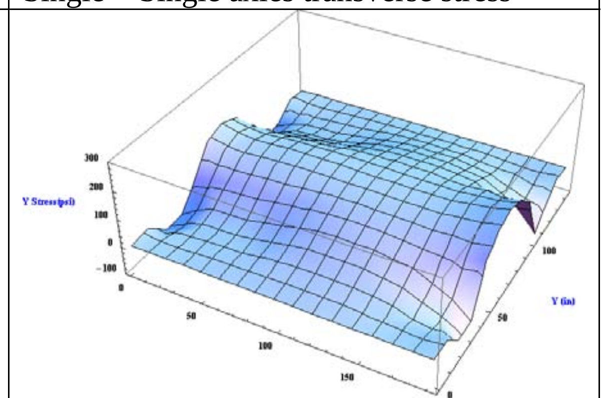

Single + Tandem axles transverse stress

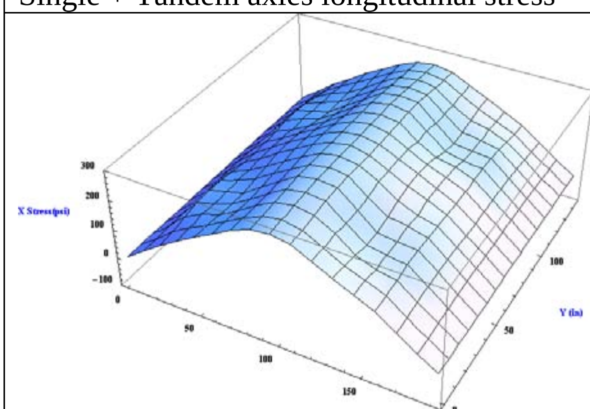

Tandem + Tandem axles longitudinal stress

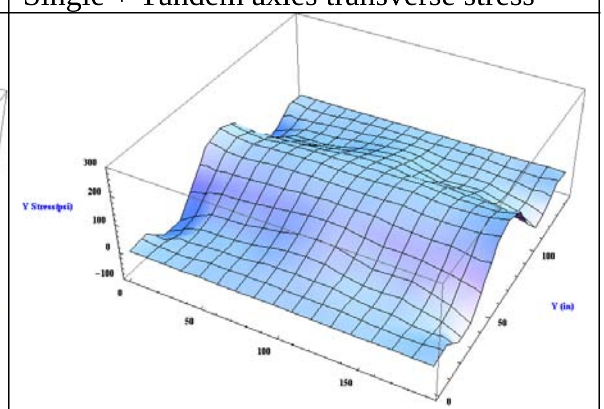

Tandem + Tandem axles transverse stress

Figure 3.13 Longitudinal and transverse stresses caused by different axle combinations placed at slab ends on curled slabs

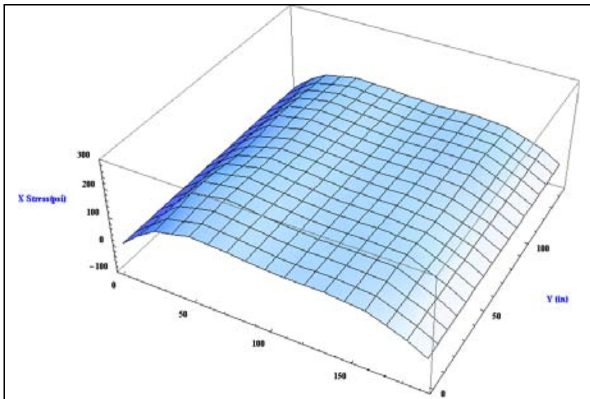

Single + Single axles longitudinal stress without curling

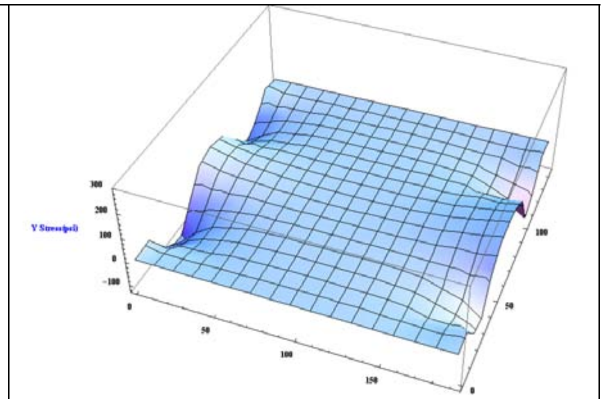

Single + Single axles transverse stress without curling

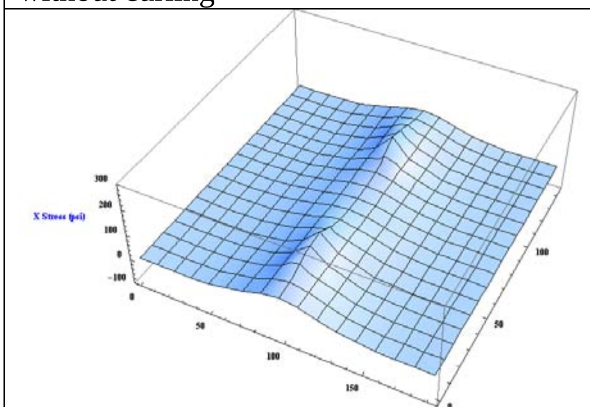

Longitudinal stresses due to single axle in the middle of slab (no curling)

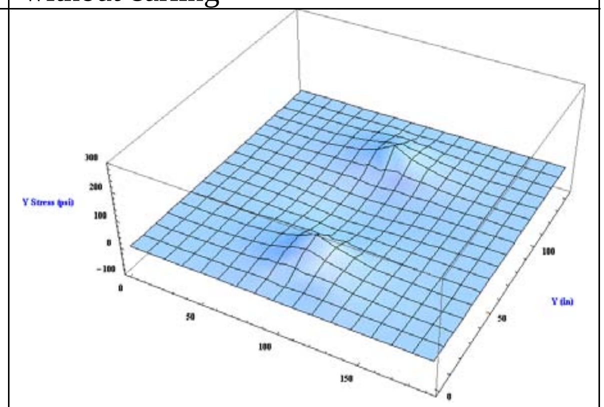

Transverse stresses due to single axle in the middle of slab (no curling)

Figure 3.14. Longitudinal and transverse stresses from single axles at middle of slab and at slab ends without curling

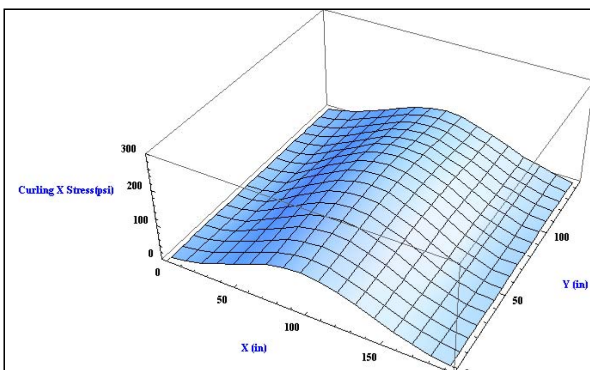

Curling longitudinal stress

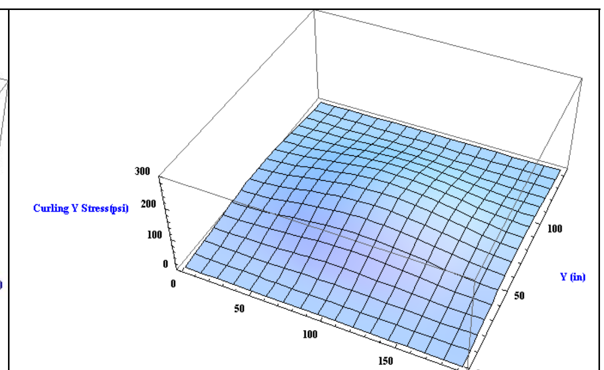

Curling transverse stress

Figure 3.15. Longitudinal and transverse curling stresses with no loading

Figure 3.16 shows vertical deflections from different conditions. The figure shows that the effect of curling is, as expected, very significant. Negative (upward) curling will lead to higher corner deflections as a given axle passes across the joint, with the effect being more significant with multiple axles. However, this has no implication on cracking.

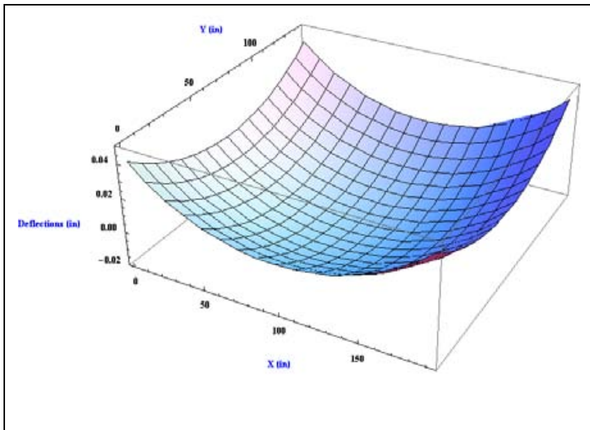	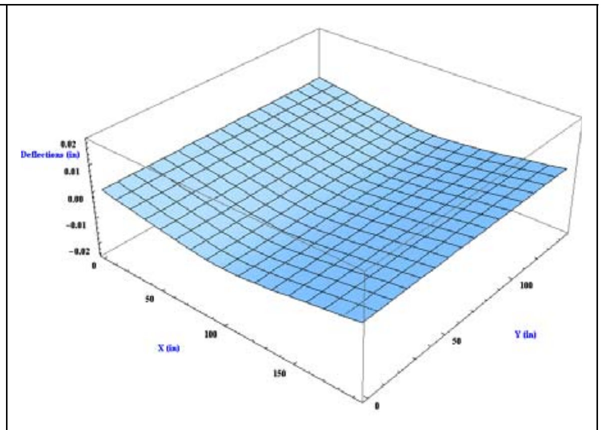
Deflections due to curling alone	Deflections due to single axle in the middle of slab (no curling)
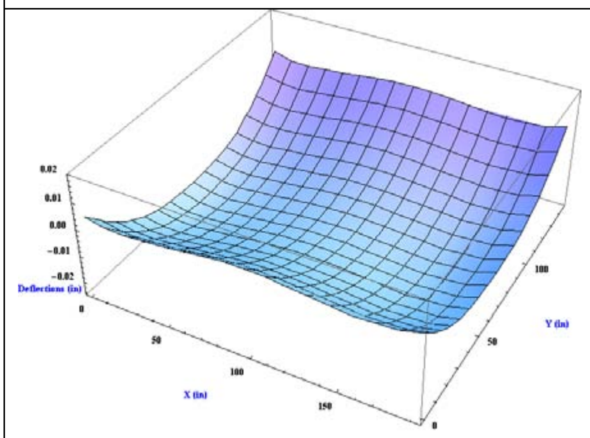	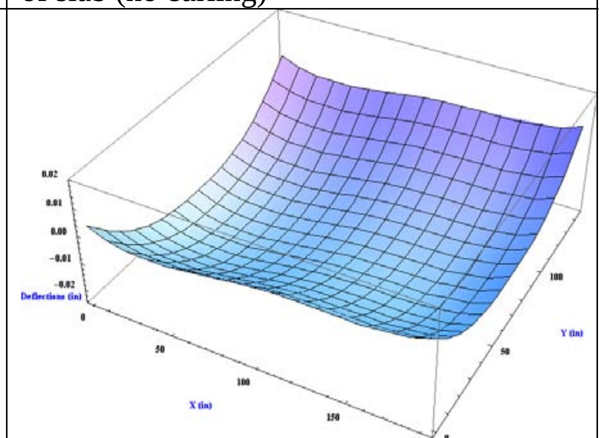
Single + Single axles deflections with curling	Single + Tandem axles deflections with curling
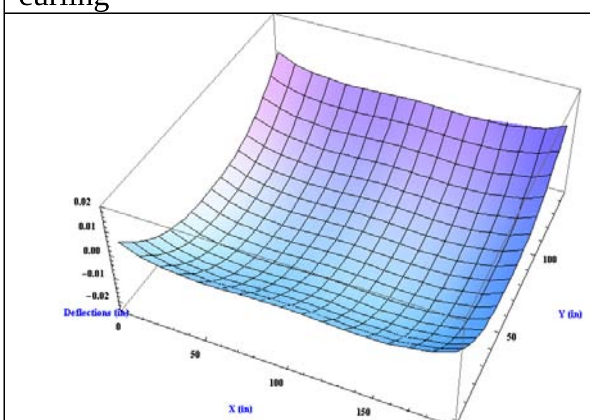	
Tandem + Tandem axles deflections with curling	

Figure 3.16. Vertical deflections caused by different loading conditions

CHAPTER 4
JOINT DETERIORATION – LABORATORY INVESTIGATION

4.1 INTRODUCTION

The effect of multiple axles moving across a joint or a crack on the joint/crack performance was investigated using DYNASLAB. The results from this analysis were used to decide on the appropriate load shape and sequence to simulate a moving multi-axle group across a joint or crack discussed in a later section in this chapter.

For this purpose, real size concrete slabs were cast and tested with a dual-actuator frame. The test setup allowed for independently controlled actuators to simulate multiple axle loads across the joint or crack, moving at different speeds. Different axle configurations were to be simulated, and the response/performance of the joint under these conditions were to be compared against that under standard single and tandem axles.

The experiment was to include single, tandem, tridem, quad, 6-axle and 8-axle groups. The results from this experiment were intended to provide a *relative* assessment of joint/crack damage from different axle combinations, and not a predictive performance model. This can be used to determine mechanistically-based axle load equivalencies and truck factors for joint/crack damage.

4.2 TEST SET-UP

Joints and/or cracks are generally the weakest points in jointed concrete pavements, and therefore are often the control factors affecting the overall performance of the jointed concrete pavement. A 7.5x15 ft (full-scale) trial concrete slab was tested under a dual-actuator frame in conjunction with a parallel study on dowel bar misalignment. It was also decided to use a slab thickness of 7 inches instead of 10 inches proposed in the original project proposal. This was done in order to shorten the duration of the tests; i.e., to aim for fewer repetitions until distress. The decision was confirmed after reviewing the results from the earlier study by Colley and Humphrey, which used 9 inch and 7 inch slabs and an axle load of 9000 lbs. In this study, the actuator loads are set at 6500 lbs (half of the legal load for individual axles within a multi-axle group).

The instrumentation details of the test set-up were worked out first, followed by an additional trial test to check the load pulses for various multiple pulses along with the data acquisition. This trial testing of the slab helped in resolving various data and analysis related issues before commencing the slab testing for the designed experiment. The test setup along with instrumentation is shown in Figures 4.1 through 4.5. Note that the metal insert shown in the figures was removed before testing.

Figure 4.1 Full-Scale Trial Slab with Loading Setup

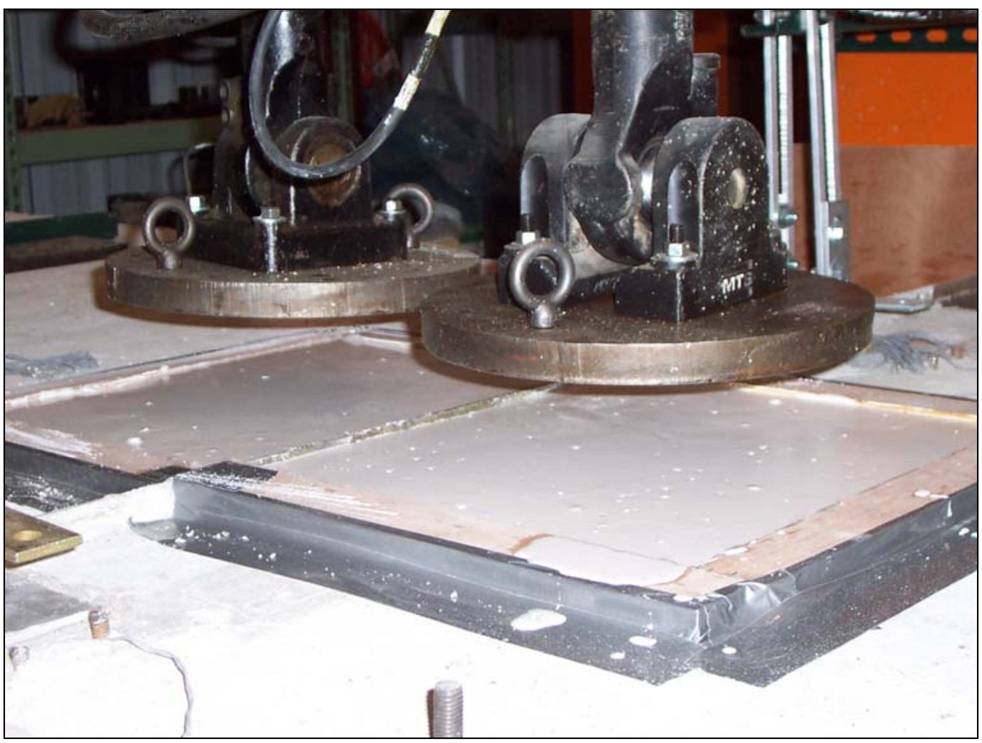

Figure 4.2 Loading Actuator at Slab Joint

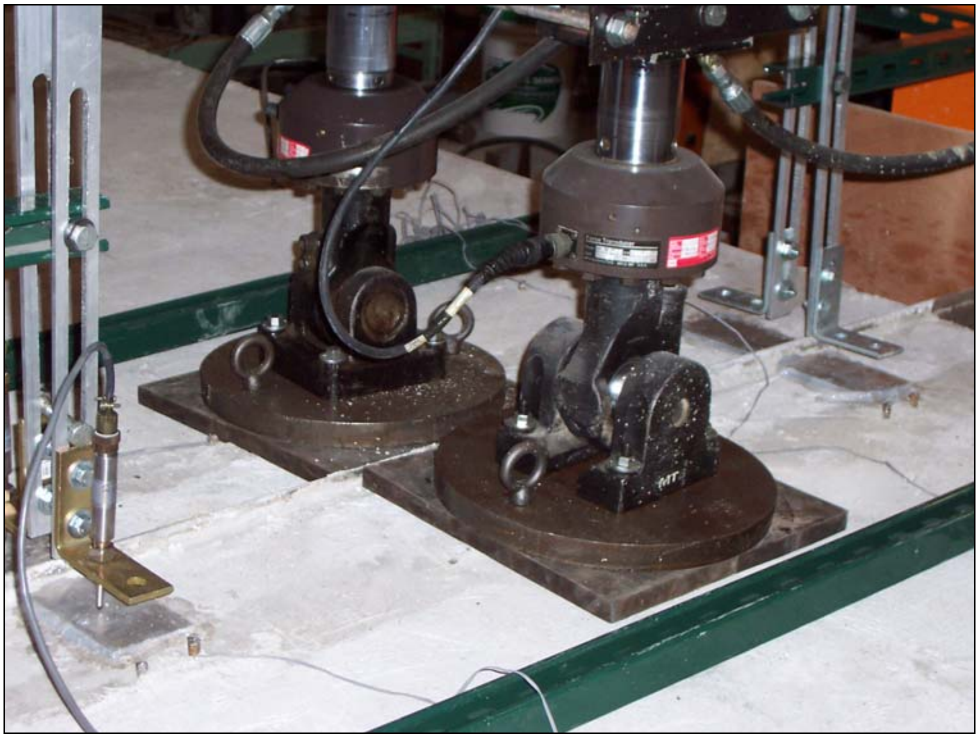

Figure 4.3 Loading Actuator at Slab Joint during Trial Test

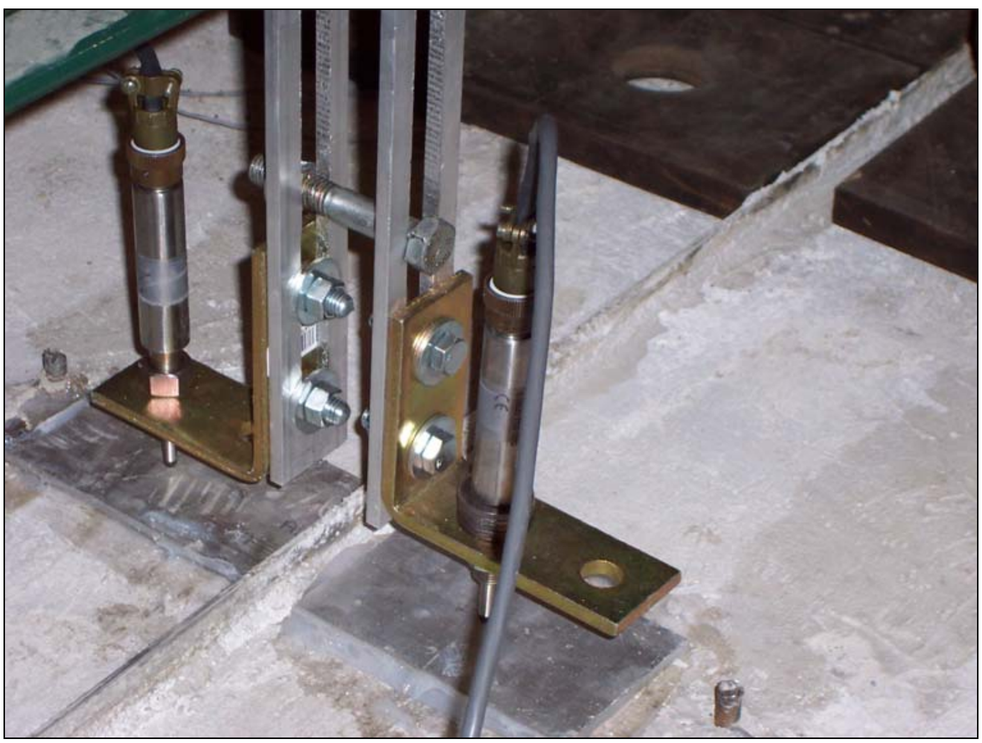

Figure 4.4 LVDTs Across Joint for Measuring Relative Deformation

Figure 4.5 Loading and Un-loading Sequence with LVDTs Across Joint

4.3 DETERMINING LOADING PULSE SHAPE

A main challenge in the full-scale slab test is to simulate moving multiple axle loads using two stationary hydraulic actuators. Researchers have divided the stress pulse for single axle as shown in Figure 4.6 (Colley and Humphrey, 1967).

A similar procedure was devised to divide the multiple axle pulses (tandem, tridem, quad and 8-axle trucks) using the DYNASLAB software program. The response (deflection) along both sides of the slab (nodes 198 and 211, see Figure 4.7) was calculated from the software for LTE 100% ($\approx 1 * 10^6$ psi) and 0% ($\approx 1 * 10^3$ psi). Figures 4.8 through Figure 4.13 show the shape of the deflection pulse at 100% and 0% LTE. At 100% LTE the deflection pulse from both sides of the slabs (nodes 198 and 211) are identical due to the continuity of the slab whereas at 0% LTE the deflection pulse is discontinuous and mirror each other. The response from each side of the slab represents the actuator action during the cyclic test. It should be noted that the response showed in Figure 4.8 through Figure 4.13 represent the deflection pulse which can be converted to force. The maximum deflection peak within the deflection pulse corresponds to 6.5 kips (half of the axle load within a multiple axle group). The tandem axle load was also simulated on the dummy sample (trial slab). However, the response from the LVDTs did not seem to represent the tandem axle.

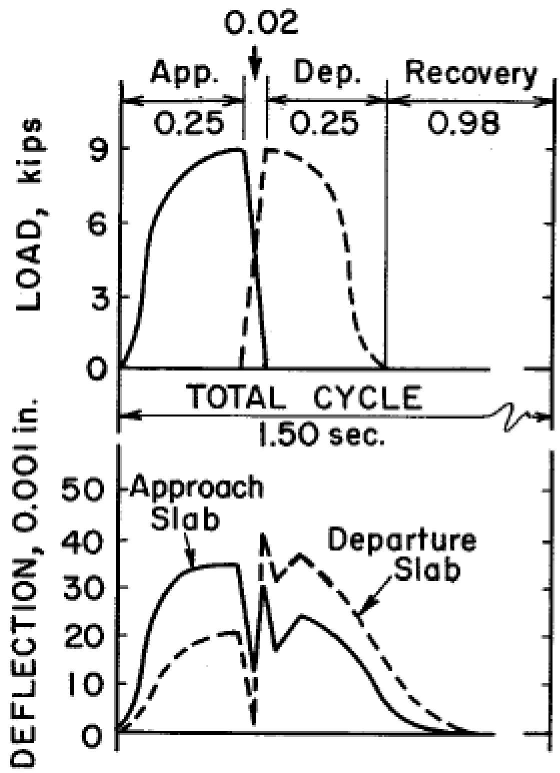

Figure 4.6 Divided stress pulse for single axle and its response (Colley and Humphrey, 1967)

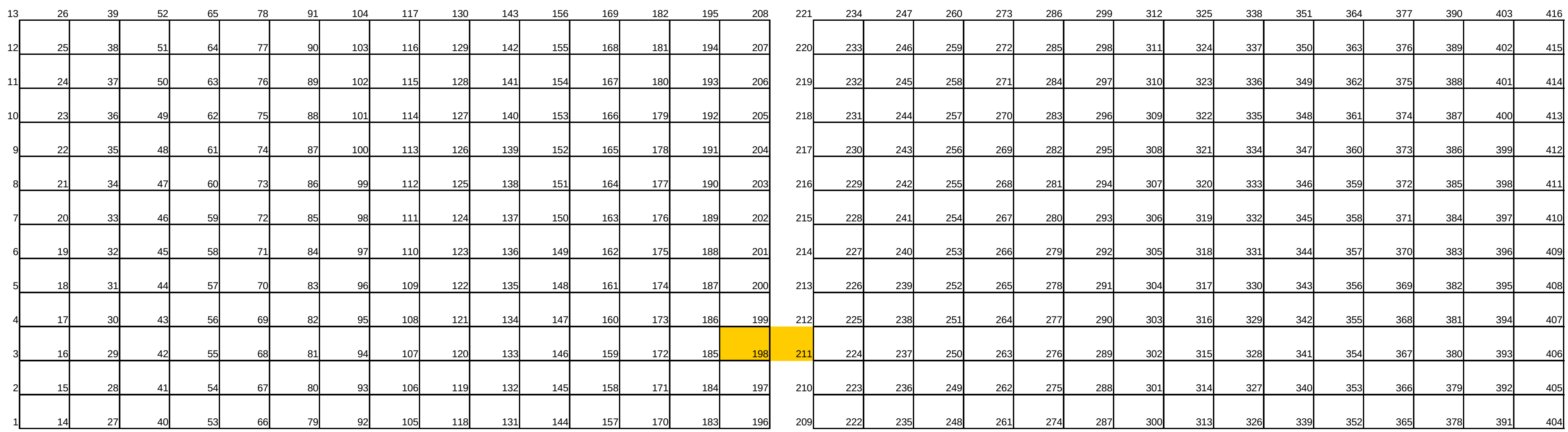

Figure 4.7 Nodes and elements for the first two slabs

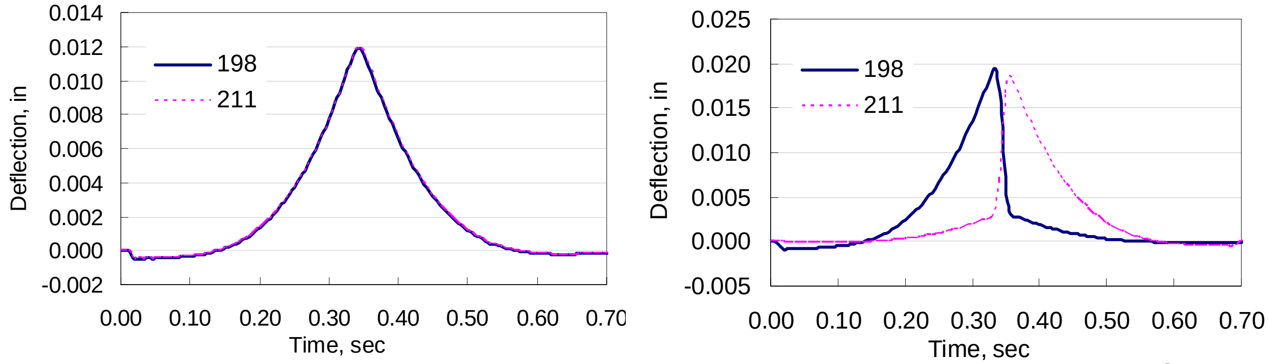

(a) Aggregate interlock factor = 1* 10^6 psi (b) Aggregate interlock factor = 1* 10^3 psi

Figure 4.8 Response under Single axle

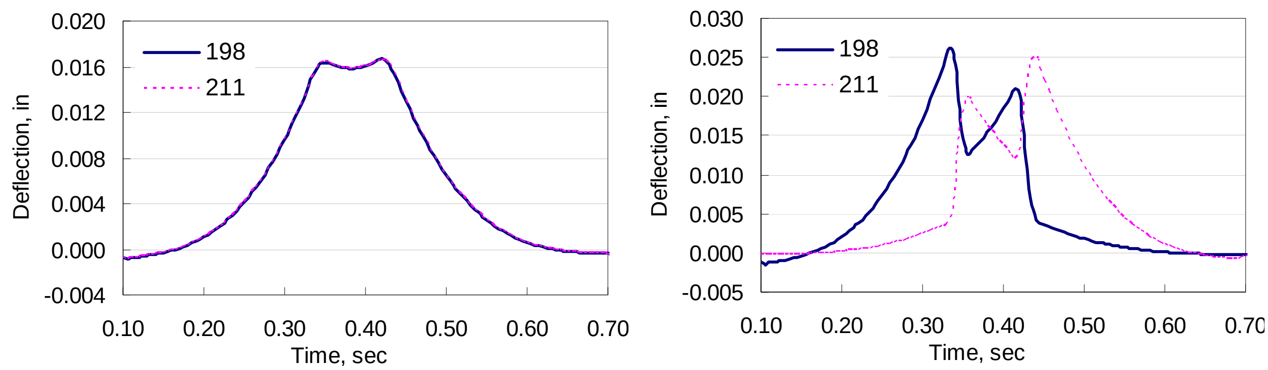

(a) Aggregate interlock factor = 1* 10^6 psi (b Aggregate interlock factor = 1* 10^3 psi

Figure 4.9 Response under Tandem axle

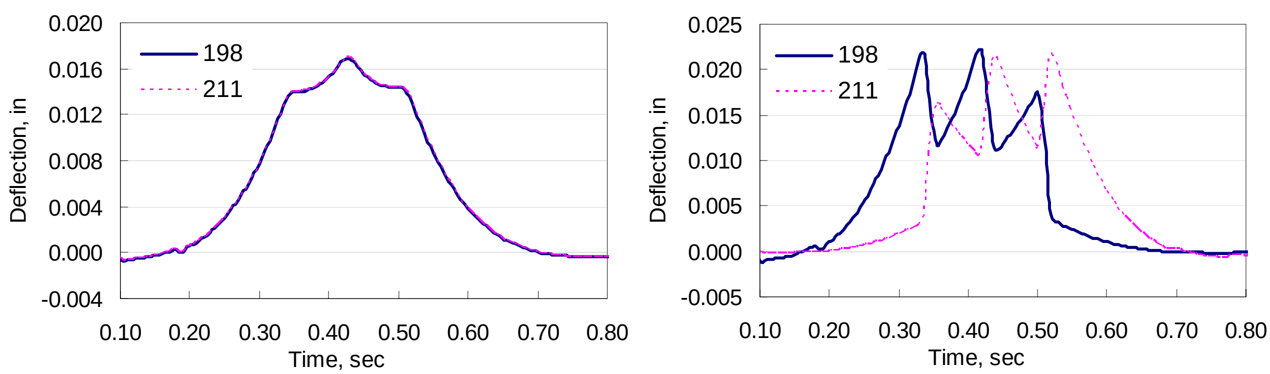

(a) Aggregate interlock factor = 1* 10^6 psi (b) Aggregate interlock factor = 1* 10^3 psi

Figure 4.10 Response under Tridem axle

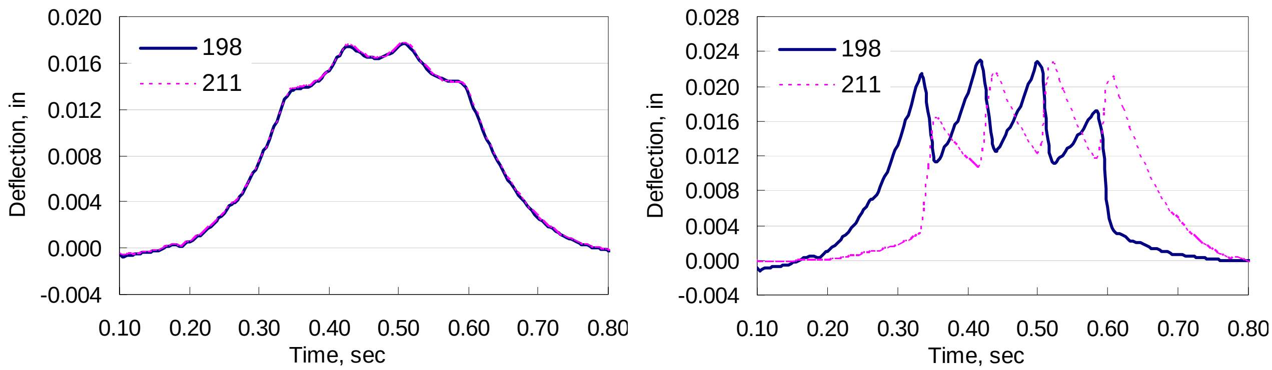

(a) Aggregate interlock factor = 1* 10^6 psi (b) Aggregate interlock factor = 1* 10^3 psi

Figure 4.11 Response under Quad axle

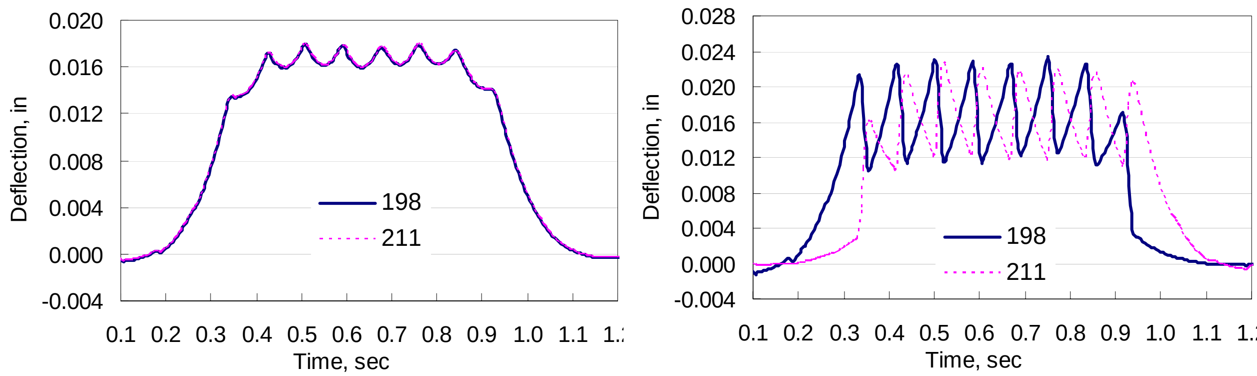

(a) Aggregate interlock factor = 1* 10^6 psi (b) Aggregate interlock factor = 1* 10^3 psi

Figure 4.12Response under Eight-axle group

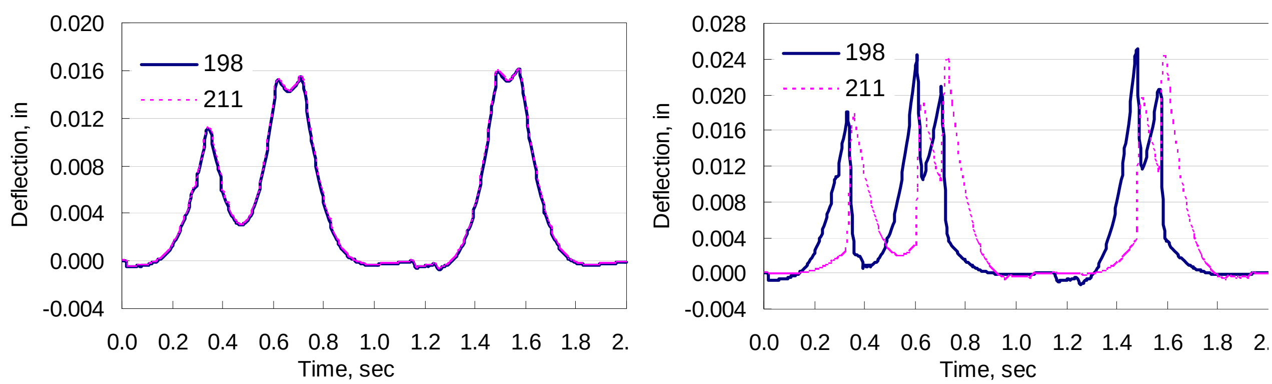

(a) Aggregate interlock factor = 1* 10^6 psi (b) Aggregate interlock factor = 1* 10^3 psi

Figure 4.13 Response under Truck S1T2

4.4 CRACK WIDTH IN THE TEST SLAB

The initial plan was to cast the slab as one piece 5 ft wide by 14 ft long with a 1-inch notch at the top and bottom at the middle of the slab, as shown in Figure 4.14. The slab was then to be pulled by a horizontal force to create a crack at the middle of the slab. Previous literature shows that the effectiveness of the joint is very sensitive to the width of the crack. Figure 4.15 (Colley and Humphrey, 1967) shows the effect of crack width versus N_f. If the crack width is too tight, (crack width = 0.025 inch) the LTE will take a longer time to decay than if the crack width is too wide (crack width = 0.085inch). The most reasonable crack width ranges from 0.035 to 0.065 inch.

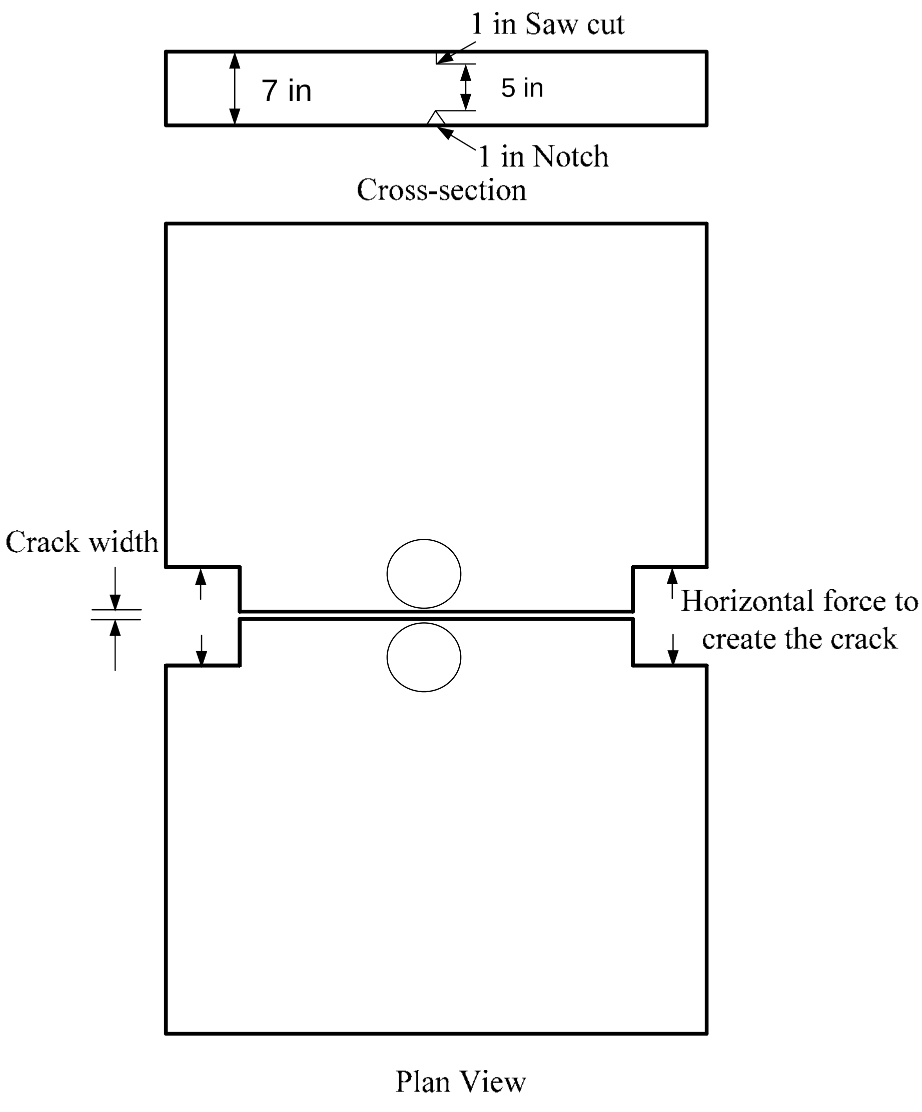

Figure 4.14 Plan and cross section of the slab

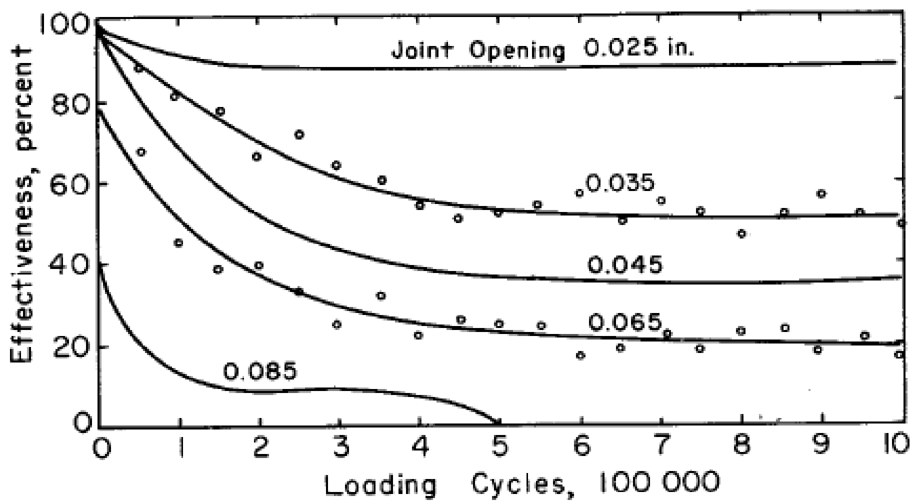

Figure 4.15 Relationship between effectiveness and N_f (Colley and Humphrey, 1967)

4.5 DOUBLE CRACK CYCLIC LOAD TEST

One of the main drawbacks of a full-scale slab test is the replication of the test specimens. Due to the inordinate amount of time it takes for the slab to harden, prepare, and actually test, there cannot be many replicates given the time constraint. An alternative for a full-scale test is a mini-test to investigate the effect of multiple axles load on crack deterioration. Several researchers have used similar tests in the past: Valle and Buyukozturk, 1993, Millard and Johnson, 1984, and White and Holley, 1972, Arnold et al, 2005. The research team proposed to use a double crack cycling load test. In this test, two cracks will be induced on a beam similar to the one used in the flexural fatigue test; the broken beam will be held together. A series of multiple pulses that simulate the axle configuration will be applied to the middle part of beam until failure occurs. Failure can be defined as a limiting amount of vertical movement in the middle part of the beam. Figure 4.16 and Figure 4.17 show a similar test setup from previous research (White and Holley, 1972, Arnold et al, 2005).

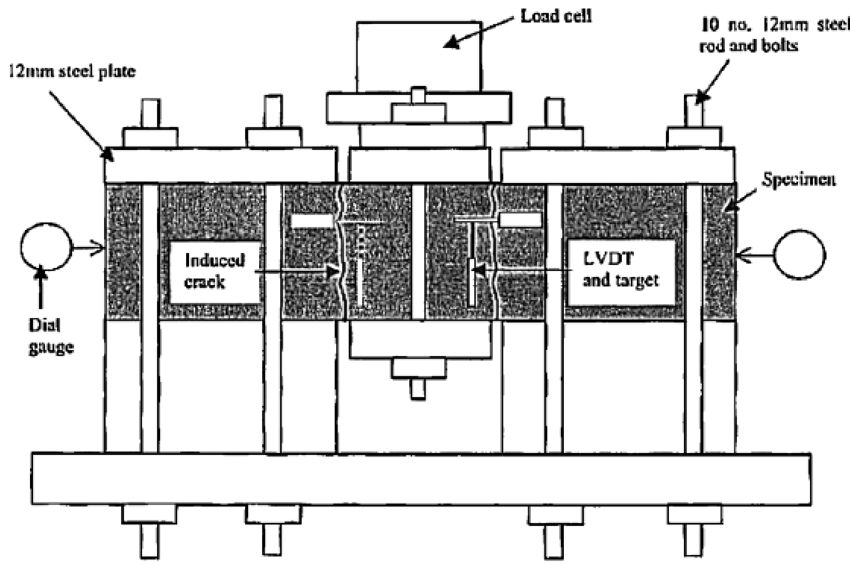

Figure 4.16 Double crack test set-up for cyclic loading (White and Holley, 1972)

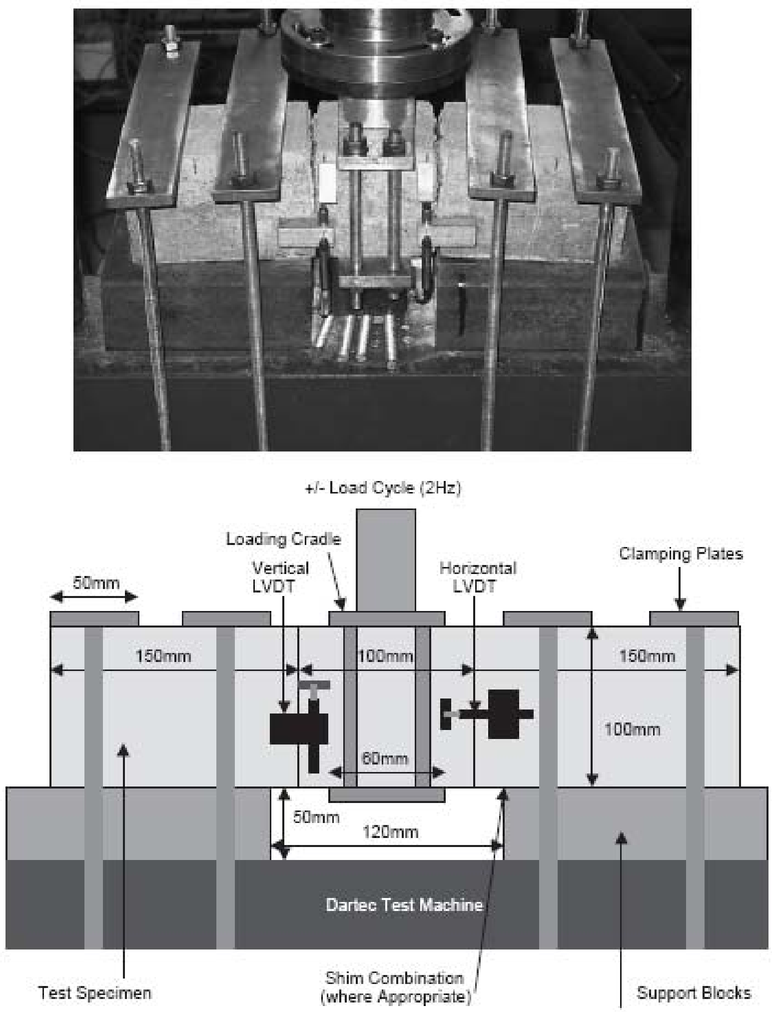

Figure 4.17 Test set up for double crack cyclic loading (Arnold et al, 2005)

4.6 MEASURES FOR JOINT DETERIORATION

(a) Load Transfer Efficiency

Three different measures to quantify the deterioration were used. The first measure was Load Transfer Efficiency (LTE), which has the following relationship:

$$LTE = \frac{\delta u}{\delta l} \tag{4.1}$$

Where δu = deflection of the unloaded slab
δl = deflection of the loaded slab

(b) Joint Efficiency

The second measure was Joint Efficiency (JE), which has the following relationship:

$$JE = \frac{2\delta u}{\delta u + \delta l} \tag{4.2}$$

This relationship relates the unloaded deflection to the total deflection experienced by both sides of the slab.

(c)Differential Energy

The third measure that was used was differential energy (DE) per stiffness K, which has the following relationship:

$$DE = \frac{1}{2}K\left(\delta_l{}^2 - \delta_u{}^2\right)$$, which can be re-written as:

$$\frac{DE}{K} = \frac{1}{2}\left(\delta_l - \delta_u\right)\left(\delta_l + \delta_u\right) \tag{4.3}$$

This measure can be a good indicator of the load transfer efficiency and its relationship to faulting. The reason is because this quantity accounts for differential deflection (compared to a ratio, which does not account for the magnitude of the deflections themselves) and is scaled by the total deflection. For example, if using LTE or JE to calculate the transfer efficiency for two deflections of 1 mil (unloaded side) and 2 mils (loaded side), the LTE would be equal to 50%, the JE would be equal to 66.67 % and the DE would be equal to 3 mils^2. If the deflections were to change to 10 mils and 20 mils respectively (10 times the initial deflection), the LTE would remain at 50% and the JE would also remain at 66.67%. The DE however, would change dramatically to 300 mils^2 thus signifying that it accounts for the magnitude of the deflection and could be a good indicator of potential faulting.

4.7 CASTING AND TESTING OF THE SLABS

The first slab was cast on 11/13/06. The crack, along the center of the slab, was formed 24 hours after casting. Figure 4.18 shows the crack along the depth at the center of the slab. The crack was created in the laboratory by lifting each end of the slab with a crane until a visible crack appeared along the depth located at the center of the slab.

Figure 4.18 Close-up of induced crack. Left: North Side of Slab; Right: South Side of Slab

The LVDT's, also shown in the figure, are located 3 ½ in. away from the crack at either side. They were used to measure the deflection at either side of the joint. Testing of the slab began 14 days after casting.

4.7.1 Single-Axle

The pavement was subjected to 40,000 single axle cycles over a period of 15 hours. The research team closely monitored the response of the slab over these 40,000 cycles. Readings were taken at cycle number 1, 50, 500, 1000, 3000, 6000, 10000, 15000, 20000, 30000, and 40000. An LTE test was conducted after the 40,000 cycles were completed. This was done by applying a 9 kip load on either side of the crack, simulating an FWD in the field. Figure 4.20 illustrates the test setup showing the leave and approach slabs, and the north and south directions.

4.7.1.1 First Reading - 1st Cycle

Figure 4.21 shows the deflection on both the leave slab and approach slab located on the south corner of the joint under one single axle cycle. The figure illustrates that the deflections on either side of the crack are relatively equal.

(a) Slab Test set-up

(b) Close-up of actuators and LVDT's

Figure 4.19 Test setup showing actuators and LVDT's on the slab

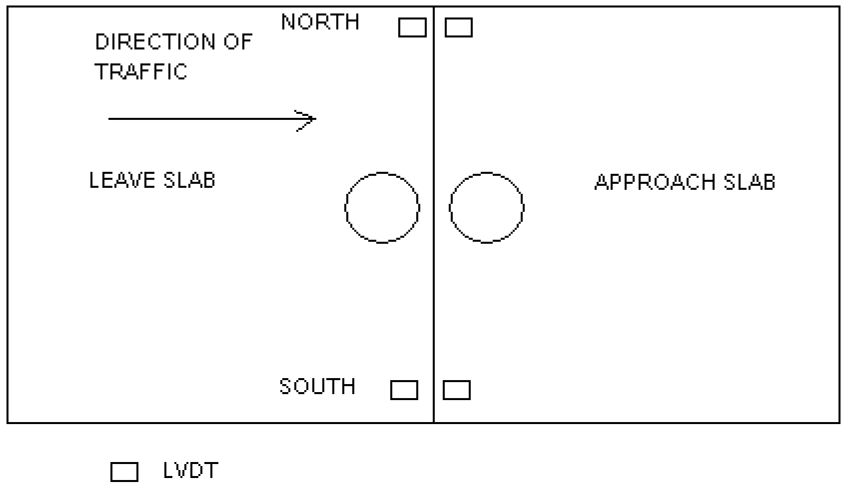

Figure 4.20 Schematic of Slab and Orientation of LVDTs

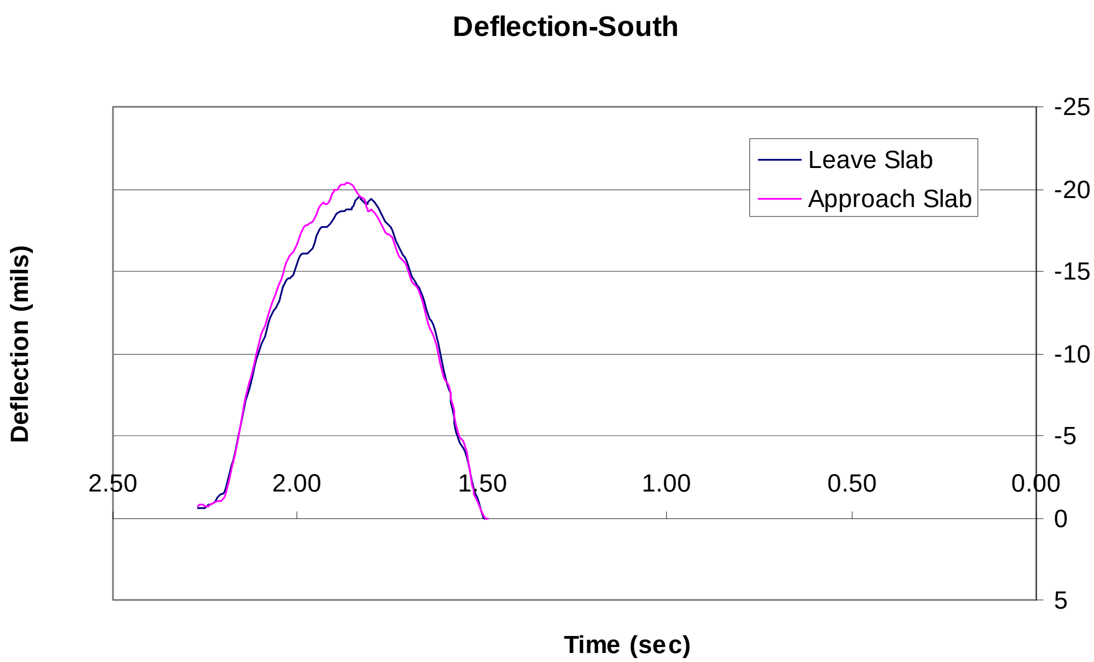

Figure 4.21 Deflection of South Corner of the Joint

The deflection on the north corner of the joint was not as uniform as the south corner of the slab. As shown in Figure 4.22, the displacement on the leave side of the slab is greater than the approach side over the entire duration of the cycle.

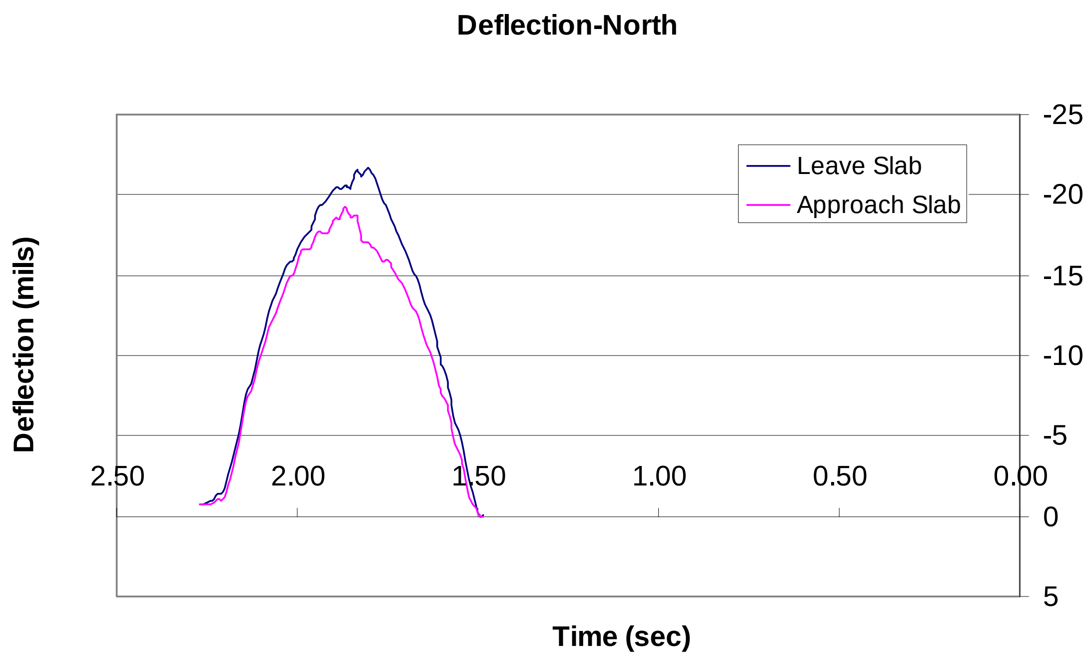

Figure 4.22 Deflection of North Corner of Joint

This result does not seem to be reasonable because when the load is applied to the approach slab it should deflect more. There are at least two reasons why this may be occurring:

1. The crack is locking into place when the load on the leave slab reaches its peak, thus not allowing the leave slab to slip back upwards.
2. The LVDT was out of range, causing erroneous results.

4.7.1.2 Joint Deterioration

An LTE reading was taken before the test began and after 40,000 cycles. Tables 4.1 and 4.2 show the LTE before testing and after 40,000 cycles.

Table 4.1 LTE values before testing

		North				
Cycles		δ_{Leave}	$\delta_{Approach}$	LTE	Average	Average of Both Sides
0	Applied Load-Leave	-21.34	-16.77	0.79	0.93	**0.94**
	Applied Load-Approach	-20.47	-19.19	1.07		
		South				
		δ_{Leave}	$\delta_{Approach}$	LTE	Average	
	Applied Load-Leave	-19.19	-18.51	0.97	0.94	
	Applied Load-Approach	-18.65	-20.22	0.92		

Table 4.2 LTE values after 40,000 cycles

		North				
Cycles		δ_{Leave}	$\delta_{Approach}$	LTE	Average	Average of Both Sides
40,000	Applied Load-Leave	-22.51	-17.72	0.79	0.94	**0.94**
	Applied Load-Approach	-21.64	-19.88	1.09		
		South				
		δ_{Leave}	$\delta_{Approach}$	LTE	Average	
	Applied Load-Leave	-21.37	-19.29	0.90	0.95	
	Applied Load-Approach	-20.75	-20.94	0.99		

4.7.1.3 Alternative Deterioration Analysis

When investigated further, the dissipated energy (area in between the stress-strain/displacement curves) may be able to explain the deterioration more accurately than the LTE. As shown in Figure 4.23, the dissipated energy has not increased over 40,000 cycles. The only thing that has occurred is a shift in the displacement (permanent deformation), but the area has remained relatively unchanged. After 40,000 cycles, no deterioration of the joint was detected. Thus, the research team decided to modify the test setup, as discussed in the following section.

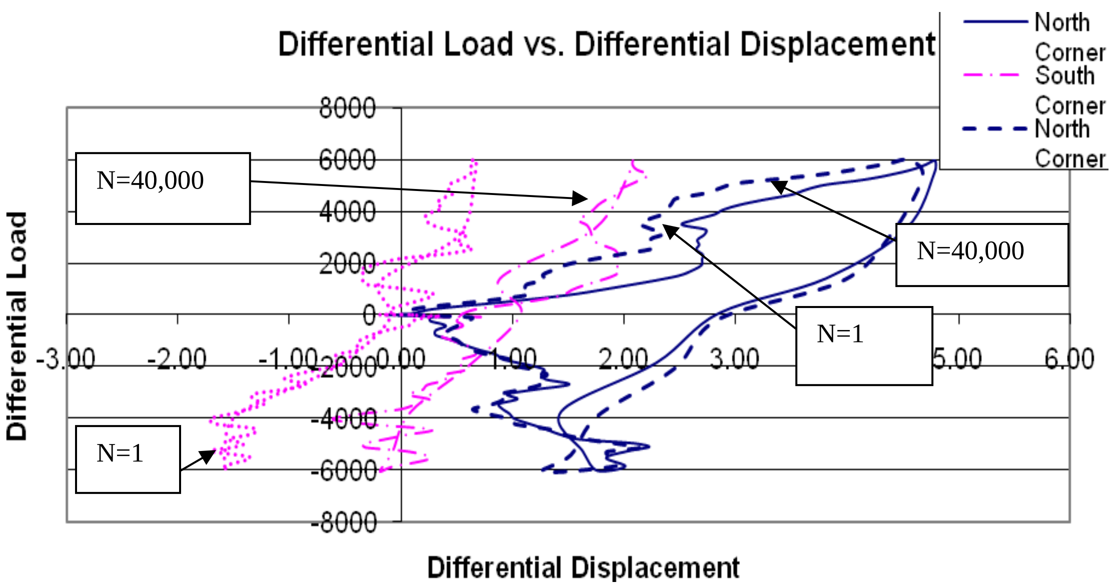

Figure 4.23 Differential Load vs. Differential Displacement – Dissipated Energy

4.8 Test Setup Modification

During the test, the research team noticed that the slab appeared to be rotating rigidly (rather than deforming). This rigid rotation caused the crack opening to fluctuate over a given loading cycle. Figure 4.24 shows this behavior in terms of the change in crack opening over time. As the load is applied, the slab rotates and causes the joint to close. As the joint closes, it's stiffness (resistance to deflection) and durability increases dramatically. Therefore, the crack opening must be held constant throughout the test.

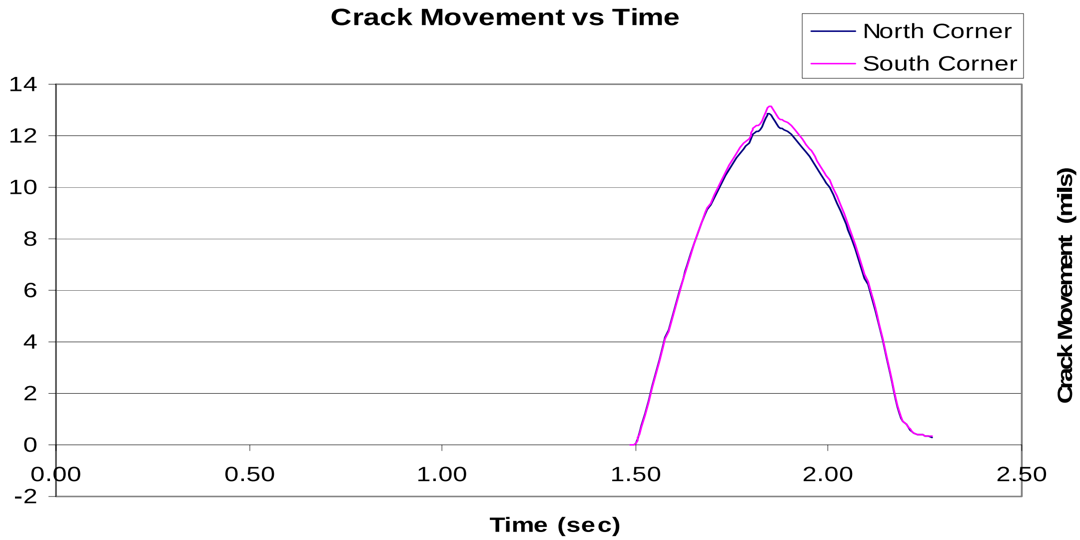

Figure 4.24 Movement of Joint Opening Under One Load Cycle

In order to prevent this crack movement, the research team designed a restraining system that was placed at either end of the slab. This would simulate real field conditions because in reality, the slab is restrained in all directions by a series of other slabs (through tie rods, dowel bars and/or aggregate interlock): One 10 ft long 14 in x 6 in steel tube was placed over the slab at each end (see figure 4.25). Two 5 ft post-tensioned concrete blocks were also placed behind the slab on either end (see figure 4.26). The steel tubes were designed to restrain the vertical displacement at the end of the slab and the concrete blocks were designed to prevent any horizontal displacement. The steel tubes were fastened to threaded rods that were post-tensioned to the floor. Two steel channels were fastened to the concrete blocks and three steel rods were made to pass through them and were forced up against the outer edge of the slab.

Figure 4.25 Steel Tube (14x6) Placed at the End of the Slab

Figure 4.26 Threaded Rods Forced Against the Ends of the Slab

After the design and placement of the restraint system, a cyclic eight-axle pulse was applied on the slab. The slab did not displace vertically or horizontally at its back edge (based on actual measurements). Unfortunately, because the slab was restrained so well (relatively no movement was recorded at the back edge of the slab), it caused a crack in the middle of both slabs (leave and approach) just after a few cycles, as shown in Figure 4.27.

Figure 4.27 Crack in the middle of the slab caused by the restraints

There could be several reasons why this crack may have occurred under this loading and restraint system:

1. Tightening of the steel tube (restraint) may have been excessive. This could cause part of the slab to rise, causing a gap between the slab and the base.

2. The base was not compacted well enough:
    i. Loss of support under the load causing a gap between slab and base.
    ii. This may have been exacerbated by the plastic sheeting underneath the slab (the plastic sheeting was used to prevent the infiltration of concrete into the base). The concrete was therefore not allowed to bond with the base.

Therefore, the test setup was again modified. Two jacks were placed on both ends of the slab (replacing the old restraint system) to improve the control of the crack opening. Figure 4.28 shows these jacks at both ends of the slab.

Figure 4.28 Photo of Jacks placed on both sides of the Slab

4.9 SLAB TESTS

Slab 2 was cast on 5/31/07 and slab 4 was cast on 7/9/2007. The crack for both slabs, were initiated 16 hours after casting. Figures 4.29 and 4.30 show the crack along the depth at the center of the slab for slab 2 and slab 4, respectively. The crack was initiated in the laboratory by pushing both ends of the pocket located at the north and south ends at mid-slab, with a hand operated hydraulic jack. The crack at the edges does not follow a clean vertical pattern. However, it should be aligned with the crack initiation groove since no visible crack at the surface (near the groove). Therefore, initiating the crack in this manner properly simulates the tensile stress field at mid-slab caused by shrinkage and thermal movements. Testing of both slabs began 7 days after casting.

Figure 4.29 Close-up of induced crack for slab 2. Left: North Side; Right: South Side

Figure 4.30 Close-up of induced crack for slab 4. Left: North Side; Right: South Side

4.9.1 Slab 2 Test Results

4.9.1.1 Single Axle

Slab 2 was tested under a single axle loading sequence for 551,000 cycles. An FWD load was applied every 10,000 cycles and the displacements on either side of the cracks were monitored. Figure 4.31 shows the Load Transfer Efficiency, Joint Efficiency, and Differential Energy of the joint with respect to the number of cycles.

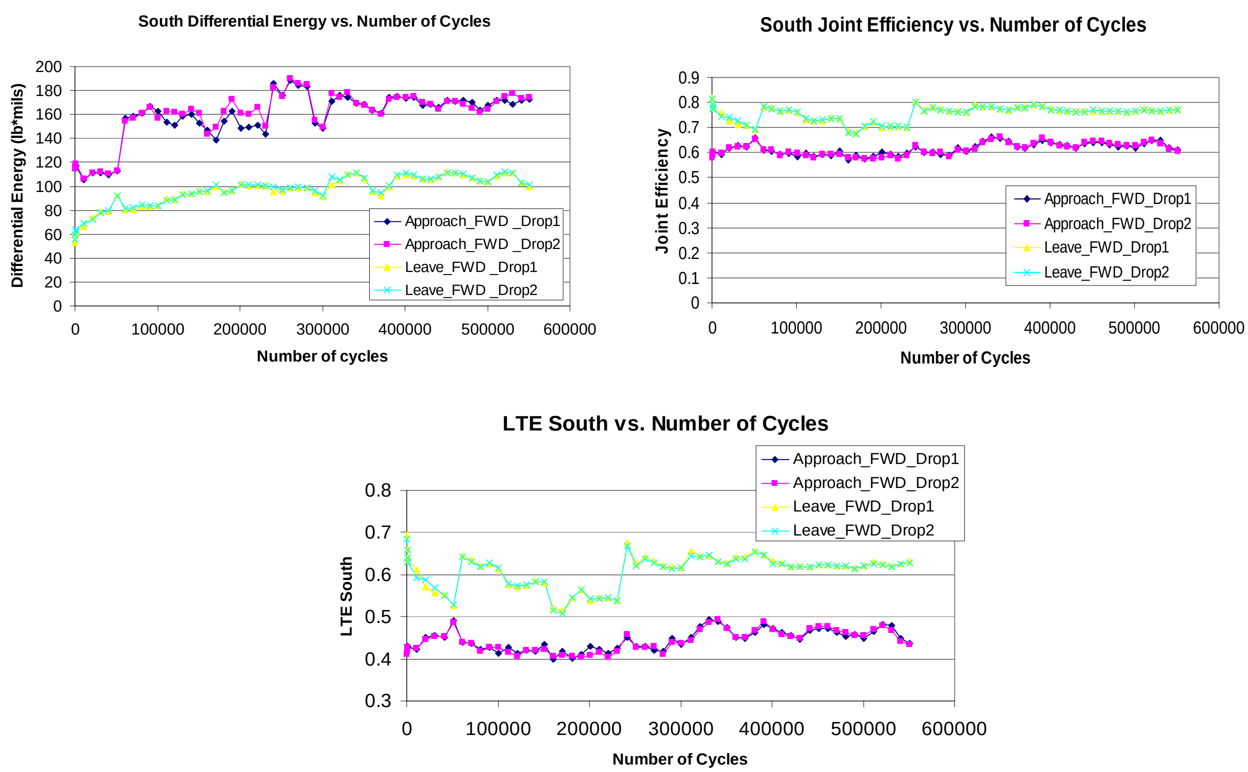

Figure 4.31 DE, JE and LTE at Southern End of the Crack under Single Axle – Slab 2

After 550,000 cycles, the crack did not appear to have deteriorated. Both the LTE and the JE were essentially constant. The Differential Energy was increasing slightly. This is most likely due to the increase in total deflection of the slab (unloaded and loaded). The leave side FWD drop in all cases produced higher load transfers (80% JE, 60% LTE, and 160 mils^2) as compared to the Approach FWD drop (60% JE, 45 % LTE, and 100 mils^2). This can be caused by the crack orientation. If the crack is not completely vertical, different transfer efficiencies may be produced depending on the location of the applied load.

In each of the three figures, there are visible jumps in transfer efficiency at several points. This jump appears to be occurring after each instance the test was stopped and restarted. Thus, it appears that the initial transfer efficiencies may not accurately represent the true characteristics of the crack. It seems that the system must stabilize itself (after a few thousand cycles) to allow for consolidation/compaction of the underlying base layer. Once that is achieved, accurate results can be tabulated.

4.9.1.2 Tandem Axle

After the single axle test was complete, a tandem axle loading sequence was implemented because relatively no deterioration was observed from the single axle test. The tandem axle was tested for 200,000 cycles. An FWD load was applied every 10,000 cycles and the displacements on either side of the cracks were monitored. Figure 4.32 shows the Load Transfer Efficiency, Joint Efficiency, and Differential Energy of the joint with respect to the number of cycles.

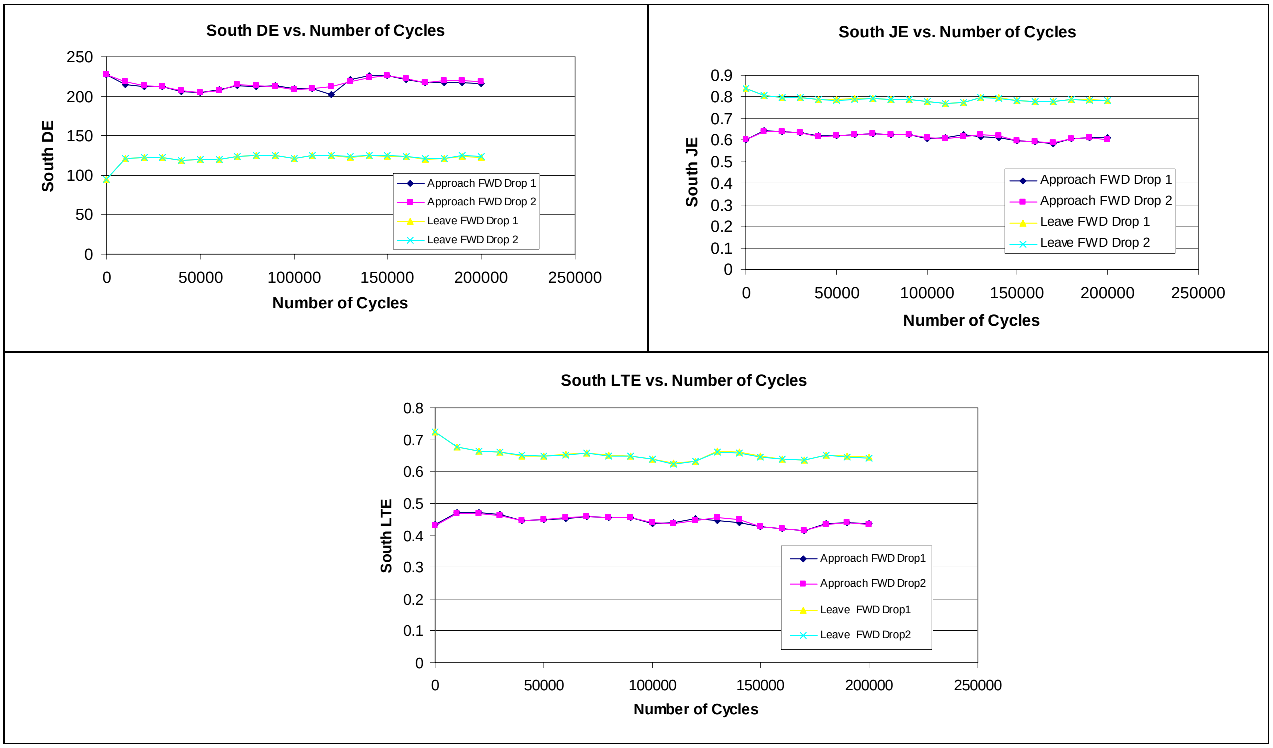

Figure 4.32 DE, JE and LTE at Southern End of the Crack under Tandem Axle – Slab 2

The Differential Energy under the tandem axle does not appear to be changing after 200,000 cycles. The Joint Efficiency and the Load Transfer Efficiency appear to have decreased slightly.

After 750,000 cycles of both single and tandem axle loading, no significant deterioration has been detected. Thus, in Slab 4, a tighter crack (0.035 in) was used to ensure a higher initial Load Transfer Efficiency and ultimately greater *potential* for deterioration.

4.9.2 Slab 3

Slab 3 was cast on 7/3/07. The research team attempted to initiate the crack 16 hours after casting using the same procedure for slabs 2 and 4 described previously. When the hydraulic jacks were pushing on both sides of the pocket, a crack was initiated approximately 8 inches from mid-slab. The slab was rendered useless because the crack was not sitting in between the west and east actuators. Thus, the slab was discarded and slab 4 was cast 6 days later.

Upon further review of the incident, it became clear as to why the crack did not initiate at mid-slab. The reason was because the steel reinforcement at the corner of the pocket was not placed properly. Figure 4.35 shows a photograph of the slab after it cracked.

4.9.3 Slab 4 Test Results

4.9.3.1 Single Axle

With the new restraining system in place (the jacks on the east and west ends of the slab), the research team was able to attain an accurate crack width measurement of 0.035 inch on both the south and north side of the crack. The crack width was measured with both an LVDT and a caliper. Both measuring devices confirmed a surface crack width of 0.035 in.

A single axle loading pulse was implemented for 250,000 cycles. After 250,000 cycles, as shown in Figure 4.33, none of the transfer efficiency measures seemed to be changing over this number of cycles.

The Differential Energy is much smaller when compared to the previously analyzed slab ($4.5 \ll 220$ mils^2). Both the Joint Efficiency and Load Transfer Efficiency are also much greater, with values hovering close to 100% throughout 250,000 cycles.

Since no damage was observed, an eight axle loading pulse was applied to test the feasibility of any potential crack deterioration for this crack width.

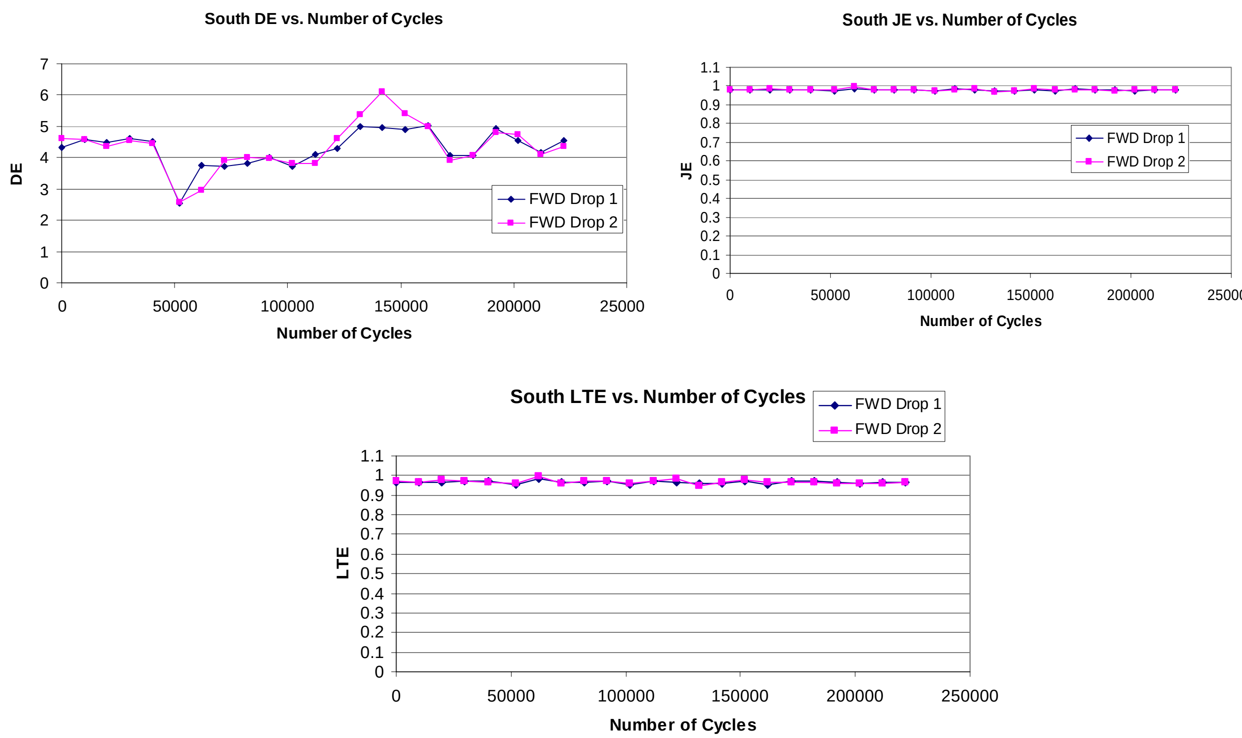

Figure 4.33 DE, JE, and LTE at Southern End of the Crack under Single Axle – Slab 4

4.9.3.2 Eight Axle

The eight axle loading sequence was tested for 135,000 cycles. An FWD load was applied every 2,500 cycles and the displacements on either side of the cracks were monitored.

Similar behavior to the single axle was observed. The Load Transfer Efficiency values were once again hovering just under 100% over the 135,000 cycles and the Differential Energy once again was essentially constant. Figure 4.34 illustrates this behavior. Note that while the fluctuations in the DE values appear to be high, they are in fact acceptable given their low magnitudes.

Since no deterioration was observed in any of the tests thus far, modifications had to be made again. The crack width in Slab 4 was increased slightly to 0.040 inches, in the hope that this will cause the slab deterioration to accelerate. However, this did not resolve the problem. As a final resort, it was decided to remove the dense base underneath the slab, and only leave the natural sand as the foundation material. Although this clearly does not reflect MDOT practice, it was done in the hope of accelerating the damage, and mainly understanding why joint deterioration was not occurring.

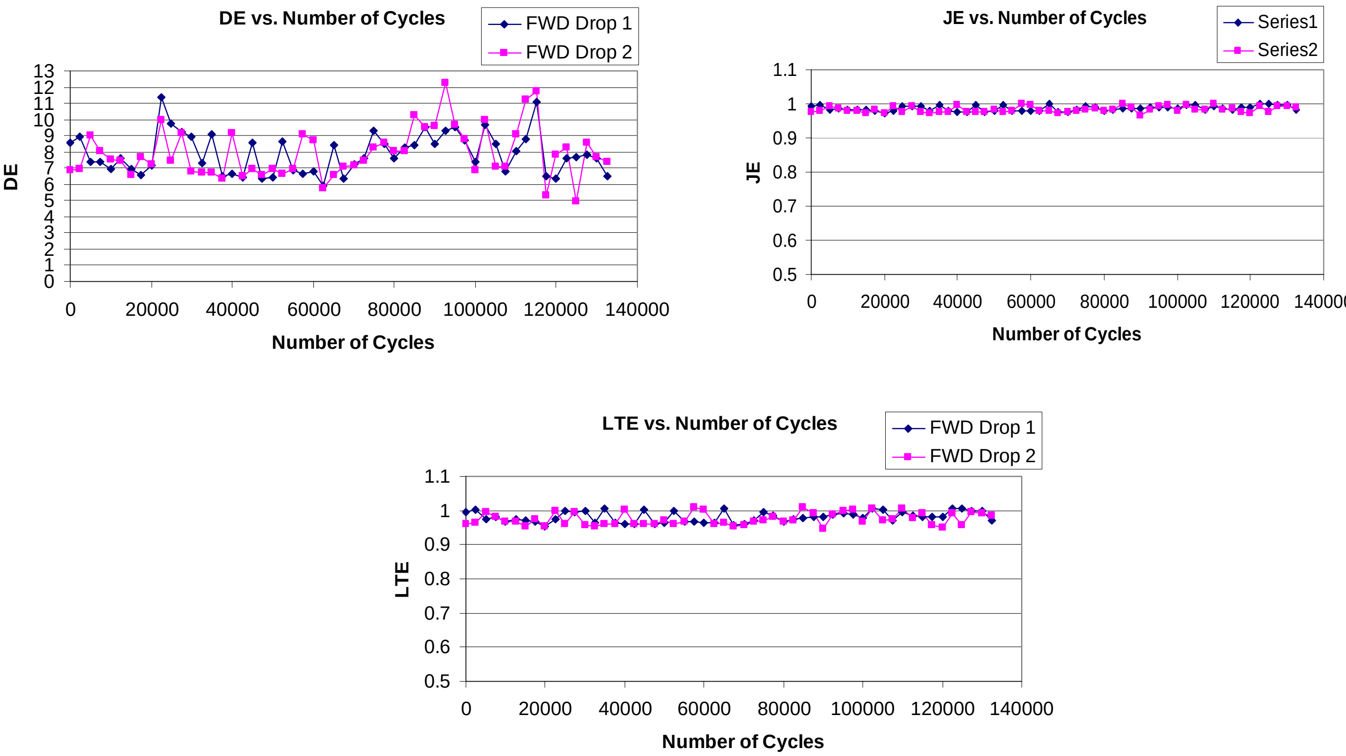

Figure 4.34 DE, JE, and LTE at Southern End of the Crack under Eight-Axle – Slab 4

Figure4.35. Photo of Slab 3 Crack

4.9.4 Slab 5

Before the casting of slab 5, the 4G base that was used in previous tests was removed from the test box and replaced with a sand base (2NS). This was done to make the base more flexible to accelerate the damage induced onto the crack.

Slab 5 was cast on September 24, 2007. The induced crack was formed 20 hours after the casting. The width of the crack was 0.045 inches. Figure 4.36 shows the crack on the north and south end of the joint, respectively.

Figure 4.36 Slab 5 - Left: North Side of Crack, Right: South Side of Crack

A 6500 lb single axle load was applied onto the pavement through the two hydraulic actuators mentioned in previous reports. The first series of tests ran for 300,000 cycles. The differential deflection on either side of the slab was monitored every 10,000 cycles. Figure 4.37 shows the Load Transfer Efficiency on the north side of the crack with respect to the number of cycles. No deterioration was observed in the crack after the 300,000 cycles. This is contrary to the findings of the PCA research where deterioration was observed after several hundred thousands cycles.

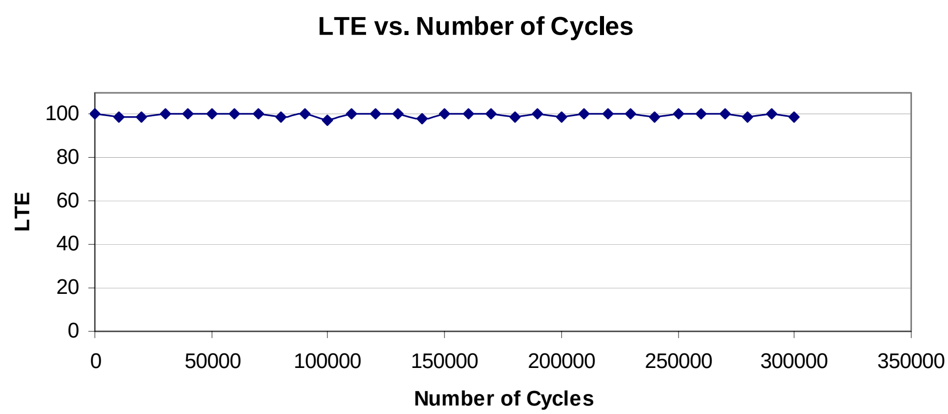

Figure 4.37 Load Transfer Efficiency vs. Number of Cycles under 6,500 lb peak load

Thus, the load was increased to 10,000 lbs from 6,500 lbs. After 200,000 cycles, once again, no deterioration was observed. Figure 4.38 shows the LTE versus number of cycles under the 10,000 lb load and new crack width.

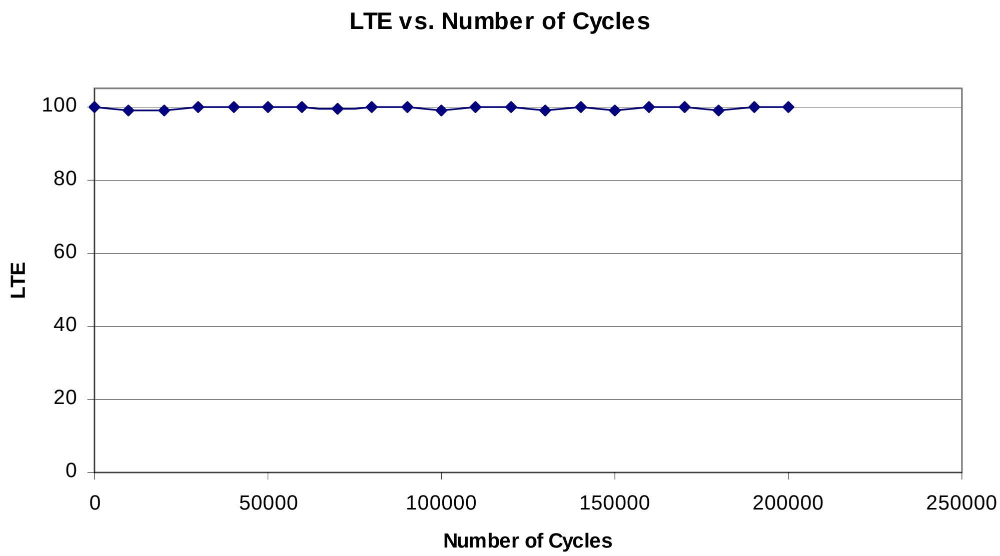

Figure 4.38 Load Transfer Efficiency vs. Number of Cycles under 10,000 lb peak load

Since no deterioration was observed through the first 500,000 cycles, the crack was re-opened and closed to 0.035 inches. After this was done, the next series of tests were conducted, and the initial LTE dropped significantly (100% to 85%). The jacks on either end of the slab were also loosened in order to release some lateral pressure that may have caused excessive restraint and retard the degradation of the crack. There was an additional 220,000 cycles applied to the slab. Figure 4.39 shows the LTE versus the number of cycles after re-opening and closing the crack. As shown below, the LTE initially started at 80 %, then dropped to approximately 70 % and remained at 70 % for the next 200,000 cycles. The reason it started at 80 % was most likely because the system had yet to stabilize. Once the system did stabilize, the LTE was 70% for the remaining 200,000 cycles. Over 720,000 cycles have been applied to the slab without any observed deterioration of the crack.

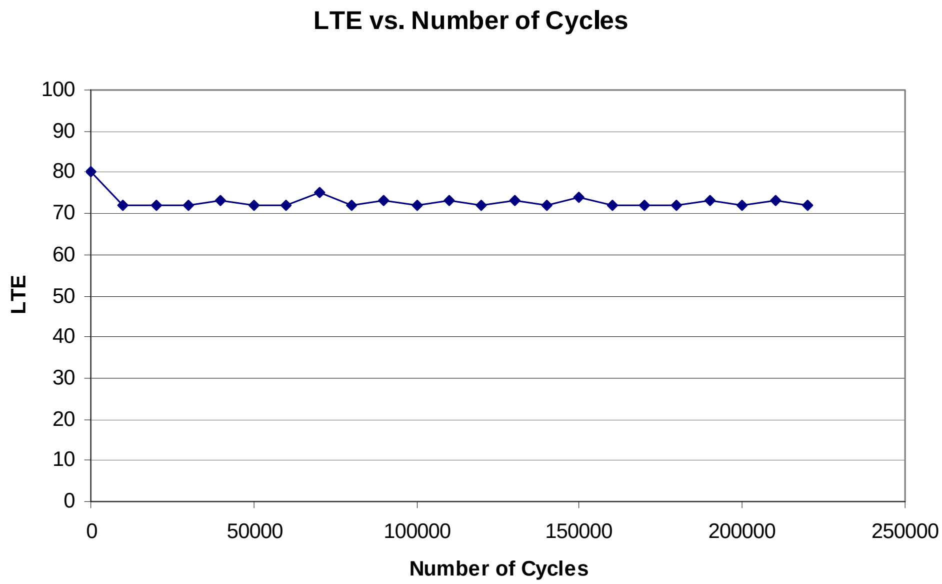

Figure 4.39 LTE vs. Number of Cycles after re-opening crack

4.10 SMALL SCALE CRACK DETERIORATION TEST

A small scale test setup was developed to test the crack deterioration of a 4 in by 4 in by 24 in beam specimen. The test is designed to simulate the behavior of a joint/crack in a concrete pavement. The details of the setup were mentioned earlier in this chapter. Figure 4.40 shows photographs of the test setup.

Figure 4.40 Test setup for the small scale crack deterioration test

The beams were cracked at two places, eight inches from either end. This created three equal portions. Each portion of the cracked beam was then clamped down to the MTS frame in preparation for the test. The total crack width was measured with a caliper.

Several modifications are still needed for the test setup before the experiment can be carried out. However, there was not enough time to implement these changes and conduct the tests. The research team plans to continue this effort beyond the end of the project.

4.11 SUMMARY

Several efforts were made to conduct full-scale slab testing in the laboratory to investigate the crack deterioration behavior under multiple axle loadings. This involved designing and building a test bed and a test frame with two large capacity actuators placed on each side of the crack. The passage of different multiple axle groups across a crack was simulated by imposing two separate loading functions for each actuator. These functions were obtained using the DYNASLAB computer program. Tests were carried out on five slabs with several modifications made for each subsequent test to try to achieve crack deterioration. However, the cracks did not show any appreciable deterioration despite the large number of load repetitions applied.

A small-scale test setup was developed to test a cracked beam under multiple axles using a small capacity MTS machine. However, because of lack of time, this testing could not be completed.

CHAPTER 5
FAULTING – MECHANISTIC ANALYSIS

5.1 INTRODUCTION

In parallel with the laboratory experiments, an analysis was performed using the computer program DYNASLAB to determine the relative damage to the jointed plain concrete pavements (JPCP) caused by trucks with different axle configurations. Chapter 3 presented the analysis in relation to fatigue in JPCP pavements. In this chapter the focus of analysis is on faulting in JPCP pavements. Four different types of trucks, as shown in figure 5.1, were considered in the analysis.

5.2 FAULTING ANALYSIS UNDER MULTIPLE AXLES

5.2.1 Detailed Sample Analysis for Calculating Axle and Truck Factors

The slab chosen in the analysis was 16 feet long and 12 feet wide with a thickness of 10 inches. These are the same dimensions as for the slabs used in fatigue analysis.

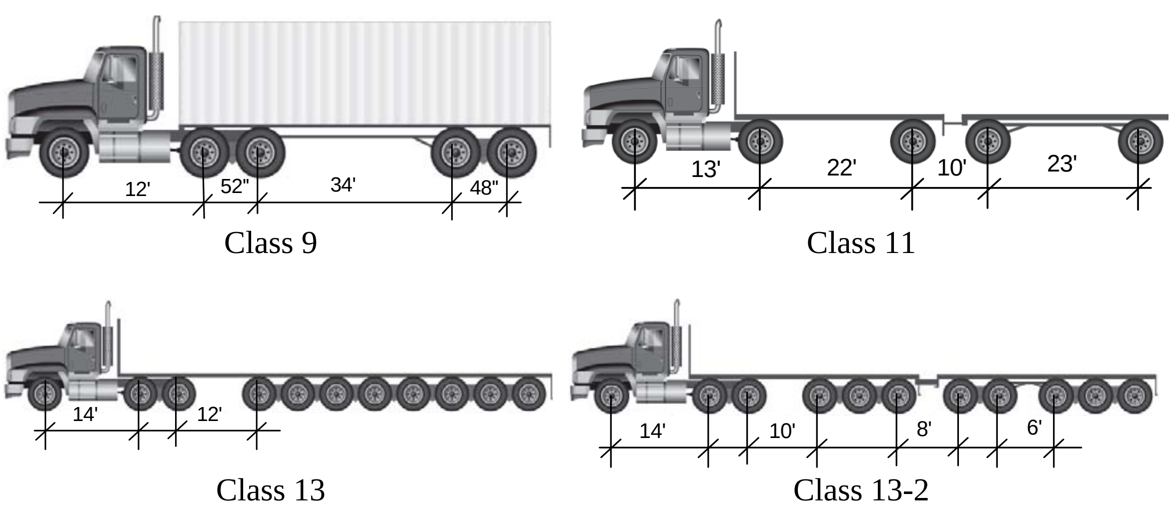

Figure 5.1 Types of trucks used in faulting and fatigue analyses

Loading per axle as applied in this analysis was as follows:

– Steering axle: 15,400 lbs
– Single axle: 18,000 lbs
– Tandem axle: 16,000 lbs
– Tridem and higher axles: 13,000 lbs

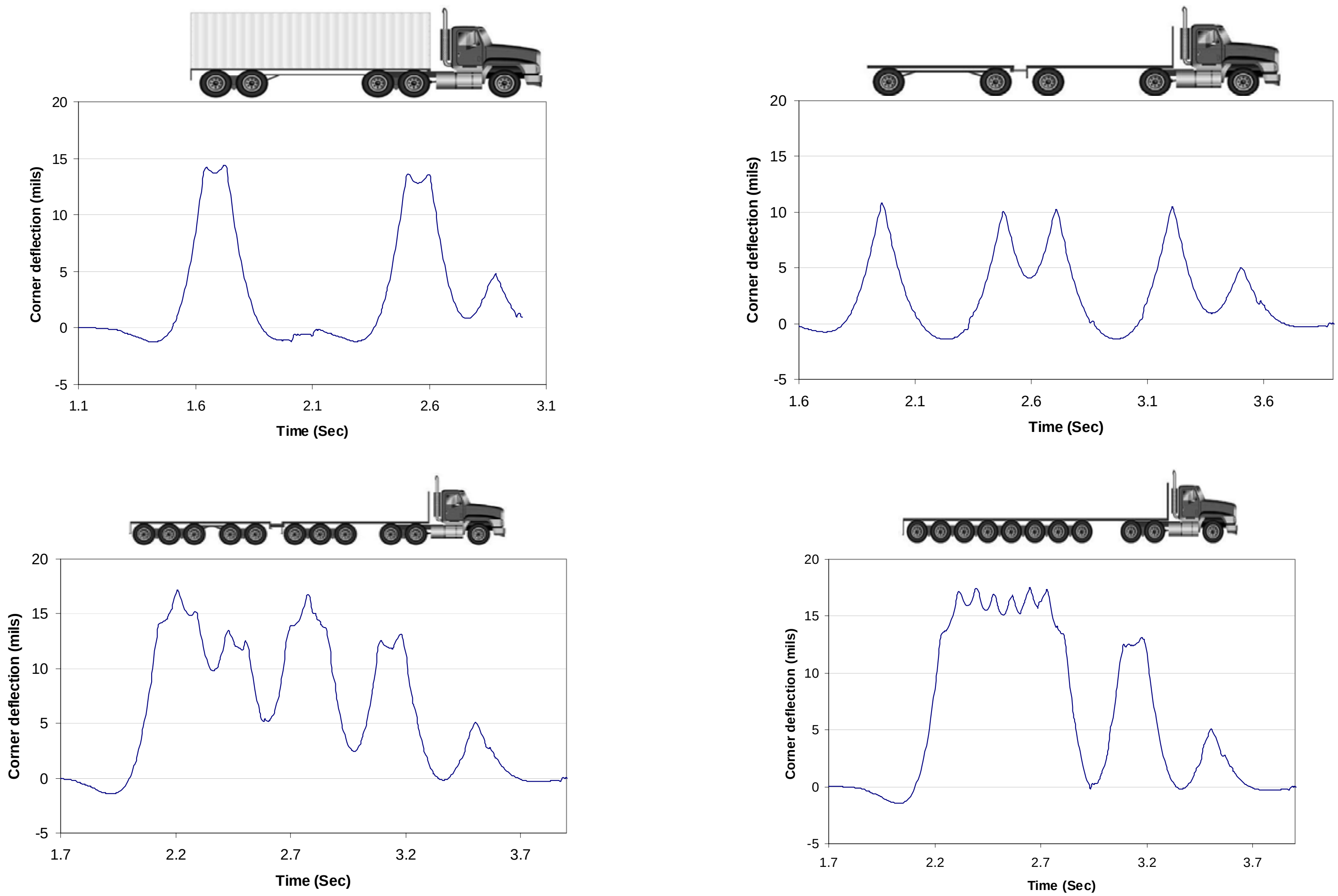

Figure 5.2 Corner deflections under various Michigan truck axle configurations

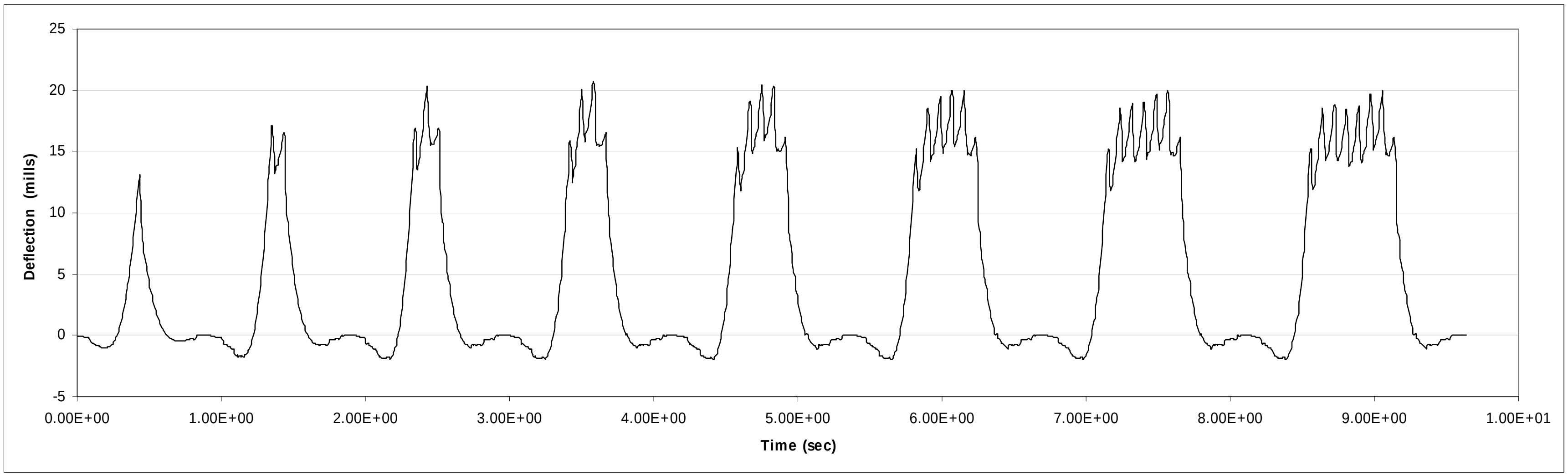

Figure 5.3 Corner deflections under different axle groups (13 kips per axle)

DYNASLAB can provide magnitudes of stresses and deflections throughout the concrete slab under a moving load. Table 5.1 shows the corner deflections in the slab obtained from the program for the above mentioned truck types.

Table 5.1 Corner deflections in concrete slab under different moving trucks (100% LTE)

Truck Type	Gross wt.	Corner Deflections (1e-4 inches)										
		Axle 1	Axle 2	Axle 3	Axle 4	Axle 5	Axle 6	Axle 7	Axle 8	Axle 9	Axle 10	Axle 11
Class 9	79400	118	162	168	177	175						
Class11	87400	124	142	142	139	149						
Class 13	151400	126	161	157	137	172	175	167	169	174	171	139
Class 13-2	151400	127	160	156	135	166	139	126	135	152	172	143

The model adopted by M-E PDG for faulting requires several steps (NCHRP, 2004). The key relationships for determining incremental faulting are shown below.

$$DE_{MONTH} = \sum_{A=1}^{3} \sum_{i=1}^{N_A} n_{i,A} \left(k_{MONTH} \frac{\delta_{L,i,A}^2}{2} - k_{MONTH} \frac{\delta_{U,i,A}^2}{2} \right)$$

where

DE_{MONTH} = Differential energy density of subgrade deformation accumulated for month MONTH.

$\delta_{L,i,A}$ = Corner deflections of the loaded slab caused by axle loading.

$\delta_{U,i,A}$ = Corner deflections of the unloaded slab caused by axle loading.

$n_{i,A}$ = Number of axle load applications for current increment and load group *j*.

N_A = Number of load categories for the axle type A.

$$\Delta Fault = C_{34} * (FMAX_{MONTH-1} - FAULT_{MONTH-1})^2 * DE_{MONTH}$$

where

$\Delta Fault$ = Increment of faulting accumulated for month MONTH.

$FAULT_{MONTH-1}$ = Magnitude of faulting at the beginning of month MONTH.
= 0 if MONTH =1.

$FMAX_{MONTH-1}$ = Maximum faulting parameter at the beginning of month MONTH.
= $FMAX_0$ if MONTH =1.

DE_{MONTH} = Differential energy density of subgrade deformation accumulated for month MONTH.

$C_{34} = C_3 + C_4 * FR^{0.25}$

FR = Base freezing index.

C_3 and C_4 are calibration parameters:

C_3 = 0.001725

C_4 = 0.0008

The above relationships show that for the sake of comparing faulting caused by different types of axles/trucks, faulting can be taken to be roughly proportional to the square of the corner deflection. Using this relationship, axle factors for each axle in the four truck configurations were calculated as the ratio of squared deflection of the given axle over that of the standard axle, and are presented in table 5.2. The rearmost axle in the truck representing class 11 having 18,000 lbs load was used as the reference single axle. Summation of the axle factors for each truck gives the truck factor. Since different classes of trucks carry varying axle and gross vehicle loads, each truck factor was divided by the gross vehicle weight (GVW) so that a truck factor per weight carried can be used for comparing the trucks. Also, to be able to compare the trucks relative to each other, the truck factor per unit gross weight was normalized using the class 9 truck as the reference truck. Table 5.3 shows details of these calculations.

Table 5.2 Axle factors for different trucks based on faulting

		Axle Factors										
	Gross wt.	Axle 1	Axle 2	Axle 3	Axle 4	Axle 5	Axle 6	Axle 7	Axle 8	Axle 9	Axle 10	Axle 11
Class 9	79400	0.63	1.18	1.27	1.41	1.38						
Class11	87400	0.69	0.91	0.91	0.87	1.00						
Class 13	151400	0.72	1.17	1.11	0.85	1.33	1.38	1.26	1.29	1.36	1.32	0.87
Class 13-2	151400	0.73	1.15	1.10	0.82	1.24	0.87	0.72	0.82	1.04	1.33	0.92

Table 5.3 Truck factors (faulting) normalized for the gross vehicle weight (100% LTE)

Truck Type	Gross wt.	Truck Factor	TF/GVW	Normalized TF/GVW
Class 9	79400	5.87	7.39E-05	1.00
Class11	87400	4.38	5.01E-05	0.68
Class 13	151400	12.64	8.35E-05	1.13
Class 13-2	151400	10.74	7.09E-05	0.96

The analysis so far assumed 100% load transfer efficiency (LTE) across the joint. Similar analysis was performed for medium and low values of load transfer efficiency. Tables 5.4 and 5.5 show truck factors corresponding to these two cases.

Table 5.4 Truck factors (faulting) corresponding to medium aggregate interlock

Truck Type	Gross wt.	Truck Factor	TF/GVW	Normalized TF/GVW
Class 9	79400	5.59	7.04E-05	1.00
Class11	87400	4.54	5.20E-05	0.74
Class 13	151400	11.30	7.46E-05	1.06
Class 13-2	151400	10.07	6.65E-05	0.94

Table 5.5 Truck factors (faulting) corresponding to low aggregate interlock

Truck Type	Gross wt.	Truck Factor	TF/GVW	Normalized TF/GVW
Class 9	79400	5.15	6.48E-05	1.00
Class11	87400	4.69	5.36E-05	0.76
Class 13	151400	9.35	6.18E-05	0.88
Class 13-2	151400	9.01	5.95E-05	0.84

Table 5.6 Effect of load transfer efficiency on truck factors for faulting

Truck Type	100% LTE	Med LTE	Low LTE
Class 9	0%	-5%	-12%
Class11	0%	4%	7%
Class 13	0%	-11%	-26%
Class 13-2	0%	-6%	-16%

The above results show that class 13 trucks (with multiple axles) are more damaging in faulting than class 9 trucks, which comprise the majority of the truck population. Within class 13, the truck with the 8-axle group is the most damaging in faulting. The least damaging truck in faulting is that of class 11, which is comprised of single axles. Comparing the results in table 5.6, it can be seen that damage caused by multiple axle groups (classes 9 and 13) decreased as LTE decreased, while the reverse trend is observed for single axles (class 11). This could be explained by the fact that multiple axles can bridge between the leave and approach slabs, while single axles cannot do that.

5.2.2 Axle Factors for Different Configurations

Similar analysis was performed to compare faulting caused by different multi-axle groups. The trucks analyzed so far had only single, tandem, tridem and 8-axle groups. Also the weights on each individual axle in the axle group were different. In the following analysis axles groups with 1, 2, 3, 4, 5, 6, 7 and 8 axles were analyzed. Each axle in all the axle groups had 13 kip load. Medium aggregate interlock was used in this analysis. Tables 5.7 through 5.9 summarize the results.

Table 5.7 Corner deflections in concrete slab under different axle groups

Axle Group	Gross Axle Wt. (lb)	Corner Deflection (1e-4 inches)							
		Axle 1	Axle 2	Axle 3	Axle 4	Axle 5	Axle 6	Axle 7	Axle 8
1 Axle	13000	131							
2 Axles	26000	165	171						
3 Axles	39000	169	203	169					
4 Axles	52000	165	206	201	159				
5 Axles	65000	162	204	204	192	153			
6 Axles	78000	162	198	200	195	185	152		
7 Axles	91000	162	198	197	191	189	185	152	
8 Axles	104000	162	200	197	187	184	189	185	152

Axle factors for the axle groups show that multi-axles are much more damaging for the pavement as far as potential for faulting is concerned. Even when these axle factors are normalized for the weight carried by the axle-groups multi-axles are more damaging. All the axle groups with four or more axles are almost twice as damaging as the single axle when comparing the normalized axle factors. The reason behind having same normalized axle factors for axle groups with more than four axles is that the pavement slabs used in this analysis are 16 feet long. Therefore, at any time only four axles can be on the slab even if there are more axles in the axle group.

Table 5.8 Axle factors for different axle groups based on faulting

Axle Group	Gross Axle Wt.	Axle Factors							
		Axle 1	Axle 2	Axle 3	Axle 4	Axle 5	Axle 6	Axle 7	Axle 8
1 Axle	13000	1.00							
2 Axles	26000	1.59	1.70						
3 Axles	39000	1.66	2.40	1.66					
4 Axles	52000	1.59	2.47	2.35	1.47				
5 Axles	65000	1.53	2.43	2.43	2.15	1.36			
6 Axles	78000	1.53	2.28	2.33	2.22	1.99	1.35		
7 Axles	91000	1.53	2.28	2.26	2.13	2.08	1.99	1.35	
8 Axles	104000	1.53	2.33	2.26	2.04	1.97	2.08	1.99	1.35

Table 5.9 Axle factors (faulting) for different axle groups normalized for the gross vehicle weight

Axle Group	Gross Axle Wt.	Axle Group Factor	TF/GAW	Normalized TF/GAW
1 Axle	13000	1.00	7.69E-05	1.00
2 Axles	26000	3.29	1.27E-04	1.65
3 Axles	39000	5.73	1.47E-04	1.91
4 Axles	52000	7.89	1.52E-04	1.97
5 Axles	65000	9.89	1.52E-04	1.98
6 Axles	78000	11.70	1.50E-04	1.95
7 Axles	91000	13.62	1.50E-04	1.95
8 Axles	104000	15.55	1.50E-04	1.94

5.2.3 Truck Factors for Legal Load Limits

This analysis was extended to include the different axle load configurations at their legal load limits. Table 5.10 lists the corresponding axle factors for each axle group. Table 5.11 shows the final truck factors relative to a standard 18 kip single axle with dual wheels. The results show trucks with multi-axle groups to be more damaging in faulting as compared to those with single or tandem axles.

Table 5.10 Axle group factors (faulting) for legal load limits

Axle Group	Gross Axle Wt.	Axle factors								Axle factor (Group)
		Axle 1	Axle 2	Axle 3	Axle 4	Axle 5	Axle 6	Axle 7	Axle 8	
Front axle	**15400**	0.799								0.799
Single axle	**18000**	1.000								1.000
2 Axles - 16k	**32000**	1.199	1.286							2.485
2 Axles - 13k	**26000**	0.850	0.913							1.762
2 Axles - 9k	**18000**	0.442	0.406							0.848
3 axles	**39000**	0.891	1.286	0.891						3.069
4 Axles	**52000**	0.850	1.324	1.261	0.789					4.224
5 Axles	**65000**	0.819	1.299	1.299	1.151	0.731				5.298
6 Axles	**78000**	0.819	1.224	1.248	1.187	1.068	0.721			6.267
7 Axles	**91000**	0.819	1.224	1.211	1.139	1.115	1.068	0.721		7.297
8 Axles	**104000**	0.819	1.248	1.211	1.091	1.057	1.115	1.068	0.721	8.331

Table 5.11 Truck factors (faulting)

Truck	Truck No.	Total Wt. (kips)	Truck Factor
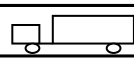	1	*33.4*	0.799
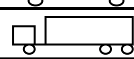	2	*47.4*	3.284
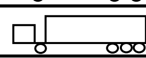	3	*54.4*	3.069
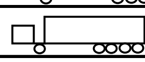	4	*67.4*	5.023
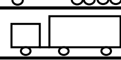	5	*51.4*	2.799
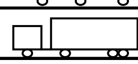	6	*65.4*	4.284
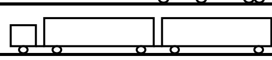	7	*87.4*	4.799
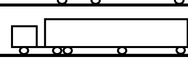	8	*83.4*	5.284
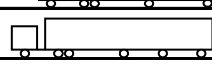	9	*101.4*	6.284
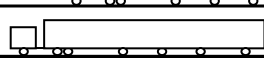	10	*119.4*	7.284
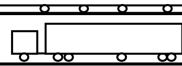	11	*91.4*	6.046
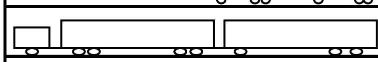	12	*117.4*	7.809
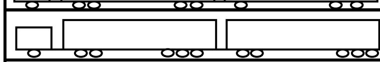	13	*151.4*	11.184
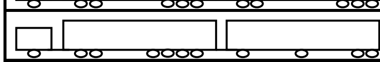	14	*161.4*	11.270
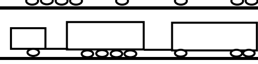	15	*117.4*	8.508
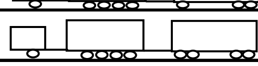	16	*125.4*	9.270
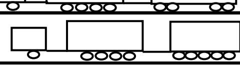	17	*132.4*	10.321
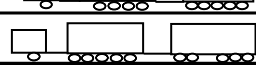	18	*143.4*	10.269
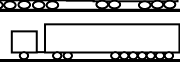	19	*138.4*	10.581
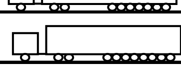	20	*151.4*	11.615
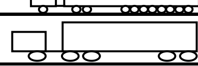	21	*79.4*	5.769

5.2.4 Faulting-based Truck Factors within AASHTO LEF Framework

This study was charged with determining the relative damage caused by multiple axles within an axle group; i.e., how much damage is caused by grouping multiple axles into one axle group. The scope of the study did not include verifying the AASHTO's "Fourth Power" damage law; i.e., we were not charged with determining how much damage is caused by increasing the load of a given axle relative to the standard 18-kip single axle. To do so would require extensive full-scale testing similar to what had been done in the original AASHO road test. Therefore, the TF's were obtained by converting multiple axle groups within each truck configuration into an equivalent number of single axles using the AF's obtained in this study, calculating the LEF of each axle group by multiplying the AF values obtained above (Table 5.8) with the Load Equivalency Factor (LEF) from AASHTO corresponding to the single axle at the legal load limit, and then summing the LEF of the different axle groups within a truck. This was done for different slab thicknesses. Table 5.12 summarizes the results.

Table 5.12 Truck Factors from Mechanistic AF and AASHTO LEF

			Truck Factors - Faulting (AASHTO Framework)					
			Slab thickness, D (in)					
Truck	Truck No.	Total Wt. (kips)	8	9	10	11	12	13
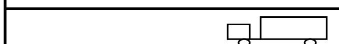	1	33.4	1.519	1.512	1.509	1.508	1.507	1.507
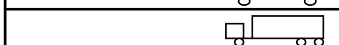	2	47.4	2.527	2.499	2.486	2.480	2.477	2.476
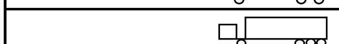	3	54.4	1.971	1.934	1.918	1.911	1.908	1.906
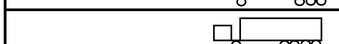	4	67.4	2.518	2.470	2.449	2.440	2.436	2.434
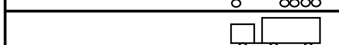	5	51.4	2.519	2.512	2.509	2.508	2.507	2.507
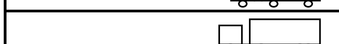	6	65.4	3.527	3.499	3.486	3.480	3.477	3.476
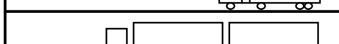	7	87.4	4.519	4.512	4.509	4.508	4.507	4.507
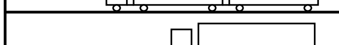	8	83.4	4.527	4.499	4.486	4.480	4.477	4.476
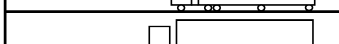	9	101.4	5.527	5.499	5.486	5.480	5.477	5.476
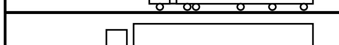	10	119.4	6.527	6.499	6.486	6.480	6.477	6.476
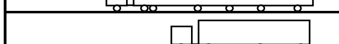	11	91.4	4.360	4.315	4.295	4.286	4.282	4.280
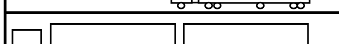	12	117.4	5.194	5.131	5.104	5.091	5.086	5.083
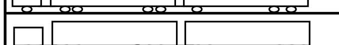	13	151.4	6.264	6.158	6.112	6.092	6.083	6.078
	14	161.4	7.359	7.272	7.234	7.218	7.210	7.206
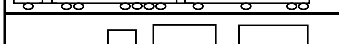	15	117.4	5.526	5.456	5.426	5.412	5.406	5.403
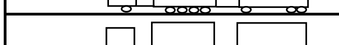	16	125.4	5.359	5.272	5.234	5.218	5.210	5.206
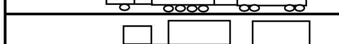	17	132.4	5.023	4.924	4.881	4.862	4.853	4.849
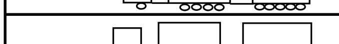	18	143.4	5.608	5.515	5.475	5.457	5.448	5.444
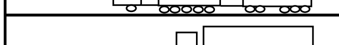	19	138.4	5.977	5.878	5.834	5.815	5.806	5.802
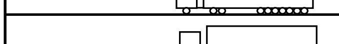	20	151.4	6.466	6.357	6.309	6.288	6.278	6.273
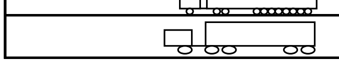	21	79.4	4.534	4.485	4.462	4.452	4.448	4.445

5.3 FAULTING PERFORMANCE WITH DIFFERENT AXLE GROUPS USING MEPDG

Similar to the analyses conducted for flexible pavements, the objective behind this analysis was to compare relative faulting damage to rigid pavements caused by the passage of different axle groups. To this end, four types of axle groups were separately simulated using MEPDG. The simulation was done using a 9 inch JPCP pavement with 8 inch thick granular base of A-1-b material as shown in figure 5.4. The traffic loading applied was equivalent to 4000 axle groups per day. Each run has only one type of axle group traffic. The axle groups simulated in this analysis were (a) Single, (b) Tandem, (c) Tridem and (d) Quad axles.

Figure 5.5 shows the performance curves output by M-E PDG. In the case of faulting, the M-E PDG predictions seem to generally agree with the fact that multiple axles are more damaging than single axles. However, there appears to be some discrepancy in the output for tandem axles. We have not been able to ascertain possible reasons behind this anomaly. There is a possibility that there is a bug in the MEPDG software which leads to erroneous output in the case of tandem axles.

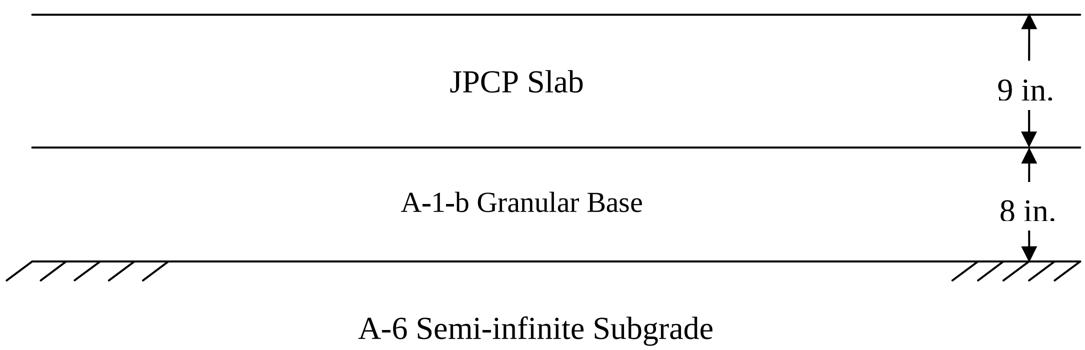

Figure 5.4 Pavement structure used in the MEPDG simulation

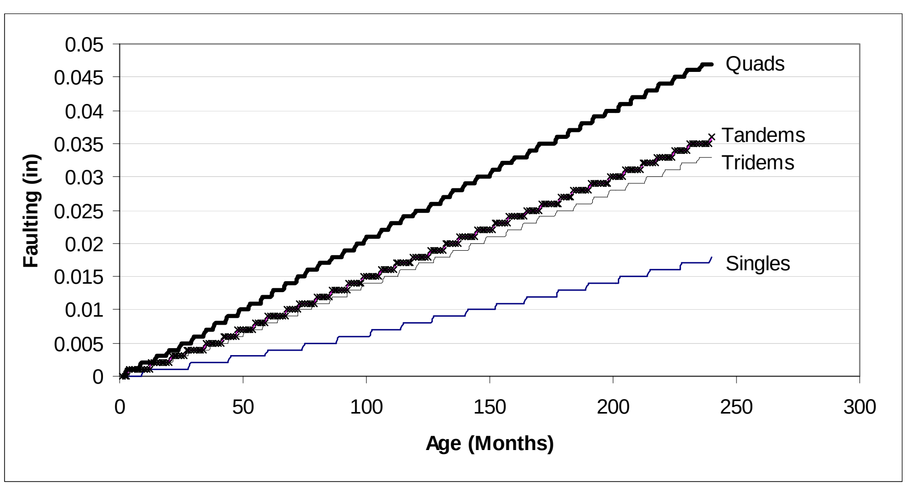

Figure 5.5 Faulting under different axle group loadings

CHAPTER 6

TRUCK FACTORS FOR RIGID PAVEMENT DESIGN

The truck factors (TF) presented in tables 2.8 and 5.12 in chapters 2 and 5 of this volume were calculated using the legal load limits for all the axles and trucks. However, not all the trucks using the roadways are always fully loaded. These truck factors could prove to be very conservative from a design point of view. Therefore, truck factors should also be calculated considering actual loads carried by the trucks in Michigan. Weigh-in-motion (WIM) data was collected from 42 weigh stations in Michigan for the year 2007. The data from these weigh stations were used to determine the axle load spectra for different classes of trucks. The load spectra were then used to calculate the average truck factor for all truck classes. This chapter presents details of this analysis.

6.1 WIM DATA

WIM data include weights of the individual axles and distances between them. WIM data from each station were analyzed to identify the axle groups and truck types based on standard axle configurations of trucks of different classes. The FHWA definition of truck class was used for this purpose and the trucks were classified into classes 5 through 13. Figure 6.1 shows the distribution of these trucks for a sample weigh station (File: W26829189) and Figure 6.2 shows the combined truck distribution of all the 42 weigh stations.

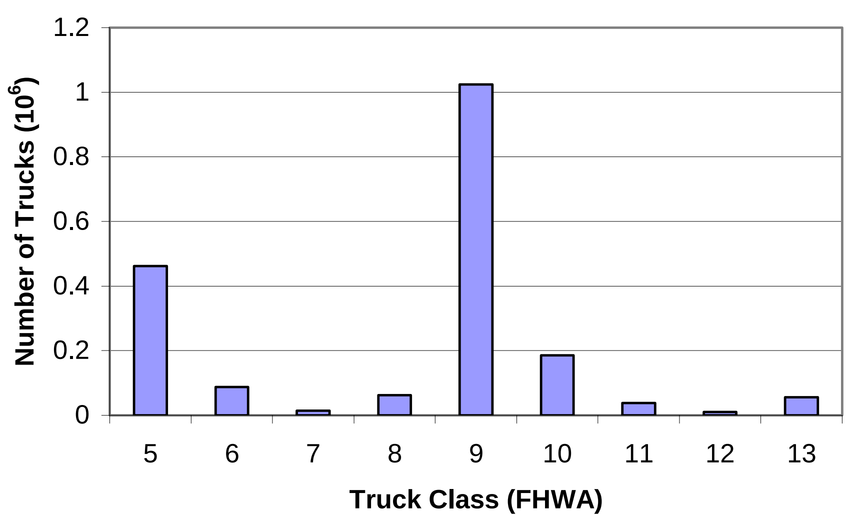

Figure 6.1. Truck distribution for sample weigh station W26829189 (year 2007)

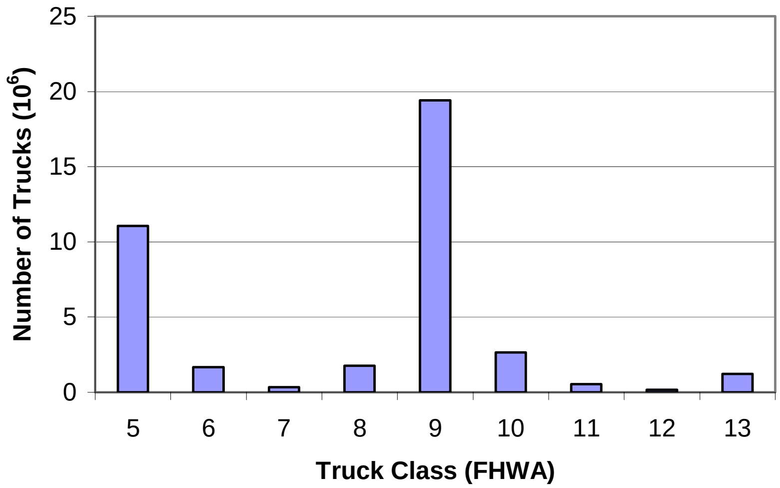

Figure 6.2. Combined truck distribution for all 42 weigh stations (year 2007)

As mentioned earlier, different trucks of the same classification have different loads on their axles. Analysis of the WIM data gave the actual load distribution spectrum for all the axle configurations of different truck classes. For example, figure 6.3 and 6.4 show the load spectra for tridem- and quad-axle groups respectively for class 7 trucks weighed at the 42 WIM stations. The WIM station data had some records with unusually high axle weights. It was also noted that the frequency of loads in excess of the legal load limits was higher than would be expected. Such records were assumed to be in error and were therefore excluded from the analysis. A threshold of 25% higher than the legal maximum load for each axle-group was used for this purpose.

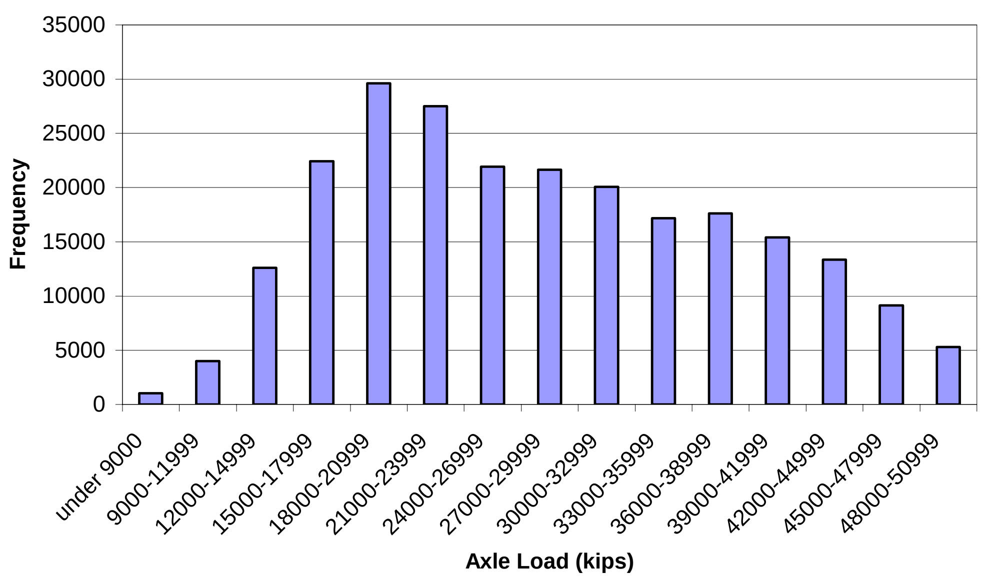

Figure 6.3.Load spectrum of tridem axles for truck class 7

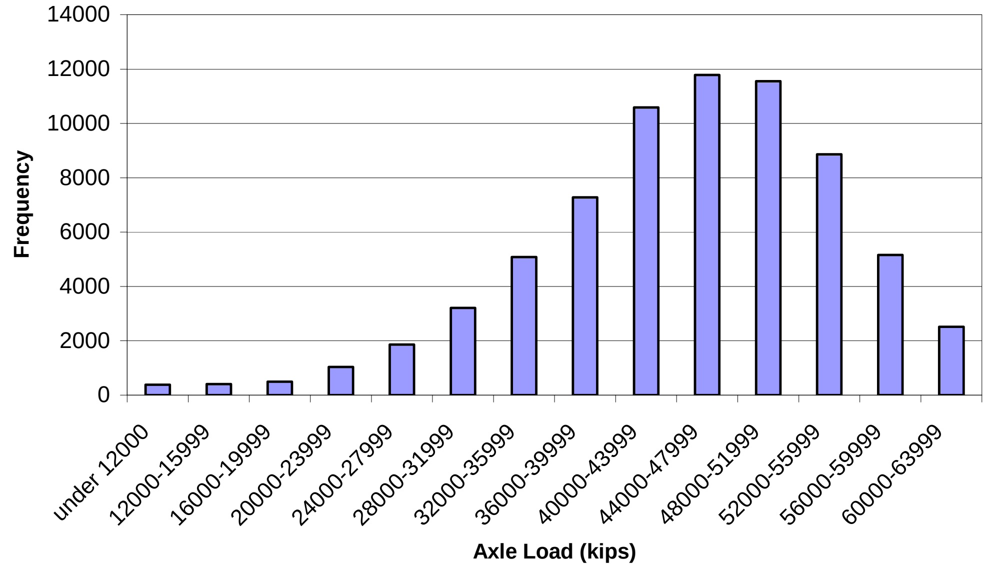

Figure 6.4. Load spectrum of quad axles for truck class 7

Calculation of truck factors for each class is an elaborate process which is presented briefly in the following sections. Details of the method can be found in the MDOT position paper entitled "Method of Calculating 18-kip Axle Equivalencies".

6.2 TRUCK FACTOR CALCULATION

This study was charged with determining the relative damage caused by multiple axles within an axle group; i.e., how much damage is caused by grouping multiple axles into one axle group. The scope of the study did not include verifying the AASHTO's "Fourth Power" damage law; i.e., we were not charged with determining how much damage is caused by increasing the load of a given axle relative to the standard 18-kip single axle. To do so would require extensive full-scale testing similar to what had been done in the original AASHO road test. Therefore, the TF's were obtained by converting multiple axle groups within each truck configuration into an equivalent number of single axles using the AF's obtained in this study, calculating the LEF of each axle group by multiplying the AF values obtained from the laboratory with the Load Equivalency Factor (LEF) from AASHTO corresponding to the single axle at the legal load limit, and then summing the LEF of the different axle groups within a truck.

Table 6.1. Load spectrum and truck factor calculation for class 7 truck (fatigue cracking)

Axle load (lb)	EALF	Number of axles	ESAL	Axle load (lb)	EALF	Number of axles	ESAL
Single axle				Tridem axle			
under 3000	0.000	1216	0.243	under 9000	0.000	1029	0.311
3000-3999	0.001	2375	3.094	9000-11999	0.002	4002	7.873
4000-4999	0.003	2769	9.117	12000-14999	0.005	12597	62.630
5000-5999	0.007	4564	32.513	15000-17999	0.011	22424	241.215
6000-6999	0.014	6089	84.016	18000-20999	0.021	29618	617.090
7000-7999	0.025	15660	385.215	21000-23999	0.037	27505	1021.646
8000-8999	0.041	25411	1044.819	24000-26999	0.062	21919	1360.871
9000-9999	0.065	44563	2908.786	27000-29999	0.099	21655	2134.383
10000-10999	0.099	45430	4513.053	30000-32999	0.150	20066	3009.992
11000-11999	0.146	26947	3933.130	33000-35999	0.220	17182	3786.854
12000-12999	0.208	25035	5210.918	36000-38999	0.314	17614	5536.070
13000-13999	0.289	17256	4992.355	39000-41999	0.437	15417	6735.070
14000-14999	0.393	20324	7992.490	42000-44999	0.594	13351	7928.001
15000-15999	0.524	14906	7813.034	45000-47999	0.791	9134	7229.305
16000-16999	0.687	16455	11297.299	48000-50999	1.037	5297	5491.407
17000-17999	0.885	11448	10135.477	51000-53999	1.337	0	0.000
18000-18999	1.126	11867	13358.825	54000-56999	1.700	0	0.000
19000-19999	1.413	7506	10606.539	57000-59999	2.134	0	0.000
20000-20999	1.753	6941	12167.905	60000-62999	2.647	0	0.000
21000-21999	2.151	4740	10197.406	63000-65999	3.249	0	0.000
22000-22999	2.614	0	0.000	66000-68999	3.947	0	0.000
23000-23999	3.146	0	0.000	69000-71999	4.750	0	0.000
24000-24999	3.753	0	0.000	72000-74999	5.668	0	0.000
25000-25999	4.442	0	0.000	75000-77999	6.707	0	0.000
26000-26999	5.216	0	0.000	78000-80999	7.877	0	0.000
27000-27999	6.082	0	0.000	81000-83999	9.184	0	0.000
28000-28999	7.044	0	0.000	84000-86999	10.637	0	0.000
29000-34999	7.563	0	0.000	87000-104999	11.420	0	0.000
35000-39999	7.563	0	0.000	105000-11199(	11.420	0	0.000
40000-50000	7.563	0	0.000	120000-15000(	11.420	0	0.000

Axle load (lb)	EALF	Number of axles	ESAL
Quadric axle			
under 12000	0.000	391	0.163
12000-15999	0.003	408	1.106
16000-19999	0.007	493	3.376
20000-23999	0.015	1038	15.381
24000-27999	0.029	1864	53.496
28000-31999	0.051	3212	164.343
32000-35999	0.086	5088	435.141
36000-39999	0.136	7280	988.398
40000-43999	0.207	10590	2188.200
44000-47999	0.304	11789	3579.054
48000-51999	0.433	11552	5001.349
52000-55999	0.602	8864	5334.066
56000-59999	0.818	5165	4224.804
60000-63999	1.090	2512	2738.682
64000-67999	1.428	0	0.000
68000-71999	1.842	0	0.000
72000-75999	2.341	0	0.000
76000-79999	2.939	0	0.000
80000-83999	3.646	0	0.000
84000-87999	4.475	0	0.000
88000-91999	5.437	0	0.000
92000-95999	6.544	0	0.000
96000-99999	7.807	0	0.000
100000-103999	9.239	0	0.000
104000-107999	10.850	0	0.000
108000-111999	12.651	0	0.000
112000-115999	14.652	0	0.000
116000-139999	15.731	0	0.000
140000-159999	15.731	0	0.000
160000-200000	15.731	0	0.000
ESAL for all trucks weighted :			176576.512

$$\text{Truck factor} = \frac{\text{18-kip ESALs for all trucks weighted}}{\text{Number of trucks weighted}} = \frac{1.766\text{E}+05}{309775} = \boxed{0.570}$$

Tables 2.8 and 5.12 in chapters 2 and 5 of this volume present the truck factors in AASHTO framework. A similar procedure for calculating ALEF was followed in this case except that entire load spectrum for each axle group and each truck class was considered to calculate the truck factor. Table 6.1 shows sample calculation of the truck factors for class 7 trucks. Other details corresponding to this example are as follows:

- Pavement type: Rigid
- Slab Thickness: 10 inches
- Distress: Fatigue cracking

These ALEF were calculated for each of the load subcategories (shown in the first column of table 6.1). Axle groups having loads above the threshold of 25% higher than the legal maximum load (for each axle-group) were excluded from the calculation. The number of axle-groups of each type for each load subcategory were then multiplied with the corresponding ALEF to obtain the cumulative ALEF for all the trucks with that axle group and load subcategory. Finally the cumulative ALEF for all the axles in the truck and for all the load subcategories were calculated. The cumulative EALF thus obtained was divided by the total number of trucks to obtain the average truck factor for the corresponding truck class.

6.3 RESULTS AND DISCUSSION

The example presented here corresponds to class 7 truck and the truck factor has been calculated from fatigue cracking point of view for rigid pavements. This procedure was repeated to obtain truck factors for other truck classes as well from fatigue point of view. Slab thickness in this example was 10 inches. Truck factors for other thicknesses of slabs were also calculated using the same procedure. Table 6.2 presents the results for the 9 different classes of trucks and 6 slab thicknesses.

Table 6.2. Final average fatigue truck factors for rigid pavements

	Truck Factors - Fatigue (AASHTO Framework)					
	Slab thickness, D (in)					
Truck Class	8 in	9 in	10 in	11 in	12 in	13 in
5	0.193	0.191	0.190	0.190	0.190	0.190
6	0.455	0.449	0.446	0.445	0.445	0.445
7	0.579	0.572	0.570	0.569	0.569	0.568
8	0.402	0.397	0.396	0.395	0.395	0.394
9	0.719	0.710	0.706	0.704	0.703	0.703
10	1.325	1.309	1.303	1.300	1.298	1.298
11	1.117	1.106	1.101	1.099	1.099	1.098
12	1.113	1.110	1.110	1.111	1.111	1.111
13	1.396	1.376	1.368	1.364	1.363	1.362

The same procedure was followed for faulting. Truck factors were calculated for the 6 different slab thicknesses for all the nine truck classes. Table 6.3 presents these results.

Table 6.3. Final average faulting truck factors for rigid pavements

	Truck Factors - Faulting (AASHTO Framework)					
	Slab thickness, D (in)					
Truck Class	8 in	9 in	10 in	11 in	12 in	13 in
5	0.193	0.191	0.190	0.190	0.190	0.190
6	0.816	0.805	0.801	0.799	0.798	0.798
7	1.229	1.209	1.200	1.197	1.195	1.194
8	0.467	0.462	0.459	0.458	0.458	0.458
9	1.550	1.531	1.523	1.519	1.517	1.517
10	2.788	2.750	2.733	2.726	2.723	2.721
11	1.117	1.106	1.101	1.099	1.099	1.098
12	1.133	1.130	1.130	1.130	1.130	1.130
13	3.456	3.405	3.383	3.373	3.368	3.366

Figure 6.5 graphically compares the current MDOT truck factors with those calculated in this study. These truck factors correspond to rigid pavements with slab thickness of 9 inches. The calculated average truck factors for fatigue cracking are either equal to (class 5, 11 and 12) or lower than that (class 6, 7, 8, 9, 10 and 13) for faulting. Also MDOT truck factors for truck class 7, 8, 11 and 12 are higher than the average truck factors calculated in this study and equal to that for class 5. Trucks belonging to class 5, 8 and 11 have only single axles. Since ALEF for single axle has been obtained using AASHTO equation in this study as well as in MDOT calculations the truck factors should be similar. The slight difference in the truck factor in class 8 and 11 is because of different load spectrum used by MDOT as compared to that in this study. The load spectrum used in this study is much more recent. The results from this study also highlight that the truck factors for faulting is almost always higher than that for fatigue cracking.

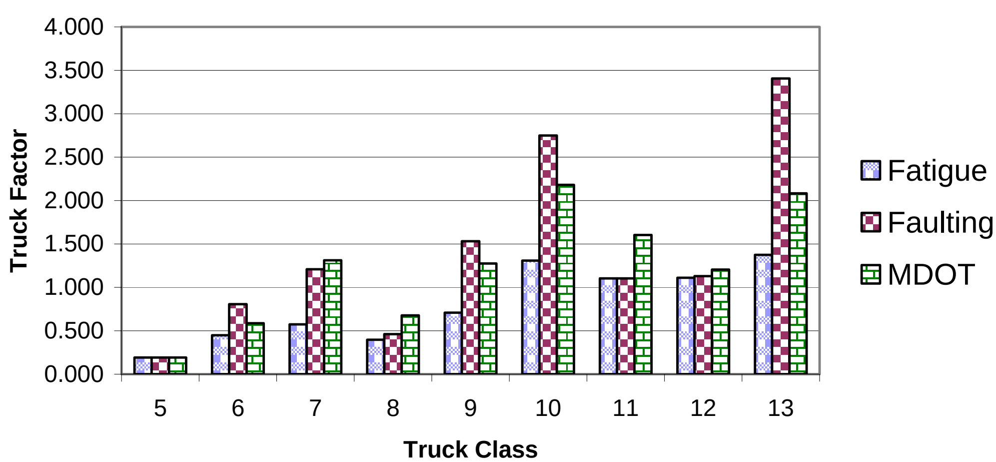

Figure 6.5. Comparing current MDOT truck factors with calculated average truck factors for slab thickness = 9 in.

CHAPTER 7
CONCLUSIONS AND RECOMMENDATIONS

Considering the increases in truck traffic and fuel prices, demands for heavier gross truck weights with larger axle groups should make this study relevant to policy–makers and pavement designers. The findings from the study are valuable for both truck weight and size policy purposes as well as pavement design protocols. The study provides updated truck factors taking into account multiple axle group effects and compatible with the AASHTO load equivalency framework for:

- Maximum legal loads for each truck type (useful for weight and size policy)
- Axle load spectra for each truck class (useful for pavement design)

The following summarizes the conclusions from the analyses of portland cement concrete pavements, and lists recommendations for truck factors of various axle configurations.

7.1 CONCLUSIONS

7.1.1 Analysis of In-service Rigid Pavement Performance Data

Based on the analyses of in-service pavement performance data to determine the effect of heavy multiple axle trucks on rigid pavement damage, the following main conclusions can be drawn:

1. Trucks with single and tandem axles affect pavement cracking (DI) more than those with multiple axles (tridem and higher).
2. Conversely, heavier trucks with multiple axles have more effect on roughness (RQI), which is an indirect measure of faulting, than those with single and tandem axles.

However, the above findings cannot be considered as definitive conclusions that can be implemented in a quantitative manner. Rather, they have highlighted general apparent trends that need to be confirmed with mechanistic analyses, controlled laboratory testing, or better yet, accelerated pavement testing (APT). The main findings of the analyses conducted in this volume (Volume III- Rigid Pavements) are summarized below. Full-scale accelerated pavement testing (APT) was outside the scope of this study. However, it is recommended that such tests be conducted in a future study. Since MDOT does not have an APT facility, it is recommended that MDOT consider joining other State Highway Agencies (SHA) in conducting a pooled fund study to support the findings of this study using full-scale APT tests.

7.1.2 Laboratory Fatigue and Joint Deterioration Testing

Based on the experimental results from flexural fatigue testing of concrete beams using cyclic multiple pulse loading, the following main conclusions can be drawn:

1. Multiple axles were found to be less damaging in fatigue per load carried compared to single axles. Increasing the number of axles carrying the same load results in less fatigue damage.
2. If one takes into consideration the stress reduction due to the interaction between axles within the same axle group, then the fatigue damage caused by multiple axles groups becomes even lower by a significant amount.

The full-scale joint deterioration testing was inconclusive due to the fact that it was not possible to accelerate joint deterioration within the constraints of the laboratory setting (slab geometry, load configuration and foundation support). Several attempts were made to allow for accelerating damage at the joint; however, these attempts were unsuccessful. A small scale beam test with a double crack was proposed as an alternative to the full-scale slab test. However, there was not sufficient time an resources to conduct a series of multiple pulses that simulate the different axle configurations. Nonetheless, full-scale slab testing as well small-scale double crack beam testing will be conducted beyond the completion of the current study. Based on the mechanistic analysis (chapter 5), it is expected that multiple axles will be more damaging in faulting than single axles. However, this needs to be confirmed using the aforementioned laboratory tests.

7.1.3 Mechanistic Analyses

Results from mechanistic analyses confirm the experimental findings; i.e., that:

1. Multiple axles are less damaging in fatigue per load carried compared to single axles.
2. Faulting damage due to different axle configurations is approximately proportional to the number of axles within an axle group, with multiple axles causing slightly more damage than a combination of smaller axle groups, for the same load carried.

Load equivalency factors (LEF) derived from mechanistic analyses for fatigue can be significantly lower than those from AASHTO, while those for faulting can be significantly higher than those from AASHTO, as can be seen in Figure 7.1. These results suggest that the AASHTO based fourth power law may need to be revised in the future.

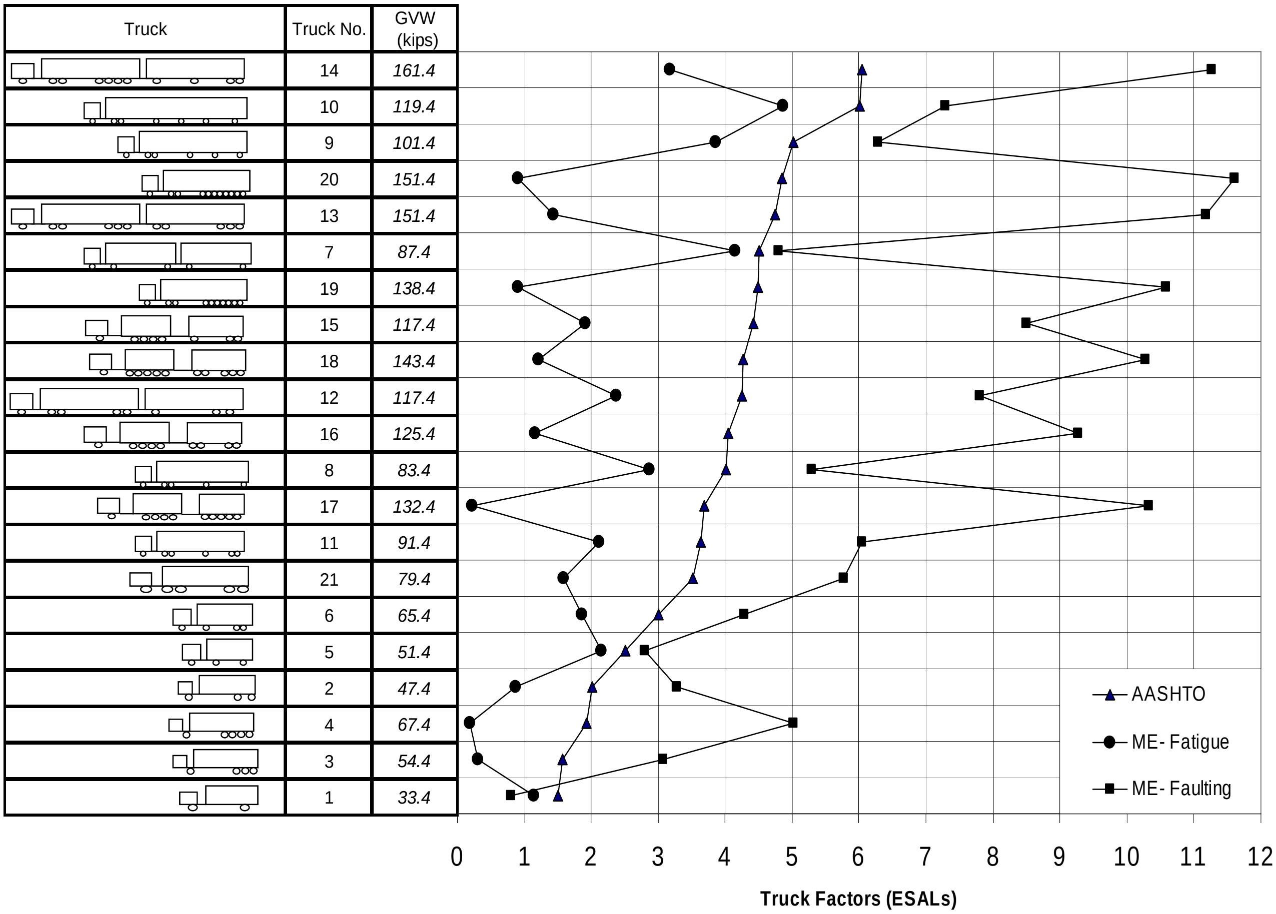

Figure 7.1 Comparison of Truck Factors from AASHTO and mechanistic analysis

7.2 RECOMMENDATIONS

Figure 7.2 summarizes the axle factors obtained from laboratory fatigue testing, and mechanistic-based fatigue and faulting analyses, and compares them to the AASHTO axle factors. AASHTO axle factors have been extrapolated for axles larger than the tridem based on a best fit curve using the axle factors from single, tandem and tridem axles.

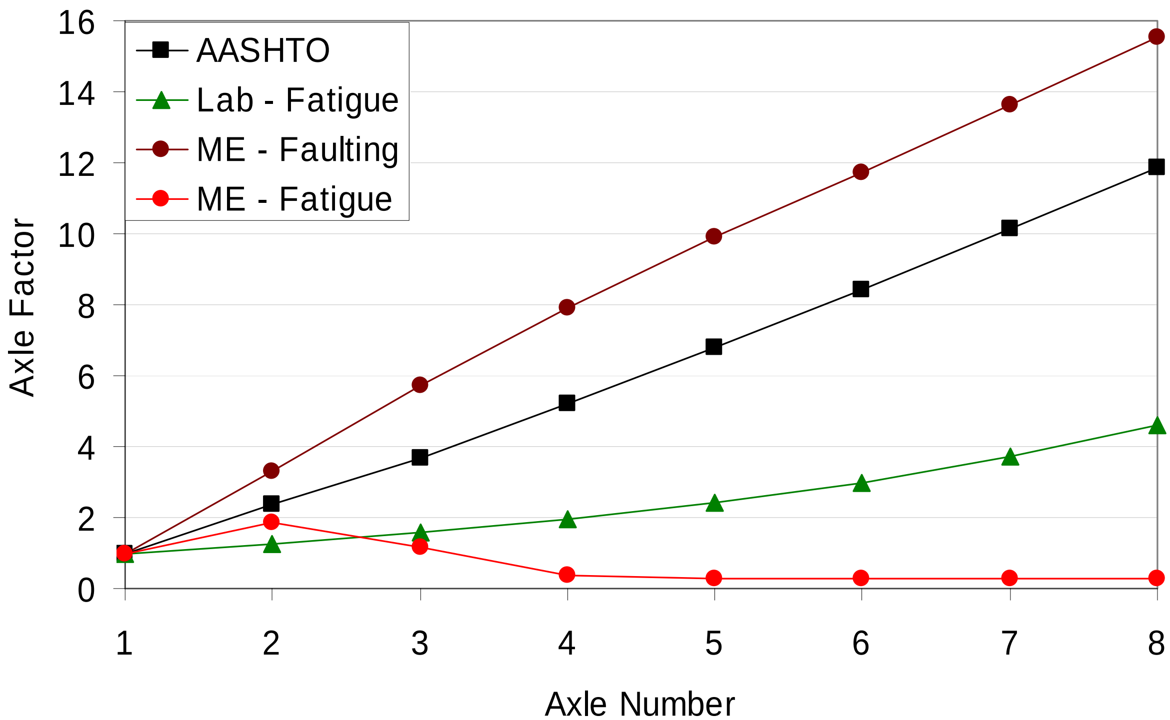

Figure 7.2 Rigid pavement axle factors for various axle configurations

7.2.1 Truck Factors Using Legal Load Limits for Weight and Size Policy

Tables 7.1 and 7.2 summarize recommended Truck Factors based on multiplying the axle factors for fatigue (laboratory) and faulting (mechanistic), respectively, by the AASHTO LEF value for a given legal load per axle (e.g., for a 39 kip tridem use 13 kip legal axle load). These truck factors are therefore based on fatigue and faulting considerations, but are provided within the AASHTO LEF framework.

Figures 7.3 and 7.4 show the same fatigue and faulting based Truck Factors for different slab thicknesses. Theses factors are ranked in descending order of relative damage caused to the pavement with slab thickness of 10 in to better show the most/least damaging truck configurations.

Table 7.1 Fatigue-based Truck Factors within AASHTO LEF Framework

Truck	Truck No.	Total Wt. (kips)	Truck Factors - Fatigue (AASHTO Framework) Slab thickness, D (in) 8	9	10	11	12	13
	1	33.4	1.519	1.512	1.509	1.508	1.507	1.507
	2	47.4	1.288	1.273	1.266	1.263	1.262	1.261
	3	54.4	0.902	0.887	0.881	0.878	0.876	0.876
	4	67.4	1.046	1.028	1.021	1.017	1.016	1.015
	5	51.4	2.519	2.512	2.509	2.508	2.507	2.507
	6	65.4	2.288	2.273	2.266	2.263	2.262	2.261
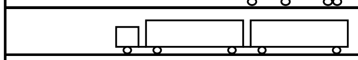	7	87.4	4.519	4.512	4.509	4.508	4.507	4.507
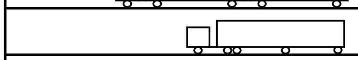	8	83.4	3.288	3.273	3.266	3.263	3.262	3.261
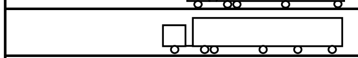	9	101.4	4.288	4.273	4.266	4.263	4.262	4.261
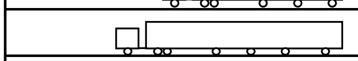	10	119.4	5.288	5.273	5.266	5.263	5.262	5.261
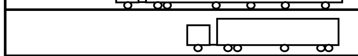	11	91.4	2.607	2.586	2.576	2.572	2.570	2.569
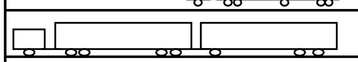	12	117.4	2.927	2.898	2.886	2.880	2.878	2.877
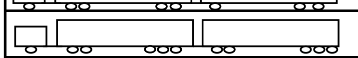	13	151.4	2.372	2.335	2.319	2.311	2.308	2.306
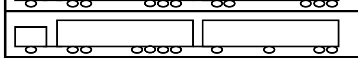	14	161.4	4.134	4.102	4.087	4.081	4.078	4.077
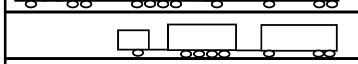	15	117.4	2.815	2.789	2.778	2.773	2.770	2.769
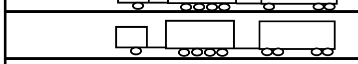	16	125.4	2.134	2.102	2.087	2.081	2.078	2.077
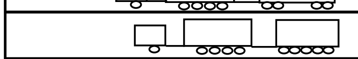	17	132.4	1.685	1.654	1.640	1.634	1.632	1.630
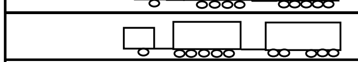	18	143.4	2.121	2.089	2.074	2.068	2.065	2.064
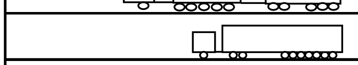	19	138.4	2.180	2.146	2.132	2.125	2.122	2.121
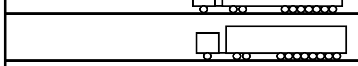	20	151.4	2.443	2.404	2.387	2.380	2.376	2.375
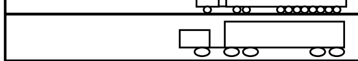	21	79.4	2.057	2.034	2.023	2.019	2.016	2.015

Table 7.2 Faulting-based Truck Factors within AASHTO LEF Framework

Truck	Truck No.	Total Wt. (kips)	Truck Factors - Faulting (AASHTO Framework) Slab thickness, D (in)					
			8	9	10	11	12	13
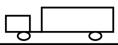	1	33.4	1.519	1.512	1.509	1.508	1.507	1.507
	2	47.4	2.527	2.499	2.486	2.480	2.477	2.476
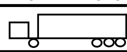	3	54.4	1.971	1.934	1.918	1.911	1.908	1.906
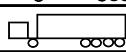	4	67.4	2.518	2.470	2.449	2.440	2.436	2.434
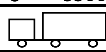	5	51.4	2.519	2.512	2.509	2.508	2.507	2.507
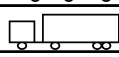	6	65.4	3.527	3.499	3.486	3.480	3.477	3.476
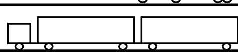	7	87.4	4.519	4.512	4.509	4.508	4.507	4.507
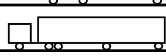	8	83.4	4.527	4.499	4.486	4.480	4.477	4.476
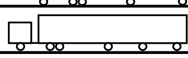	9	101.4	5.527	5.499	5.486	5.480	5.477	5.476
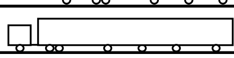	10	119.4	6.527	6.499	6.486	6.480	6.477	6.476
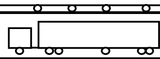	11	91.4	4.360	4.315	4.295	4.286	4.282	4.280
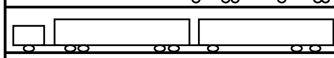	12	117.4	5.194	5.131	5.104	5.091	5.086	5.083
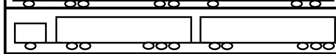	13	151.4	6.264	6.158	6.112	6.092	6.083	6.078
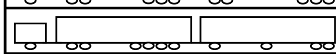	14	161.4	7.359	7.272	7.234	7.218	7.210	7.206
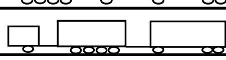	15	117.4	5.526	5.456	5.426	5.412	5.406	5.403
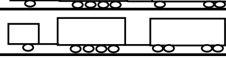	16	125.4	5.359	5.272	5.234	5.218	5.210	5.206
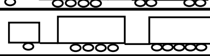	17	132.4	5.023	4.924	4.881	4.862	4.853	4.849
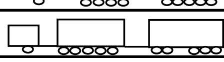	18	143.4	5.608	5.515	5.475	5.457	5.448	5.444
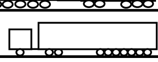	19	138.4	5.977	5.878	5.834	5.815	5.806	5.802
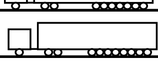	20	151.4	6.466	6.357	6.309	6.288	6.278	6.273
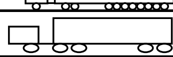	21	79.4	4.534	4.485	4.462	4.452	4.448	4.445

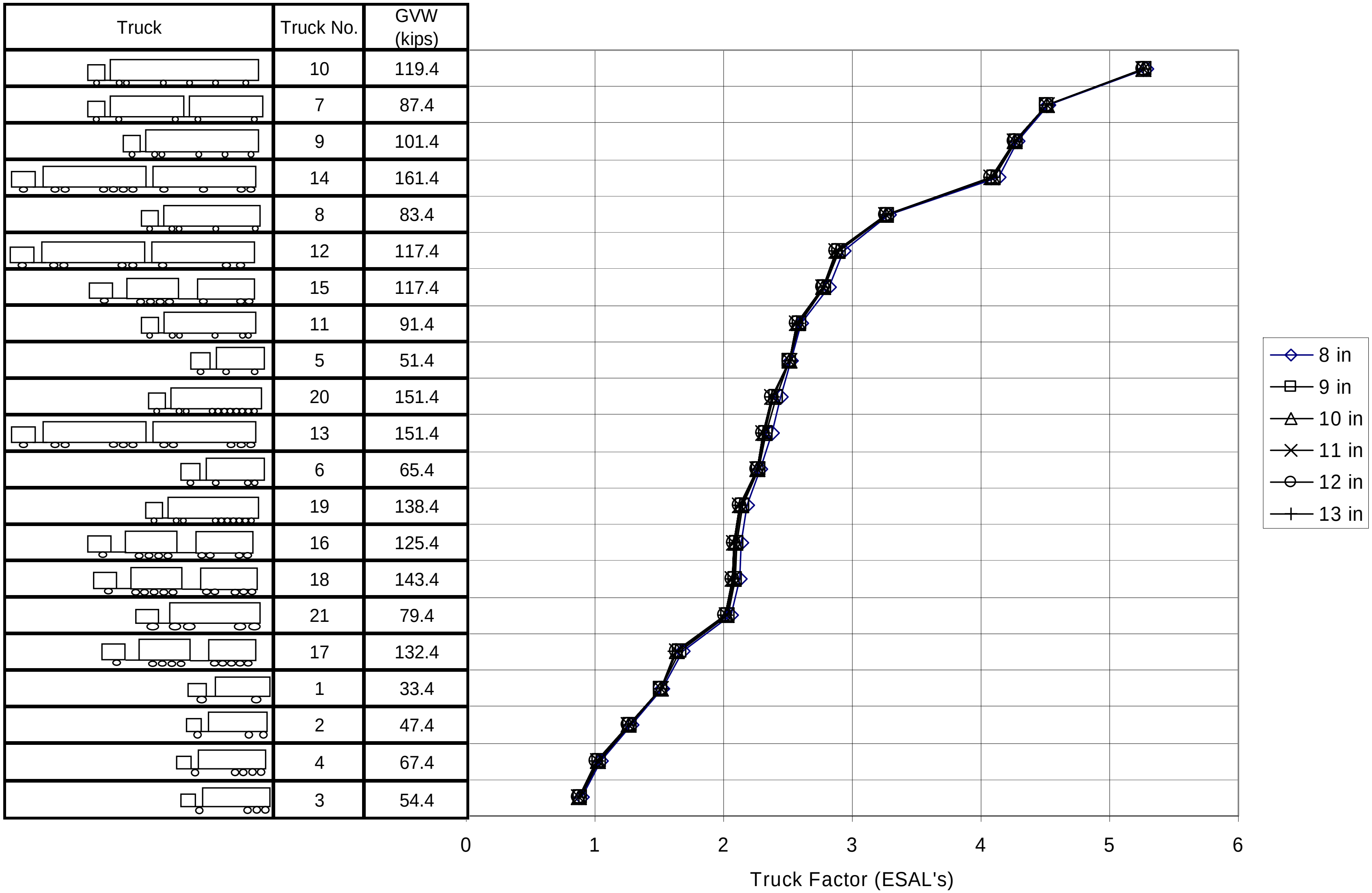

Figure 7.3 Fatigue-based Truck Factors within AASHTO LEF framework

Truck No.	GVW (kips)
14	161.4
10	119.4
20	151.4
13	151.4
19	138.4
18	143.4
9	101.4
15	117.4
16	125.4
12	117.4
17	132.4
21	79.4
8	83.4
7	87.4
11	91.4
6	65.4
2	47.4
5	51.4
4	67.4
3	54.4
1	33.4

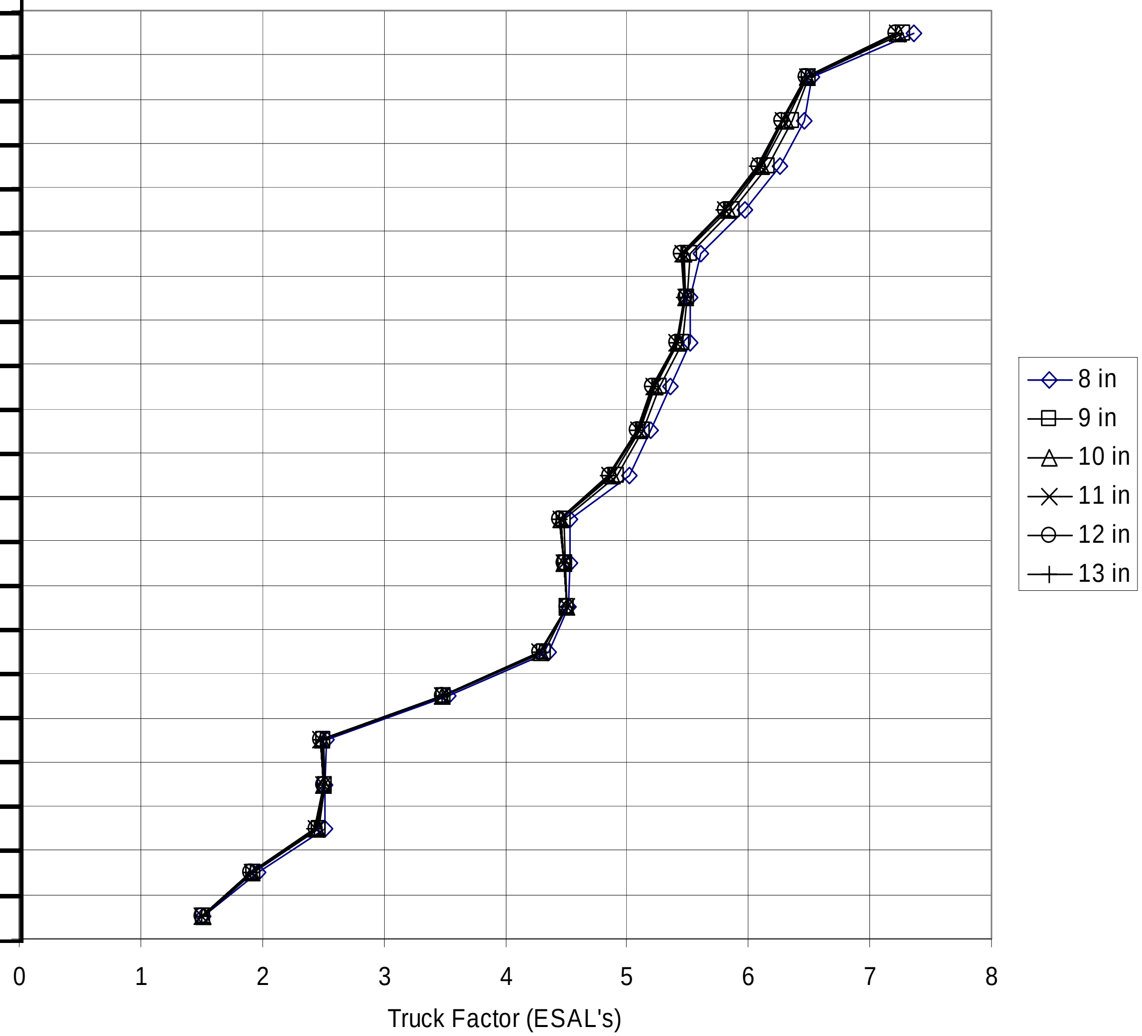

Figure 7.4 Faulting-based Truck Factors within AASHTO LEF framework

7.2.2 Truck Factors Using Axle Load Spectra for Pavement Design

Tables 7.3 and 7.4 summarize recommended Truck Factors based on multiplying the axle factors for fatigue cracking and faulting, respectively, by the AASHTO LEF value using the axle load spectra from 42 WIM stations in Michigan. These truck factors are therefore useful for pavement design, taking into account fatigue and faultiing considerations, and are provided within the AASHTO LEF framework. Table 7.5 and figure 7.5 compare the TFs from this study to those currently used by MDOT.

Table 7.3. Fatigue-based Truck Factors for Rigid Pavement Design - AASHTO LEF Framework

	Truck Factors - Fatigue (AASHTO Framework)					
	Slab thickness, D (in)					
Truck Class	8 in	9 in	10 in	11 in	12 in	13 in
5	0.193	0.191	0.190	0.190	0.190	0.190
6	0.455	0.449	0.446	0.445	0.445	0.445
7	0.579	0.572	0.570	0.569	0.569	0.568
8	0.402	0.397	0.396	0.395	0.395	0.394
9	0.719	0.710	0.706	0.704	0.703	0.703
10	1.325	1.309	1.303	1.300	1.298	1.298
11	1.117	1.106	1.101	1.099	1.099	1.098
12	1.113	1.110	1.110	1.111	1.111	1.111
13	1.396	1.376	1.368	1.364	1.363	1.362

Table 7.4. Faulting-based Truck Factors for Rigid Pavement Design - AASHTO LEF Framework

	Truck Factors - Faulting (AASHTO Framework)					
	Slab thickness, D (in)					
Truck Class	8 in	9 in	10 in	11 in	12 in	13 in
5	0.193	0.191	0.190	0.190	0.190	0.190
6	0.816	0.805	0.801	0.799	0.798	0.798
7	1.229	1.209	1.200	1.197	1.195	1.194
8	0.467	0.462	0.459	0.458	0.458	0.458
9	1.550	1.531	1.523	1.519	1.517	1.517
10	2.788	2.750	2.733	2.726	2.723	2.721
11	1.117	1.106	1.101	1.099	1.099	1.098
12	1.133	1.130	1.130	1.130	1.130	1.130
13	3.456	3.405	3.383	3.373	3.368	3.366

Table 7.5. Comparison of Truck Factors for Rigid Pavement Design

Rigid Pavement (D = 9 in.)

Truck Class	Truck Factors		
	Fatigue Cracking	Faulting	MDOT
5	0.191	0.191	0.1895
6	0.449	0.805	0.5854
7	0.572	1.209	1.3111
8	0.397	0.462	0.6759
9	0.710	1.531	1.2736
10	1.309	2.750	2.1806
11	1.106	1.106	1.604
12	1.110	1.130	1.2039
13	1.376	3.405	2.0837

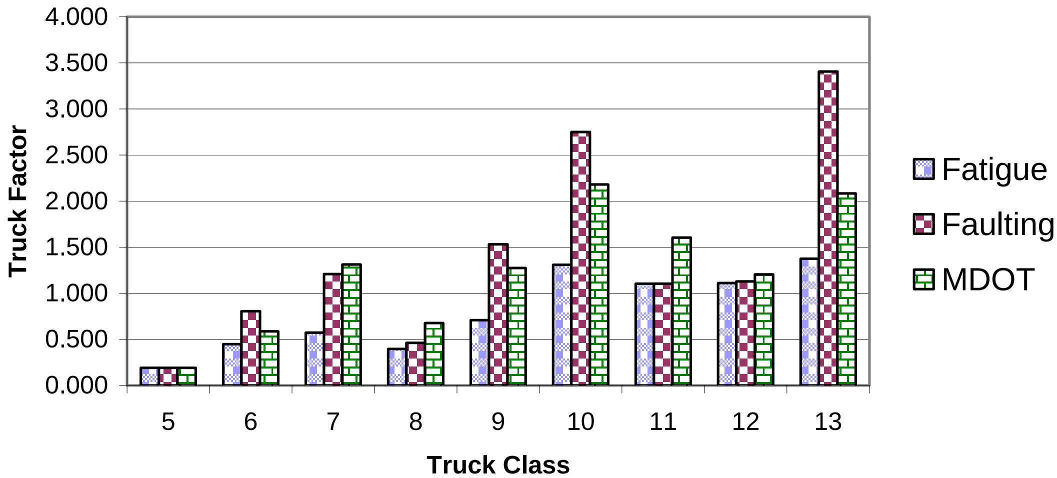

Figure 7.5. Comparison of current MDOT truck factors with those from this study for 9 inch slab

REFERENCES

Chatti, K, J. Lysmer and C. L. Monismith, "Dynamic Finite-Element Analysis of Jointed Concrete Pavements"; Transportation Research Record, No. 1449; pp. 79-90, 1994.

Colley, B.E., and Humphrey, H.A., “Aggregate Interlock at Joints in Concrete Pavements,” In Highway Research Record 189, HRB, National Research Council, Washington, D.C., 1967, pp. 1-18

Darter, M.I., Design of Zero-Maintenance Plain Jointed Concrete Pavements, Vol. I – Development of Design Procedures, FHWA-RD-77-111, Federal Highway Research Record No. 370, Highway Research Board, pp. 48-60, Washington D.C., 1971.

Hilsdorf, H.K. and Kesler, C.E.., Fatigue Strength of Concrete Under Varying Flexural Stresses, Journal of the American Concrete Institute, vol. 63, pp. 1059-1075, 1966.

NCHRP 1-37A, “Guide for Mechanistic-Empirical Design of New and Rehabilitated Pavement Structures,” National Cooperative Highway Research Program, Washington, D.C., 2004.

Oh, B.H. , Fatigue Analysis of Plain Concrete in Flexure, Journal of Structural Engineering, ASCE, V. 112, No.2, Feb. pp. 273-288, 1986.

Roesler, J.R., Fatigue of Concrete Beams and Slabs, Ph.D. dissertation, University of Illinois, 1998.

Tabatabaie, A. M and E. J. Barenberg, “Finite Element Analysis of Jointed or Cracked Concrete Pavements,” Transportation Research Record, No. 671, pp. 11-19, 1978.

Zhang B., Phillips D.V. and Wu K. Effect of loading frequency and stress reversal on fatigue life of plain concrete. Magazine of Concrete Research, 48, No.177, 361-375, 1996.

APPENDIX A1

PCC Fatigue-based Truck Factors by Class using WIM Data within AASHTO LEF Framework

Calculation of Truck Factor for Class 5

Axle load (lb)	EALF	Number of axles	ESAL
Single axle			
under 3000	0.000	480085	96.093
3000-3999	0.001	3212970	4186.188
4000-4999	0.003	3689060	12146.648
5000-5999	0.007	3088150	21999.466
6000-6999	0.014	1664410	22965.524
7000-7999	0.025	1789680	44023.755
8000-8999	0.041	1204850	49539.563
9000-9999	0.065	1243800	81187.251
10000-10999	0.099	1217440	120941.464
11000-11999	0.146	752855	109885.216
12000-12999	0.208	716939	149227.493
13000-13999	0.289	438587	126888.145
14000-14999	0.393	434099	170711.083
15000-15999	0.524	271202	142151.513
16000-16999	0.687	266017	182635.889
17000-17999	0.885	166753	147634.621
18000-18999	1.126	161392	181680.926
19000-19999	1.413	99249	140246.255
20000-20999	1.753	90997	159522.090
21000-21999	2.151	62930	135384.551
22000-22999	2.614	0	0.000
23000-23999	3.146	0	0.000
24000-24999	3.753	0	0.000
25000-25999	4.442	0	0.000
26000-26999	5.216	0	0.000
27000-27999	6.082	0	0.000
28000-28999	7.044	0	0.000
29000-34999	7.563	0	0.000
35000-39999	7.563	0	0.000
40000-50000	7.563	0	0.000

ESAL for all trucks weighted : 2003053.734

$$\text{Truck factor} = \frac{\text{18-kip ESALs for all trucks weighted}}{\text{Number of trucks weighted}} = \frac{2.003E+06}{1.053E+07} = \boxed{0.190}$$

Calculation of Truck Factor for Class 6

Axle load (lb)	EALF	Number of axles	ESAL	Axle load (lb)	EALF	Number of axles	ESAL
Single axle				Tandem axle			
under 3000	0.000	2847	0.570	under 6000	3E-04	48965	12.34893
3000-3999	0.001	9521	12.405	6000-7999	0.002	214535	352.1931
4000-4999	0.003	13215	43.512	8000-9999	0.004	185744	770.5948
5000-5999	0.007	20551	146.402	10000-11999	0.009	101730	913.1315
6000-6999	0.014	26885	370.959	12000-13999	0.017	92258	1603.949
7000-7999	0.025	70099	1724.342	14000-15999	0.031	85209	2640.996
8000-8999	0.041	106476	4377.951	16000-17999	0.052	77065	3992.518
9000-9999	0.065	212628	13878.986	18000-19999	0.082	77577	6380.296
10000-10999	0.099	314914	31283.809	20000-21999	0.125	95732	11982.72
11000-11999	0.146	214373	31289.456	22000-23999	0.184	93970	17281.75
12000-12999	0.208	185032	38513.544	24000-25999	0.262	98041	25712.54
13000-13999	0.289	109224	31599.730	26000-27999	0.365	94082	34295.91
14000-14999	0.393	101579	39946.328	28000-29999	0.495	83694	41470.36
15000-15999	0.524	55406	29041.256	30000-31999	0.66	70361	46468.77
16000-16999	0.687	46389	31848.702	32000-33999	0.865	53421	46212.48
17000-17999	0.885	24667	21838.907	34000-35999	1.116	36263	40452.82
18000-18999	1.126	21560	24270.353	36000-37999	1.418	23820	33786.22
19000-19999	1.413	12625	17840.069	38000-39999	1.78	15517	27627.62
20000-20999	1.753	10941	19180.096	40000-41999	2.209	0	0
21000-21999	2.151	6724	14465.688	42000-43999	2.711	0	0
22000-22999	2.614	0	0.000	44000-45999	3.293	0	0
23000-23999	3.146	0	0.000	46000-47999	3.964	0	0
24000-24999	3.753	0	0.000	48000-49999	4.729	0	0
25000-25999	4.442	0	0.000	50000-51999	5.597	0	0
26000-26999	5.216	0	0.000	52000-53999	6.573	0	0
27000-27999	6.082	0	0.000	54000-55999	7.664	0	0
28000-28999	7.044	0	0.000	56000-57999	8.876	0	0
29000-34999	7.563	0	0.000	58000-69999	9.53	0	0
35000-39999	7.563	0	0.000	70000-79999	9.53	0	0
40000-50000	7.563	0	0.000	80000-100000	9.53	0	0

ESAL for all trucks weighted : 693630.279

$$\text{Truck factor} = \frac{\text{18-kip ESALs for all trucks weighted}}{\text{Number of trucks weighted}} = \frac{6.936E+05}{1.55E+06} = \boxed{0.446}$$

Calculation of Truck Factor for Class 7

Axle load (lb)	EALF	Number of axles	ESAL	Axle load (lb)	EALF	Number of axles	ESAL
Single axle				Tridem axle			
under 3000	0.000	1216	0.243	under 9000	3E-04	1029	0.311003
3000-3999	0.001	2375	3.094	9000-11999	0.002	4002	7.873469
4000-4999	0.003	2769	9.117	12000-14999	0.005	12597	62.63034
5000-5999	0.007	4564	32.513	15000-17999	0.011	22424	241.2147
6000-6999	0.014	6089	84.016	18000-20999	0.021	29618	617.0903
7000-7999	0.025	15660	385.215	21000-23999	0.037	27505	1021.646
8000-8999	0.041	25411	1044.819	24000-26999	0.062	21919	1360.871
9000-9999	0.065	44563	2908.786	27000-29999	0.099	21655	2134.383
10000-10999	0.099	45430	4513.053	30000-32999	0.15	20066	3009.992
11000-11999	0.146	26947	3933.130	33000-35999	0.22	17182	3786.854
12000-12999	0.208	25035	5210.918	36000-38999	0.314	17614	5536.07
13000-13999	0.289	17256	4992.355	39000-41999	0.437	15417	6735.07
14000-14999	0.393	20324	7992.490	42000-44999	0.594	13351	7928.001
15000-15999	0.524	14906	7813.034	45000-47999	0.791	9134	7229.305
16000-16999	0.687	16455	11297.299	48000-50999	1.037	5297	5491.407
17000-17999	0.885	11448	10135.477	51000-53999	1.337	0	0
18000-18999	1.126	11867	13358.825	54000-56999	1.7	0	0
19000-19999	1.413	7506	10606.539	57000-59999	2.134	0	0
20000-20999	1.753	6941	12167.905	60000-62999	2.647	0	0
21000-21999	2.151	4740	10197.406	63000-65999	3.249	0	0
22000-22999	2.614	0	0.000	66000-68999	3.947	0	0
23000-23999	3.146	0	0.000	69000-71999	4.75	0	0
24000-24999	3.753	0	0.000	72000-74999	5.668	0	0
25000-25999	4.442	0	0.000	75000-77999	6.707	0	0
26000-26999	5.216	0	0.000	78000-80999	7.877	0	0
27000-27999	6.082	0	0.000	81000-83999	9.184	0	0
28000-28999	7.044	0	0.000	84000-86999	10.64	0	0
29000-34999	7.563	0	0.000	87000-104999	11.42	0	0
35000-39999	7.563	0	0.000	105000-11199	11.42	0	0
40000-50000	7.563	0	0.000	120000-15000	11.42	0	0

Axle load (lb)	EALF	Number of axles	ESAL
Quad axle			
under 12000	0.000	391	0.163
12000-15999	0.003	408	1.106
16000-19999	0.007	493	3.376
20000-23999	0.015	1038	15.381
24000-27999	0.029	1864	53.496
28000-31999	0.051	3212	164.343
32000-35999	0.086	5088	435.141
36000-39999	0.136	7280	988.398
40000-43999	0.207	10590	2188.200
44000-47999	0.304	11789	3579.054
48000-51999	0.433	11552	5001.349
52000-55999	0.602	8864	5334.066
56000-59999	0.818	5165	4224.804
60000-63999	1.090	2512	2738.682
64000-67999	1.428	0	0.000
68000-71999	1.842	0	0.000
72000-75999	2.341	0	0.000
76000-79999	2.939	0	0.000
80000-83999	3.646	0	0.000
84000-87999	4.475	0	0.000
88000-91999	5.437	0	0.000
92000-95999	6.544	0	0.000
96000-99999	7.807	0	0.000
100000-103999	9.239	0	0.000
104000-107999	10.850	0	0.000
108000-111999	12.651	0	0.000
112000-115999	14.652	0	0.000
116000-139999	15.731	0	0.000
140000-159999	15.731	0	0.000
160000-200000	15.731	0	0.000

ESAL for all trucks weighted : 176576.512

$$\text{Truck factor} = \frac{\text{18-kip ESALs for all trucks weighted}}{\text{Number of trucks weighted}} = \frac{1.766\text{E}+05}{309775} = \boxed{0.570}$$

Calculation of Truck Factor for Class 8

Axle load (lb)	EALF	Number of axles	ESAL	Axle load (lb)	EALF	Number of axles	ESAL
Single axle				Tandem axle			
under 3000	0.000	47700	9.548	under 6000	3E-04	117362	29.59859
3000-3999	0.001	216420	281.974	6000-7999	0.002	222021	364.4825
4000-4999	0.003	306637	1009.637	8000-9999	0.004	254319	1055.091
5000-5999	0.007	312311	2224.852	10000-11999	0.009	207204	1859.869
6000-6999	0.014	227648	3141.086	12000-13999	0.017	149541	2599.841
7000-7999	0.025	341950	8411.517	14000-15999	0.031	115820	3589.763
8000-8999	0.041	372547	15317.936	16000-17999	0.052	91408	4735.588
9000-9999	0.065	466409	30444.175	18000-19999	0.082	73370	6034.292
10000-10999	0.099	347090	34480.199	20000-21999	0.125	64690	8097.209
11000-11999	0.146	185099	27016.681	22000-23999	0.184	40702	7485.386
12000-12999	0.208	191005	39756.796	24000-25999	0.262	26797	7027.864
13000-13999	0.289	132793	38418.506	26000-27999	0.365	16757	6108.465
14000-14999	0.393	142793	56153.890	28000-29999	0.495	9886	4898.511
15000-15999	0.524	93963	49251.048	30000-31999	0.66	5987	3954.016
16000-16999	0.687	95644	65665.078	32000-33999	0.865	3608	3121.144
17000-17999	0.885	60271	53360.876	34000-35999	1.116	2271	2533.391
18000-18999	1.126	53720	60473.254	36000-37999	1.418	1299	1842.498
19000-19999	1.413	29430	41586.790	38000-39999	1.78	761	1354.941
20000-20999	1.753	24439	42842.735	40000-41999	2.209	0	0
21000-21999	2.151	15012	32296.089	42000-43999	2.711	0	0
22000-22999	2.614	0	0.000	44000-45999	3.293	0	0
23000-23999	3.146	0	0.000	46000-47999	3.964	0	0
24000-24999	3.753	0	0.000	48000-49999	4.729	0	0
25000-25999	4.442	0	0.000	50000-51999	5.597	0	0
26000-26999	5.216	0	0.000	52000-53999	6.573	0	0
27000-27999	6.082	0	0.000	54000-55999	7.664	0	0
28000-28999	7.044	0	0.000	56000-57999	8.876	0	0
29000-34999	7.563	0	0.000	58000-69999	9.53	0	0
35000-39999	7.563	0	0.000	70000-79999	9.53	0	0
40000-50000	7.563	0	0.000	80000-10000C	9.53	0	0

ESAL for all trucks weighted : 668834.618

$$\text{Truck factor} = \frac{\text{18-kip ESALs for all trucks weighted}}{\text{Number of trucks weighted}} = \frac{6.688E+05}{1.69E+06} = \boxed{0.396}$$

Calculation of Truck Factor for Class 9

Axle load (lb)	EALF	Number of axles	ESAL	Axle load (lb)	EALF	Number of axles	ESAL
Single axle				Tandem axle			
under 3000	0.000	217586	43.552	under 6000	3E-04	263474	66.4479
3000-3999	0.001	474182	617.813	6000-7999	0.002	851432	1397.76
4000-4999	0.003	392627	1292.769	8000-9999	0.004	2289300	9497.602
5000-5999	0.007	435776	3104.396	10000-11999	0.009	3283180	29469.92
6000-6999	0.014	415293	5730.212	12000-13999	0.017	3237820	56291.04
7000-7999	0.025	880848	21667.693	14000-15999	0.031	2874240	89085.14
8000-8999	0.041	1489430	61240.578	16000-17999	0.052	2601420	134772.2
9000-9999	0.065	3683550	240438.414	18000-19999	0.082	2387830	196386.3
10000-10999	0.099	5998950	595940.496	20000-21999	0.125	2503490	313360.4
11000-11999	0.146	3725460	543760.721	22000-23999	0.184	2037270	374668.4
12000-12999	0.208	2170990	451881.394	24000-25999	0.262	1845260	483943.6
13000-13999	0.289	633693	183334.502	26000-27999	0.365	1793390	653748.3
14000-14999	0.393	428790	168623.298	28000-29999	0.495	1942570	962543
15000-15999	0.524	292044	153075.923	30000-31999	0.66	2107480	1391851
16000-16999	0.687	365772	251123.403	32000-33999	0.865	1873360	1620573
17000-17999	0.885	260477	230613.081	34000-35999	1.116	1197970	1336383
18000-18999	1.126	236156	265843.665	36000-37999	1.418	644266	913825.1
19000-19999	1.413	119596	168998.087	38000-39999	1.78	342570	609937
20000-20999	1.753	86395	151454.564	40000-41999	2.209	0	0
21000-21999	2.151	47271	101696.538	42000-43999	2.711	0	0
22000-22999	2.614	0	0.000	44000-45999	3.293	0	0
23000-23999	3.146	0	0.000	46000-47999	3.964	0	0
24000-24999	3.753	0	0.000	48000-49999	4.729	0	0
25000-25999	4.442	0	0.000	50000-51999	5.597	0	0
26000-26999	5.216	0	0.000	52000-53999	6.573	0	0
27000-27999	6.082	0	0.000	54000-55999	7.664	0	0
28000-28999	7.044	0	0.000	56000-57999	8.876	0	0
29000-34999	7.563	0	0.000	58000-69999	9.53	0	0
35000-39999	7.563	0	0.000	70000-79999	9.53	0	0
40000-50000	7.563	0	0.000	80000-10000C	9.53	0	0

ESAL for all trucks weighted : 12778279.930

$$\text{Truck factor} = \frac{\text{18-kip ESALs for all trucks weighted}}{\text{Number of trucks weighted}} = \frac{1.278E+07}{1.81E+07} = \boxed{0.706}$$

Calculation of Truck Factor for Class 10

Axle load (lb)	EALF	Number of axles	ESAL	Axle load (lb)	EALF	Number of axles	ESAL
Single axle				Tandem axle			
under 3000	0.000	253446	50.729	under 6000	3E-04	31067	7.835069
3000-3999	0.001	381335	496.843	6000-7999	0.002	66836	109.7218
4000-4999	0.003	419770	1382.140	8000-9999	0.004	144459	599.316
5000-5999	0.007	455130	3242.270	10000-11999	0.009	261587	2348.013
6000-6999	0.014	311176	4293.606	12000-13999	0.017	287843	5004.288
7000-7999	0.025	351943	8657.331	14000-15999	0.031	237582	7363.695
8000-8999	0.041	292155	12012.475	16000-17999	0.052	198224	10269.42
9000-9999	0.065	472821	30862.709	18000-19999	0.082	175094	14400.55
10000-10999	0.099	746091	74117.277	20000-21999	0.125	174420	21832.05
11000-11999	0.146	607189	88624.097	22000-23999	0.184	153058	28148.45
12000-12999	0.208	613503	127697.774	24000-25999	0.262	166578	43687.26
13000-13999	0.289	371182	107387.121	26000-27999	0.365	192553	70191.76
14000-14999	0.393	366007	143933.645	28000-29999	0.495	216873	107460.5
15000-15999	0.524	225922	118417.837	30000-31999	0.66	220489	145618.3
16000-16999	0.687	218932	150309.343	32000-33999	0.865	194198	167993.3
17000-17999	0.885	134400	118990.921	34000-35999	1.116	146968	163948.7
18000-18999	1.126	124175	139785.299	36000-37999	1.418	96892	137431.3
19000-19999	1.413	68353	96587.898	38000-39999	1.78	58771	104640.2
20000-20999	1.753	55958	98097.048	40000-41999	2.209	0	0
21000-21999	2.151	34217	73612.795	42000-43999	2.711	0	0
22000-22999	2.614	0	0.000	44000-45999	3.293	0	0
23000-23999	3.146	0	0.000	46000-47999	3.964	0	0
24000-24999	3.753	0	0.000	48000-49999	4.729	0	0
25000-25999	4.442	0	0.000	50000-51999	5.597	0	0
26000-26999	5.216	0	0.000	52000-53999	6.573	0	0
27000-27999	6.082	0	0.000	54000-55999	7.664	0	0
28000-28999	7.044	0	0.000	56000-57999	8.876	0	0
29000-34999	7.563	0	0.000	58000-69999	9.53	0	0
35000-39999	7.563	0	0.000	70000-79999	9.53	0	0
40000-50000	7.563	0	0.000	80000-100000	9.53	0	0

Axle load (lb)	EALF	Number of axles	ESAL	Axle load (lb)	EALF	Number of axles	ESAL
7-axle				8-axle			
under 21000	0.001	8708	6.135	under 24000	9E-04	30507	27.84436
21000-27999	0.005	22195	101.791	24000-31999	0.006	78497	466.3693
28000-34999	0.012	17913	207.612	32000-39999	0.015	36058	541.3862
35000-41999	0.025	9262	232.253	40000-47999	0.032	13208	429.0577
42000-48999	0.049	5508	267.518	48000-55999	0.063	6664	419.2913
49000-55999	0.087	5638	488.179	56000-63999	0.112	7991	896.3501
56000-62999	0.145	7530	1089.825	64000-71999	0.187	13736	2575.398
63000-69999	0.230	10257	2356.678	72000-79999	0.298	22316	6642.3
70000-76999	0.350	15219	5321.774	80000-87999	0.453	39277	17792.25
77000-83999	0.514	22345	11480.240	88000-95999	0.666	67015	44603.07
84000-90999	0.733	27555	20188.763	96000-103999	0.949	99997	94911.42
91000-97999	1.018	24471	24920.668	104000-111999	1.319	113115	149228
98000-104999	1.384	17000	23532.308	112000-119999	1.793	91930	164852.3
105000-111999	1.845	10834	19988.955	120000-127999	2.39	56756	135654.8
112000-118999	2.417	0	0.000	128000-135999	3.131	0	0
119000-125999	3.116	0	0.000	136000-143999	4.037	0	0
126000-132999	3.963	0	0.000	144000-151999	5.133	0	0
133000-139999	4.974	0	0.000	152000-159999	6.444	0	0
140000-146999	6.171	0	0.000	160000-167999	7.994	0	0
147000-153999	7.573	0	0.000	168000-175999	9.81	0	0
154000-160999	9.200	0	0.000	176000-183999	11.92	0	0
161000-167999	11.074	0	0.000	184000-191999	14.35	0	0
168000-174999	13.212	0	0.000	192000-199999	17.12	0	0
175000-181999	15.636	0	0.000	200000-207999	20.26	0	0
182000-188999	18.362	0	0.000	208000-215999	23.79	0	0
189000-195999	21.410	0	0.000	216000-223999	27.74	0	0
196000-202999	24.796	0	0.000	224000-231999	32.12	0	0
203000-244999	26.623	0	0.000	232000-279999	34.49	0	0
245000-279999	26.623	0	0.000	280000-319999	34.49	0	0
280000-350000	26.623	0	0.000	320000-400000	34.49	0	0

ESAL for all trucks weighted : 3158836.534

$$\text{Truck factor} = \frac{\text{18-kip ESALs for all trucks weighted}}{\text{Number of trucks weighted}} = \frac{3.159E+06}{2.43E+06} = \boxed{1.303}$$

Calculation of Truck Factor for Class 11

Axle load (lb)	EALF	Number of axles	ESAL
Single axle			
under 3000	0.000	45199	9.047
3000-3999	0.001	88280	115.020
4000-4999	0.003	108165	356.146
5000-5999	0.007	163914	1167.696
6000-6999	0.014	131316	1811.898
7000-7999	0.025	173850	4276.479
8000-8999	0.041	184295	7577.619
9000-9999	0.065	318663	20800.268
10000-10999	0.099	314038	31196.786
11000-11999	0.146	174981	25539.878
12000-12999	0.208	187849	39099.889
13000-13999	0.289	140541	40660.090
14000-14999	0.393	162424	63873.856
15000-15999	0.524	108747	57000.135
16000-16999	0.687	103746	71227.564
17000-17999	0.885	59837	52976.635
18000-18999	1.126	50726	57102.872
19000-19999	1.413	26155	36958.970
20000-20999	1.753	19239	33726.886
21000-21999	2.151	9745	20964.921
22000-22999	2.614	0	0.000
23000-23999	3.146	0	0.000
24000-24999	3.753	0	0.000
25000-25999	4.442	0	0.000
26000-26999	5.216	0	0.000
27000-27999	6.082	0	0.000
28000-28999	7.044	0	0.000
29000-34999	7.563	0	0.000
35000-39999	7.563	0	0.000
40000-50000	7.563	0	0.000

ESAL for all trucks weighted : 566442.654

$$\text{Truck factor} = \frac{\text{18-kip ESALs for all trucks weighted}}{\text{Number of trucks weighted}} = \frac{5.664E+05}{514342} = \boxed{1.101}$$

Calculation of Truck Factor for Class 12

Axle load (lb)	EALF	Number of axles	ESAL	Axle load (lb)	EALF	Number of axles	ESAL
Single axle				Tandem axle			
under 3000	0.000	10067	2.015	under 6000	0.0003	17822	4.494692
3000-3999	0.001	7138	9.300	6000-7999	0.0016	32409	53.20449
4000-4999	0.003	12932	42.580	8000-9999	0.0041	39129	162.3342
5000-5999	0.007	29544	210.467	10000-11999	0.009	27951	250.889
6000-6999	0.014	26015	358.955	12000-13999	0.0174	13549	235.5558
7000-7999	0.025	39028	960.037	14000-15999	0.031	7438	230.5358
8000-8999	0.041	45508	1871.143	16000-17999	0.0518	4017	208.1093
9000-9999	0.065	67223	4387.884	18000-19999	0.0822	1730	142.2833
10000-10999	0.099	64947	6451.887	20000-21999	0.1252	708	88.61994
11000-11999	0.146	38598	5633.687	22000-23999	0.1839	238	43.76989
12000-12999	0.208	36550	7607.711	24000-25999	0.2623	105	27.53762
13000-13999	0.289	24510	7091.018	26000-27999	0.3645	56	20.4138
14000-14999	0.393	24950	9811.682	28000-29999	0.4955	53	26.26149
15000-15999	0.524	16947	8882.832	30000-31999	0.6604	32	21.13387
16000-16999	0.687	18526	12719.159	32000-33999	0.8651	34	29.41211
17000-17999	0.885	12949	11464.386	34000-35999	1.1155	21	23.42634
18000-18999	1.126	14252	16043.649	36000-37999	1.4184	21	29.78634
19000-19999	1.413	10011	14146.291	38000-39999	1.7805	16	28.48759
20000-20999	1.753	10984	19255.477	40000-41999	2.2088	0	0
21000-21999	2.151	10038	21595.267	42000-43999	2.7107	0	0
22000-22999	2.614	0	0.000	44000-45999	3.2933	0	0
23000-23999	3.146	0	0.000	46000-47999	3.9639	0	0
24000-24999	3.753	0	0.000	48000-49999	4.7294	0	0
25000-25999	4.442	0	0.000	50000-51999	5.5968	0	0
26000-26999	5.216	0	0.000	52000-53999	6.5728	0	0
27000-27999	6.082	0	0.000	54000-55999	7.6637	0	0
28000-28999	7.044	0	0.000	56000-57999	8.876	0	0
29000-34999	7.563	0	0.000	58000-69999	9.5296	0	0
35000-39999	7.563	0	0.000	70000-79999	9.5296	0	0
40000-50000	7.563	0	0.000	80000-100000	9.5296	0	0

ESAL for all trucks weighted : 150171.682

$$\text{Truck factor} = \frac{\text{18-kip ESALs for all trucks weighted}}{\text{Number of trucks weighted}} = \frac{1.502E+05}{135230} = \boxed{1.110}$$

Calculation of Truck Factor for Class 13

Axle load (lb)	EALF	Number of axles	ESAL	Axle load (lb)	EALF	Number of axles	ESAL	Axle load (lb)	EALF	Number of axles	ESAL
Single axle				Tandem axle				Tridem axle			
under 3000	0.000	37912	7.588	under 6000	3E-04	110640	27.9033	under 9000	0.0003	13424	4.057251
3000-3999	0.001	50635	65.972	6000-7999	0.002	175169	287.568	9000-11999	0.002	18709	36.80778
4000-4999	0.003	50241	165.424	8000-9999	0.004	187700	778.71	12000-14999	0.005	8146	40.50066
5000-5999	0.007	57596	410.304	10000-11999	0.009	168902	1516.07	15000-17999	0.0108	3992	42.9419
6000-6999	0.014	42627	588.167	12000-13999	0.017	145258	2525.38	18000-20999	0.0208	2624	54.67098
7000-7999	0.025	54693	1345.375	14000-15999	0.031	117638	3646.11	21000-23999	0.0371	2248	83.49971
8000-8999	0.041	58670	2412.322	16000-17999	0.052	100302	5196.36	24000-26999	0.0621	2276	141.3085
9000-9999	0.065	129457	8450.119	18000-19999	0.082	106080	8724.52	27000-29999	0.0986	3684	363.1064
10000-10999	0.099	264804	26305.841	20000-21999	0.125	155153	19420.4	30000-32999	0.15	6454	968.1297
11000-11999	0.146	238781	34851.999	22000-23999	0.184	190807	35090.8	33000-35999	0.2204	10130	2232.617
12000-12999	0.208	244839	50962.090	24000-25999	0.262	229448	60175.7	36000-38999	0.3143	16456	5172.111
13000-13999	0.289	132753	38406.934	26000-27999	0.365	230076	83870.1	39000-41999	0.4369	18422	8047.834
14000-14999	0.393	108003	42472.591	28000-29999	0.495	198100	98158.5	42000-44999	0.5938	18147	10775.93
15000-15999	0.524	55565	29124.597	30000-31999	0.66	156011	103035	45000-47999	0.7915	14142	11193
16000-16999	0.687	49355	33885.031	32000-33999	0.865	112550	97362.7	48000-50999	1.0367	8858	9183.101
17000-17999	0.885	29025	25697.258	34000-35999	1.116	77717	86696.4	51000-53999	1.3369	0	0
18000-18999	1.126	26415	29735.685	36000-37999	1.418	50780	72026.2	54000-56999	1.6998	0	0
19000-19999	1.413	14836	20964.377	38000-39999	1.78	32271	57457.7	57000-59999	2.1337	0	0
20000-20999	1.753	12490	21895.567	40000-41999	2.209	0	0	60000-62999	2.6471	0	0
21000-21999	2.151	8105	17436.704	42000-43999	2.711	0	0	63000-65999	3.2485	0	0
22000-22999	2.614	0	0.000	44000-45999	3.293	0	0	66000-68999	3.9467	0	0
23000-23999	3.146	0	0.000	46000-47999	3.964	0	0	69000-71999	4.7503	0	0
24000-24999	3.753	0	0.000	48000-49999	4.729	0	0	72000-74999	5.6678	0	0
25000-25999	4.442	0	0.000	50000-51999	5.597	0	0	75000-77999	6.7073	0	0
26000-26999	5.216	0	0.000	52000-53999	6.573	0	0	78000-80999	7.8769	0	0
27000-27999	6.082	0	0.000	54000-55999	7.664	0	0	81000-83999	9.1843	0	0
28000-28999	7.044	0	0.000	56000-57999	8.876	0	0	84000-86999	10.637	0	0
29000-34999	7.563	0	0.000	58000-69999	9.53	0	0	87000-104999	11.42	0	0
35000-39999	7.563	0	0.000	70000-79999	9.53	0	0	105000-11199	11.42	0	0
40000-50000	7.563	0	0.000	80000-100000	9.53	0	0	120000-15000	11.42	0	0

Axle load (lb)	EALF	Number of axles	ESAL	Axle load (lb)	EALF	Number of axles	ESAL
quad axle				5-axle			
under 12000	0.000	3538	1.473	under 15000	5E-04	583	0.29406
12000-15999	0.003	9028	24.466	15000-19999	0.003	489	1.60554
16000-19999	0.007	33481	229.299	20000-24999	0.008	330	2.73814
20000-23999	0.015	42015	622.560	25000-29999	0.018	286	5.13429
24000-27999	0.029	26040	747.344	30000-34999	0.035	342	11.8917
28000-31999	0.051	17060	872.879	35000-39999	0.062	479	29.6926
32000-35999	0.086	13599	1163.026	40000-44999	0.104	835	86.5179
36000-39999	0.136	15151	2057.036	45000-49999	0.164	1287	211.698
40000-43999	0.207	23421	4839.455	50000-54999	0.25	2168	542.735
44000-47999	0.304	35393	10745.055	55000-59999	0.368	3633	1336.27
48000-51999	0.433	54083	23414.816	60000-64999	0.525	5839	3062.71
52000-55999	0.602	79669	47942.204	65000-69999	0.729	6749	4920.45
56000-59999	0.818	101051	82656.475	70000-74999	0.991	5540	5490.14
60000-63999	1.090	97171	105939.668	75000-79999	1.321	3611	4769.65
64000-67999	1.428	0	0.000	80000-84999	1.73	0	0
68000-71999	1.842	0	0.000	85000-89999	2.231	0	0
72000-75999	2.341	0	0.000	90000-94999	2.837	0	0
76000-79999	2.939	0	0.000	95000-99999	3.561	0	0
80000-83999	3.646	0	0.000	100000-10499	4.418	0	0
84000-87999	4.475	0	0.000	105000-10999	5.421	0	0
88000-91999	5.437	0	0.000	110000-11499	6.587	0	0
92000-95999	6.544	0	0.000	115000-11999	7.928	0	0
96000-99999	7.807	0	0.000	120000-12499	9.459	0	0
100000-103999	9.239	0	0.000	125000-12999	11.19	0	0
104000-107999	10.850	0	0.000	130000-13499	13.15	0	0
108000-111999	12.651	0	0.000	135000-13999	15.33	0	0
112000-115999	14.652	0	0.000	140000-14499	17.75	0	0
116000-139999	15.731	0	0.000	145000-17499	19.06	0	0
140000-159999	15.731	0	0.000	175000-19999	19.06	0	0
160000-200000	15.731	0	0.000	200000-25000	19.06	0	0

ESAL for all trucks weighted : 1471246.927

$$\text{Truck factor} = \frac{\text{18-kip ESALs for all trucks weighted}}{\text{Number of trucks weighted}} = \frac{1.471\text{E}+06}{1.08\text{E}+06} = \boxed{1.368}$$

APPENDIX A2

PCC Faulting-based Truck Factors by Class using WIM Data within AASHTO LEF Framework

Calculation of Truck Factor for Class 5

Axle load (lb)	EALF	Number of axles	ESAL
Single axle			
under 3000	0.000	480085	96.093
3000-3999	0.001	3212970	4186.188
4000-4999	0.003	3689060	12146.648
5000-5999	0.007	3088150	21999.466
6000-6999	0.014	1664410	22965.524
7000-7999	0.025	1789680	44023.755
8000-8999	0.041	1204850	49539.563
9000-9999	0.065	1243800	81187.251
10000-10999	0.099	1217440	120941.464
11000-11999	0.146	752855	109885.216
12000-12999	0.208	716939	149227.493
13000-13999	0.289	438587	126888.145
14000-14999	0.393	434099	170711.083
15000-15999	0.524	271202	142151.513
16000-16999	0.687	266017	182635.889
17000-17999	0.885	166753	147634.621
18000-18999	1.126	161392	181680.926
19000-19999	1.413	99249	140246.255
20000-20999	1.753	90997	159522.090
21000-21999	2.151	62930	135384.551
22000-22999	2.614	0	0.000
23000-23999	3.146	0	0.000
24000-24999	3.753	0	0.000
25000-25999	4.442	0	0.000
26000-26999	5.216	0	0.000
27000-27999	6.082	0	0.000
28000-28999	7.044	0	0.000
29000-34999	7.563	0	0.000
35000-39999	7.563	0	0.000
40000-50000	7.563	0	0.000

ESAL for all trucks weighted : 2003053.734

$$\text{Truck factor} = \frac{\text{18-kip ESALs for all trucks weighted}}{\text{Number of trucks weighted}} = \frac{2.003E+06}{1.053E+07} = \boxed{0.190}$$

Calculation of Truck Factor for Class 6

Axle load (lb)	EALF	Number of axles	ESAL	Axle load (lb)	EALF	Number of axles	ESAL
Single axle				Tandem axle			
under 3000	0.000	2847	0.570	under 6000	7E-04	48965	32.24442
3000-3999	0.001	9521	12.405	6000-7999	0.004	214535	919.6152
4000-4999	0.003	13215	43.512	8000-9999	0.011	185744	2012.109
5000-5999	0.007	20551	146.402	10000-11999	0.023	101730	2384.288
6000-6999	0.014	26885	370.959	12000-13999	0.045	92258	4188.09
7000-7999	0.025	70099	1724.342	14000-15999	0.081	85209	6895.933
8000-8999	0.041	106476	4377.951	16000-17999	0.135	77065	10424.91
9000-9999	0.065	212628	13878.986	18000-19999	0.215	77577	16659.66
10000-10999	0.099	314914	31283.809	20000-21999	0.327	95732	31288.21
11000-11999	0.146	214373	31289.456	22000-23999	0.48	93970	45124.57
12000-12999	0.208	185032	38513.544	24000-25999	0.685	98041	67138.29
13000-13999	0.289	109224	31599.730	26000-27999	0.952	94082	89550.44
14000-14999	0.393	101579	39946.328	28000-29999	1.294	83694	108283.7
15000-15999	0.524	55406	29041.256	30000-31999	1.724	70361	121335.1
16000-16999	0.687	46389	31848.702	32000-33999	2.259	53421	120665.9
17000-17999	0.885	24667	21838.907	34000-35999	2.913	36263	105626.8
18000-18999	1.126	21560	24270.353	36000-37999	3.704	23820	88219.58
19000-19999	1.413	12625	17840.069	38000-39999	4.649	15517	72138.78
20000-20999	1.753	10941	19180.096	40000-41999	5.768	0	0
21000-21999	2.151	6724	14465.688	42000-43999	7.078	0	0
22000-22999	2.614	0	0.000	44000-45999	8.599	0	0
23000-23999	3.146	0	0.000	46000-47999	10.35	0	0
24000-24999	3.753	0	0.000	48000-49999	12.35	0	0
25000-25999	4.442	0	0.000	50000-51999	14.61	0	0
26000-26999	5.216	0	0.000	52000-53999	17.16	0	0
27000-27999	6.082	0	0.000	54000-55999	20.01	0	0
28000-28999	7.044	0	0.000	56000-57999	23.18	0	0
29000-34999	7.563	0	0.000	58000-69999	24.88	0	0
35000-39999	7.563	0	0.000	70000-79999	24.88	0	0
40000-50000	7.563	0	0.000	80000-100000	24.88	0	0

ESAL for all trucks weighted : 1244561.348

$$\text{Truck factor} = \frac{\text{18-kip ESALs for all trucks weighted}}{\text{Number of trucks weighted}} = \frac{1.245E+06}{1.55E+06} = \boxed{0.801}$$

Calculation of Truck Factor for Class 7

Axle load (lb)	EALF	Number of axles	ESAL	Axle load (lb)	EALF	Number of axles	ESAL
Single axle				Tridem axle			
under 3000	0.000	1216	0.243	under 9000	0.0011	1029	1.180166
3000-3999	0.001	2375	3.094	9000-11999	0.0075	4002	29.87747
4000-4999	0.003	2769	9.117	12000-14999	0.0189	12597	237.6635
5000-5999	0.007	4564	32.513	15000-17999	0.0408	22424	915.3379
6000-6999	0.014	6089	84.016	18000-20999	0.0791	29618	2341.674
7000-7999	0.025	15660	385.215	21000-23999	0.141	27505	3876.841
8000-8999	0.041	25411	1044.819	24000-26999	0.2356	21919	5164.099
9000-9999	0.065	44563	2908.786	27000-29999	0.374	21655	8099.349
10000-10999	0.099	45430	4513.053	30000-32999	0.5692	20066	11422.02
11000-11999	0.146	26947	3933.130	33000-35999	0.8363	17182	14369.98
12000-12999	0.208	25035	5210.918	36000-38999	1.1927	17614	21007.74
13000-13999	0.289	17256	4992.355	39000-41999	1.6578	15417	25557.58
14000-14999	0.393	20324	7992.490	42000-44999	2.2533	13351	30084.4
15000-15999	0.524	14906	7813.034	45000-47999	3.0034	9134	27433.06
16000-16999	0.687	16455	11297.299	48000-50999	3.934	5297	20838.25
17000-17999	0.885	11448	10135.477	51000-53999	5.0731	0	0
18000-18999	1.126	11867	13358.825	54000-56999	6.4503	0	0
19000-19999	1.413	7506	10606.539	57000-59999	8.0969	0	0
20000-20999	1.753	6941	12167.905	60000-62999	10.045	0	0
21000-21999	2.151	4740	10197.406	63000-65999	12.327	0	0
22000-22999	2.614	0	0.000	66000-68999	14.977	0	0
23000-23999	3.146	0	0.000	69000-71999	18.026	0	0
24000-24999	3.753	0	0.000	72000-74999	21.508	0	0
25000-25999	4.442	0	0.000	75000-77999	25.452	0	0
26000-26999	5.216	0	0.000	78000-80999	29.89	0	0
27000-27999	6.082	0	0.000	81000-83999	34.852	0	0
28000-28999	7.044	0	0.000	84000-86999	40.365	0	0
29000-34999	7.563	0	0.000	87000-104999	43.337	0	0
35000-39999	7.563	0	0.000	105000-11199(	43.337	0	0
40000-50000	7.563	0	0.000	120000-15000(	43.337	0	0

Axle load (lb)	EALF	Number of axles	ESAL
Quad axle			
under 12000	0.002	391	0.617
12000-15999	0.010	408	4.194
16000-19999	0.026	493	12.808
20000-23999	0.056	1038	58.343
24000-27999	0.109	1864	202.927
28000-31999	0.194	3212	623.396
32000-35999	0.324	5088	1650.606
36000-39999	0.515	7280	3749.261
40000-43999	0.784	10590	8300.431
44000-47999	1.152	11789	13576.315
48000-51999	1.642	11552	18971.463
52000-55999	2.283	8864	20233.548
56000-59999	3.103	5165	16025.820
60000-63999	4.136	2512	10388.557
64000-67999	5.417	0	0.000
68000-71999	6.985	0	0.000
72000-75999	8.882	0	0.000
76000-79999	11.149	0	0.000
80000-83999	13.832	0	0.000
84000-87999	16.974	0	0.000
88000-91999	20.622	0	0.000
92000-95999	24.821	0	0.000
96000-99999	29.615	0	0.000
100000-103999	35.047	0	0.000
104000-107999	41.158	0	0.000
108000-111999	47.989	0	0.000
112000-115999	55.581	0	0.000
116000-139999	59.674	0	0.000
140000-159999	59.674	0	0.000
160000-200000	59.674	0	0.000

ESAL for all trucks weighted : 371863.580

$$\text{Truck factor} = \frac{\text{18-kip ESALs for all trucks weighted}}{\text{Number of trucks weighted}} = \frac{3.719E+05}{309775} = \boxed{1.200}$$

Calculation of Truck Factor for Class 8

Axle load (lb)	EALF	Number of axles	ESAL	Axle load (lb)	EALF	Number of axles	ESAL
Single axle				Tandem axle			
under 3000	0.000	47700	9.548	under 6000	0.00066	117362	77.2852
3000-3999	0.001	216420	281.974	6000-7999	0.00429	222021	951.7043
4000-4999	0.003	306637	1009.637	8000-9999	0.01083	254319	2754.961
5000-5999	0.007	312311	2224.852	10000-11999	0.02344	207204	4856.325
6000-6999	0.014	227648	3141.086	12000-13999	0.0454	149541	6788.475
7000-7999	0.025	341950	8411.517	14000-15999	0.08093	115820	9373.271
8000-8999	0.041	372547	15317.936	16000-17999	0.13527	91408	12365.15
9000-9999	0.065	466409	30444.175	18000-19999	0.21475	73370	15756.21
10000-10999	0.099	347090	34480.199	20000-21999	0.32683	64690	21142.71
11000-11999	0.146	185099	27016.681	22000-23999	0.4802	40702	19545.18
12000-12999	0.208	191005	39756.796	24000-25999	0.6848	26797	18350.53
13000-13999	0.289	132793	38418.506	26000-27999	0.95183	16757	15949.88
14000-14999	0.393	142793	56153.890	28000-29999	1.29381	9886	12790.56
15000-15999	0.524	93963	49251.048	30000-31999	1.72447	5987	10324.37
16000-16999	0.687	95644	65665.078	32000-33999	2.25877	3608	8149.654
17000-17999	0.885	60271	53360.876	34000-35999	2.9128	2271	6614.966
18000-18999	1.126	53720	60473.254	36000-37999	3.70359	1299	4810.967
19000-19999	1.413	29430	41586.790	38000-39999	4.64902	761	3537.901
20000-20999	1.753	24439	42842.735	40000-41999	5.76753	0	0
21000-21999	2.151	15012	32296.089	42000-43999	7.07795	0	0
22000-22999	2.614	0	0.000	44000-45999	8.5992	0	0
23000-23999	3.146	0	0.000	46000-47999	10.3501	0	0
24000-24999	3.753	0	0.000	48000-49999	12.349	0	0
25000-25999	4.442	0	0.000	50000-51999	14.6139	0	0
26000-26999	5.216	0	0.000	52000-53999	17.1622	0	0
27000-27999	6.082	0	0.000	54000-55999	20.0108	0	0
28000-28999	7.044	0	0.000	56000-57999	23.1762	0	0
29000-34999	7.563	0	0.000	58000-69999	24.883	0	0
35000-39999	7.563	0	0.000	70000-79999	24.883	0	0
40000-50000	7.563	0	0.000	80000-100000	24.883	0	0

ESAL for all trucks weighted : 776282.764

$$\text{Truck factor} = \frac{\text{18-kip ESALs for all trucks weighted}}{\text{Number of trucks weighted}} = \frac{7.763E+05}{1.69E+06} = \boxed{0.459}$$

Calculation of Truck Factor for Class 9

Axle load (lb)	EALF	Number of axles	ESAL	Axle load (lb)	EALF	Number of axles	ESAL
Single axle				Tandem axle			
under 3000	0.000	217586	43.552	under 6000	0.0007	263474	173.5028
3000-3999	0.001	474182	617.813	6000-7999	0.0043	851432	3649.707
4000-4999	0.003	392627	1292.769	8000-9999	0.0108	2289300	24799.29
5000-5999	0.007	435776	3104.396	10000-11999	0.0234	3283180	76949.24
6000-6999	0.014	415293	5730.212	12000-13999	0.0454	3237820	146982.2
7000-7999	0.025	880848	21667.693	14000-15999	0.0809	2874240	232611.2
8000-8999	0.041	1489430	61240.578	16000-17999	0.1353	2601420	351905.1
9000-9999	0.065	3683550	240438.414	18000-19999	0.2148	2387830	512786.5
10000-10999	0.099	5998950	595940.496	20000-21999	0.3268	2503490	818218.7
11000-11999	0.146	3725460	543760.721	22000-23999	0.4802	2037270	978300.8
12000-12999	0.208	2170990	451881.394	24000-25999	0.6848	1845260	1263631
13000-13999	0.289	633693	183334.502	26000-27999	0.9518	1793390	1707009
14000-14999	0.393	428790	168623.298	28000-29999	1.2938	1942570	2513307
15000-15999	0.524	292044	153075.923	30000-31999	1.7245	2107480	3634276
16000-16999	0.687	365772	251123.403	32000-33999	2.2588	1873360	4231495
17000-17999	0.885	260477	230613.081	34000-35999	2.9128	1197970	3489445
18000-18999	1.126	236156	265843.665	36000-37999	3.7036	644266	2386099
19000-19999	1.413	119596	168998.087	38000-39999	4.649	342570	1592613
20000-20999	1.753	86395	151454.564	40000-41999	5.7675	0	0
21000-21999	2.151	47271	101696.538	42000-43999	7.0779	0	0
22000-22999	2.614	0	0.000	44000-45999	8.5992	0	0
23000-23999	3.146	0	0.000	46000-47999	10.35	0	0
24000-24999	3.753	0	0.000	48000-49999	12.349	0	0
25000-25999	4.442	0	0.000	50000-51999	14.614	0	0
26000-26999	5.216	0	0.000	52000-53999	17.162	0	0
27000-27999	6.082	0	0.000	54000-55999	20.011	0	0
28000-28999	7.044	0	0.000	56000-57999	23.176	0	0
29000-34999	7.563	0	0.000	58000-69999	24.883	0	0
35000-39999	7.563	0	0.000	70000-79999	24.883	0	0
40000-50000	7.563	0	0.000	80000-100000	24.883	0	0

ESAL for all trucks weighted : 27564733.603

$$\text{Truck factor} = \frac{\text{18-kip ESALs for all trucks weighted}}{\text{Number of trucks weighted}} = \frac{2.756E+07}{1.81E+07} = \boxed{1.523}$$

Calculation of Truck Factor for Class 10

Axle load (lb)	EALF	Number of axles	ESAL	Axle load (lb)	EALF	Number of axles	ESAL
Single axle				Tandem axle			
under 3000	0.000	253446	50.729	under 6000	7E-04	31067	20.45823
3000-3999	0.001	381335	496.843	6000-7999	0.004	66836	286.4959
4000-4999	0.003	419770	1382.140	8000-9999	0.011	144459	1564.881
5000-5999	0.007	455130	3242.270	10000-11999	0.023	261587	6130.922
6000-6999	0.014	311176	4293.606	12000-13999	0.045	287843	13066.75
7000-7999	0.025	351943	8657.331	14000-15999	0.081	237582	19227.43
8000-8999	0.041	292155	12012.475	16000-17999	0.135	198224	26814.6
9000-9999	0.065	472821	30862.709	18000-19999	0.215	175094	37601.44
10000-10999	0.099	746091	74117.277	20000-21999	0.327	174420	57005.9
11000-11999	0.146	607189	88624.097	22000-23999	0.48	153058	73498.73
12000-12999	0.208	613503	127697.774	24000-25999	0.685	166578	114072.3
13000-13999	0.289	371182	107387.121	26000-27999	0.952	192553	183278.5
14000-14999	0.393	366007	143933.645	28000-29999	1.294	216873	280591.4
15000-15999	0.524	225922	118417.837	30000-31999	1.724	220489	380225.7
16000-16999	0.687	218932	150309.343	32000-33999	2.259	194198	438649.2
17000-17999	0.885	134400	118990.921	34000-35999	2.913	146968	428088.2
18000-18999	1.126	124175	139785.299	36000-37999	3.704	96892	358848.5
19000-19999	1.413	68353	96587.898	38000-39999	4.649	58771	273227.3
20000-20999	1.753	55958	98097.048	40000-41999	5.768	0	0
21000-21999	2.151	34217	73612.795	42000-43999	7.078	0	0
22000-22999	2.614	0	0.000	44000-45999	8.599	0	0
23000-23999	3.146	0	0.000	46000-47999	10.35	0	0
24000-24999	3.753	0	0.000	48000-49999	12.35	0	0
25000-25999	4.442	0	0.000	50000-51999	14.61	0	0
26000-26999	5.216	0	0.000	52000-53999	17.16	0	0
27000-27999	6.082	0	0.000	54000-55999	20.01	0	0
28000-28999	7.044	0	0.000	56000-57999	23.18	0	0
29000-34999	7.563	0	0.000	58000-69999	24.88	0	0
35000-39999	7.563	0	0.000	70000-79999	24.88	0	0
40000-50000	7.563	0	0.000	80000-100000	24.88	0	0

Axle load (lb)	EALF	Number of axles	ESAL	Axle load (lb)	EALF	Number of axles	ESAL
7-axle				8-axle			
under 21000	0.003	8708	23.739	under 24000	0.003	30507	94.95172
21000-27999	0.018	22195	393.862	24000-31999	0.02	78497	1590.36
28000-34999	0.045	17913	803.316	32000-39999	0.051	36058	1846.175
35000-41999	0.097	9262	898.660	40000-47999	0.111	13208	1463.124
42000-48999	0.188	5508	1035.111	48000-55999	0.215	6664	1429.82
49000-55999	0.335	5638	1888.921	56000-63999	0.383	7991	3056.632
56000-62999	0.560	7530	4216.880	64000-71999	0.639	13736	8782.332
63000-69999	0.889	10257	9118.738	72000-79999	1.015	22316	22650.83
70000-76999	1.353	15219	20591.637	80000-87999	1.545	39277	60673.12
77000-83999	1.988	22345	44420.700	88000-95999	2.27	67015	152100.4
84000-90999	2.835	27555	78116.749	96000-103999	3.237	99997	323656.3
91000-97999	3.940	24471	96425.992	104000-111999	4.499	113115	508880.6
98000-104999	5.356	17000	91053.986	112000-119999	6.115	91930	562160.8
105000-111999	7.139	10834	77343.628	120000-127999	8.151	56756	462594.8
112000-118999	9.351	0	0.000	128000-135999	10.68	0	0
119000-125999	12.058	0	0.000	136000-143999	13.77	0	0
126000-132999	15.332	0	0.000	144000-151999	17.5	0	0
133000-139999	19.246	0	0.000	152000-159999	21.97	0	0
140000-146999	23.877	0	0.000	160000-167999	27.26	0	0
147000-153999	29.301	0	0.000	168000-175999	33.45	0	0
154000-160999	35.599	0	0.000	176000-183999	40.64	0	0
161000-167999	42.847	0	0.000	184000-191999	48.92	0	0
168000-174999	51.123	0	0.000	192000-199999	58.37	0	0
175000-181999	60.499	0	0.000	200000-207999	69.07	0	0
182000-188999	71.049	0	0.000	208000-215999	81.12	0	0
189000-195999	82.841	0	0.000	216000-223999	94.58	0	0
196000-202999	95.945	0	0.000	224000-231999	109.5	0	0
203000-244999	103.011	0	0.000	232000-279999	117.6	0	0
245000-279999	103.011	0	0.000	280000-319999	117.6	0	0
280000-350000	103.011	0	0.000	320000-400000	117.6	0	0

ESAL for all trucks weighted : 6628069.997

$$\text{Truck factor} = \frac{\text{18-kip ESALs for all trucks weighted}}{\text{Number of trucks weighted}} = \frac{6.628E+06}{2.43E+06} = \boxed{2.733}$$

Calculation of Truck Factor for Class 11

Axle load (lb)	EALF	Number of axles	ESAL
Single axle			
under 3000	0.000	45199	9.047
3000-3999	0.001	88280	115.020
4000-4999	0.003	108165	356.146
5000-5999	0.007	163914	1167.696
6000-6999	0.014	131316	1811.898
7000-7999	0.025	173850	4276.479
8000-8999	0.041	184295	7577.619
9000-9999	0.065	318663	20800.268
10000-10999	0.099	314038	31196.786
11000-11999	0.146	174981	25539.878
12000-12999	0.208	187849	39099.889
13000-13999	0.289	140541	40660.090
14000-14999	0.393	162424	63873.856
15000-15999	0.524	108747	57000.135
16000-16999	0.687	103746	71227.564
17000-17999	0.885	59837	52976.635
18000-18999	1.126	50726	57102.872
19000-19999	1.413	26155	36958.970
20000-20999	1.753	19239	33726.886
21000-21999	2.151	9745	20964.921
22000-22999	2.614	0	0.000
23000-23999	3.146	0	0.000
24000-24999	3.753	0	0.000
25000-25999	4.442	0	0.000
26000-26999	5.216	0	0.000
27000-27999	6.082	0	0.000
28000-28999	7.044	0	0.000
29000-34999	7.563	0	0.000
35000-39999	7.563	0	0.000
40000-50000	7.563	0	0.000

ESAL for all trucks weighted : 566442.654

$$\text{Truck factor} = \frac{\text{18-kip ESALs for all trucks weighted}}{\text{Number of trucks weighted}} = \frac{5.664E+05}{514342} = \boxed{1.101}$$

Calculation of Truck Factor for Class 12

Axle load (lb)	EALF	Number of axles	ESAL	Axle load (lb)	EALF	Number of axles	ESAL
Single axle				Tandem axle			
under 3000	0.000	10067	2.015	under 6000	0.0007	17822	11.73614
3000-3999	0.001	7138	9.300	6000-7999	0.0043	32409	138.9228
4000-4999	0.003	12932	42.580	8000-9999	0.0108	39129	423.8726
5000-5999	0.007	29544	210.467	10000-11999	0.0234	27951	655.0991
6000-6999	0.014	26015	358.955	12000-13999	0.0454	13549	615.0624
7000-7999	0.025	39028	960.037	14000-15999	0.0809	7438	601.9546
8000-8999	0.041	45508	1871.143	16000-17999	0.1353	4017	543.3966
9000-9999	0.065	67223	4387.884	18000-19999	0.2148	1730	371.5175
10000-10999	0.099	64947	6451.887	20000-21999	0.3268	708	231.3965
11000-11999	0.146	38598	5633.687	22000-23999	0.4802	238	114.288
12000-12999	0.208	36550	7607.711	24000-25999	0.6848	105	71.9038
13000-13999	0.289	24510	7091.018	26000-27999	0.9518	56	53.3027
14000-14999	0.393	24950	9811.682	28000-29999	1.2938	53	68.57167
15000-15999	0.524	16947	8882.832	30000-31999	1.7245	32	55.18289
16000-16999	0.687	18526	12719.159	32000-33999	2.2588	34	76.79829
17000-17999	0.885	12949	11464.386	34000-35999	2.9128	21	61.16877
18000-18999	1.126	14252	16043.649	36000-37999	3.7036	21	77.77545
19000-19999	1.413	10011	14146.291	38000-39999	4.649	16	74.38425
20000-20999	1.753	10984	19255.477	40000-41999	5.7675	0	0
21000-21999	2.151	10038	21595.267	42000-43999	7.0779	0	0
22000-22999	2.614	0	0.000	44000-45999	8.5992	0	0
23000-23999	3.146	0	0.000	46000-47999	10.35	0	0
24000-24999	3.753	0	0.000	48000-49999	12.349	0	0
25000-25999	4.442	0	0.000	50000-51999	14.614	0	0
26000-26999	5.216	0	0.000	52000-53999	17.162	0	0
27000-27999	6.082	0	0.000	54000-55999	20.011	0	0
28000-28999	7.044	0	0.000	56000-57999	23.176	0	0
29000-34999	7.563	0	0.000	58000-69999	24.883	0	0
35000-39999	7.563	0	0.000	70000-79999	24.883	0	0
40000-50000	7.563	0	0.000	80000-100000	24.883	0	0

ESAL for all trucks weighted : 152791.761

$$\text{Truck factor} = \frac{\text{18-kip ESALs for all trucks weighted}}{\text{Number of trucks weighted}} = \frac{1.528E+05}{135230} = \boxed{1.130}$$

Calculation of Truck Factor for Class 13

Axle load (lb)	EALF	Number of axles	ESAL	Axle load (lb)	EALF	Number of axles	ESAL	Axle load (lb)	EALF	Number of axles	ESAL
Single axle				Tandem axle				Tridem axle			
under 3000	0.000	37912	7.588	under 6000	7E-04	110640	72.8586	under 9000	0.00115	13424	15.39606
3000-3999	0.001	50635	65.972	6000-7999	0.004	175169	750.871	9000-11999	0.00747	18709	139.6746
4000-4999	0.003	50241	165.424	8000-9999	0.011	187700	2033.3	12000-14999	0.01887	8146	153.6879
5000-5999	0.007	57596	410.304	10000-11999	0.023	168902	3958.63	15000-17999	0.04082	3992	162.9517
6000-6999	0.014	42627	588.167	12000-13999	0.045	145258	6594.05	18000-20999	0.07906	2624	207.4601
7000-7999	0.025	54693	1345.375	14000-15999	0.081	117638	9520.4	21000-23999	0.14095	2248	316.8565
8000-8999	0.041	58670	2412.322	16000-17999	0.135	100302	13568.3	24000-26999	0.2356	2276	536.2238
9000-9999	0.065	129457	8450.119	18000-19999	0.215	106080	22780.7	27000-29999	0.37402	3684	1377.88
10000-10999	0.099	264804	26305.841	20000-21999	0.327	155153	50708.8	30000-32999	0.56922	6454	3673.764
11000-11999	0.146	238781	34851.999	22000-23999	0.48	190807	91625.9	33000-35999	0.83634	10130	8472.118
12000-12999	0.208	244839	50962.090	24000-25999	0.685	229448	157126	36000-38999	1.19267	16456	19626.62
13000-13999	0.289	132753	38406.934	26000-27999	0.952	230076	218994	39000-41999	1.65775	18422	30539.13
14000-14999	0.393	108003	42472.591	28000-29999	1.294	198100	256303	42000-44999	2.25334	18147	40891.44
15000-15999	0.524	55565	29124.597	30000-31999	1.724	156011	269036	45000-47999	3.0034	14142	42474.09
16000-16999	0.687	49355	33885.031	32000-33999	2.259	112550	254225	48000-50999	3.93397	8858	34847.13
17000-17999	0.885	29025	25697.258	34000-35999	2.913	77717	226374	51000-53999	5.07305	0	0
18000-18999	1.126	26415	29735.685	36000-37999	3.704	50780	188068	54000-56999	6.45033	0	0
19000-19999	1.413	14836	20964.377	38000-39999	4.649	32271	150028	57000-59999	8.09692	0	0
20000-20999	1.753	12490	21895.567	40000-41999	5.768	0	0	60000-62999	10.045	0	0
21000-21999	2.151	8105	17436.704	42000-43999	7.078	0	0	63000-65999	12.3272	0	0
22000-22999	2.614	0	0.000	44000-45999	8.599	0	0	66000-68999	14.9767	0	0
23000-23999	3.146	0	0.000	46000-47999	10.35	0	0	69000-71999	18.0261	0	0
24000-24999	3.753	0	0.000	48000-49999	12.35	0	0	72000-74999	21.5075	0	0
25000-25999	4.442	0	0.000	50000-51999	14.61	0	0	75000-77999	25.4522	0	0
26000-26999	5.216	0	0.000	52000-53999	17.16	0	0	78000-80999	29.8905	0	0
27000-27999	6.082	0	0.000	54000-55999	20.01	0	0	81000-83999	34.8516	0	0
28000-28999	7.044	0	0.000	56000-57999	23.18	0	0	84000-86999	40.3647	0	0
29000-34999	7.563	0	0.000	58000-69999	24.88	0	0	87000-104999	43.3372	0	0
35000-39999	7.563	0	0.000	70000-79999	24.88	0	0	105000-11199(	43.3372	0	0
40000-50000	7.563	0	0.000	80000-100000	24.88	0	0	120000-15000(	43.3372	0	0

Axle load (lb)	EALF	Number of axles	ESAL	Axle load (lb)	EALF	Number of axles	ESAL
quad axle				5-axle			
under 12000	0.002	3538	5.587	under 15000	0.002	583	1.15408
12000-15999	0.010	9028	92.807	15000-19999	0.013	489	6.30111
16000-19999	0.026	33481	869.793	20000-24999	0.033	330	10.7461
20000-23999	0.056	42015	2361.539	25000-29999	0.07	286	20.15
24000-27999	0.109	26040	2834.876	30000-34999	0.136	342	46.6701
28000-31999	0.194	17060	3311.065	35000-39999	0.243	479	116.532
32000-35999	0.324	13599	4411.671	40000-44999	0.407	835	339.549
36000-39999	0.515	15151	7802.892	45000-49999	0.646	1287	830.83
40000-43999	0.784	23421	18357.354	50000-54999	0.982	2168	2130.02
44000-47999	1.152	35393	40758.886	55000-59999	1.444	3633	5244.33
48000-51999	1.642	54083	88818.700	60000-64999	2.059	5839	12019.9
52000-55999	2.283	79669	181857.687	65000-69999	2.861	6749	19310.8
56000-59999	3.103	101051	313538.265	70000-74999	3.889	5540	21546.6
60000-63999	4.136	97171	401857.682	75000-79999	5.184	3611	18719
64000-67999	5.417	0	0.000	80000-84999	6.79	0	0
68000-71999	6.985	0	0.000	85000-89999	8.756	0	0
72000-75999	8.882	0	0.000	90000-94999	11.13	0	0
76000-79999	11.149	0	0.000	95000-99999	13.98	0	0
80000-83999	13.832	0	0.000	100000-104999	17.34	0	0
84000-87999	16.974	0	0.000	105000-109999	21.28	0	0
88000-91999	20.622	0	0.000	110000-114999	25.85	0	0
92000-95999	24.821	0	0.000	115000-119999	31.11	0	0
96000-99999	29.615	0	0.000	120000-124999	37.12	0	0
100000-103999	35.047	0	0.000	125000-129999	43.93	0	0
104000-107999	41.158	0	0.000	130000-134999	51.59	0	0
108000-111999	47.989	0	0.000	135000-139999	60.15	0	0
112000-115999	55.581	0	0.000	140000-144999	69.67	0	0
116000-139999	59.674	0	0.000	145000-174999	74.8	0	0
140000-159999	59.674	0	0.000	175000-199999	74.8	0	0
160000-200000	59.674	0	0.000	200000-250000	74.8	0	0

ESAL for all trucks weighted : 3637607.352

$$\text{Truck factor} = \frac{\text{18-kip ESALs for all trucks weighted}}{\text{Number of trucks weighted}} = \frac{3.638E+06}{1.08E+06} = \boxed{3.383}$$